CHESTER

Compressed Heat Energy Storage for Energy from Renewable sources

D2.2 Description of CHESTER simulation model and results

PROJECT	**CHESTER**
PROJECT NO.	**764042**
DELIVERABLE NO.	**D2.2**
DOCUMENT VERSION	**V3.7**
DOCUMENT PREPARATION DATE	**12/12/2018**
RESPONSIBLE PARTNER	**PlanEnergi**
DISSEMINATION LEVEL	**Public**

Type of Deliverable		
R	Document, Report	**X**
DEM	Demonstrator, pilot, prototype	
DEC	Websites, patent fillings, videos, etc.	
OTHER		
ETHICS	Ethics requirements	
ORDP	Open Research Data Pilot	

This project has received funding from the European Union's Horizon 2020 research and innovation programme under grant agreement No. 764042.

This deliverable reflects only the author's views and neither Agency nor the Commission are responsible for any use that may be made of the information contained therein.

EC Grant Agreement	No.764042
Project Acronym	CHESTER
Project Title	Compressed Heat Energy Storage for Energy from Renewable sources
Programme	HORIZON 2020
Start Date of Project	01-04-2018
Duration	48 Months

Financial/Administrative Coordinator	
Project Coordinator Organization Name	TECNALIA
Address	Parque Tecnológico de Bizkaia C/Astondo, Edificio 700 (Spain)
Phone Numbers	+34 946 430 850
E-mail Address	eduardo.zabala@tecnalia.com
Project web-site	www.chester-project.eu

Version Management			
Filename	CHESTER D2.2 - Description of CHESTER simulation model and results		
Authors	Federico Bava, Henning Jockenhöfer, Sven Stark		
Reviewed by	Silvia Alonso		
Approved by	Eduardo Zabala		
Revision No.	**Date**	**Author**	**Modification description**
0.1	04/09/2018	F. Bava	Description of the TRNSYS model
0.2	28/09/2018	H. Jockenhöfer	Description of the DLR model
1.0	14/10/2018	F. Bava	Update of the TRNSYS model's description
2.0	07/11/2018	F. Bava	Results from Aalborg case study
2.1	16/11/2018	S. Stark	Results from Alpha Ventus case study
3.0	18/11/2018	F. Bava	Preparation of the report for internal revision
3.1	23/11/2018	A. Carrera	Internal revision
3.2	30/11/2018	S. Ochoa de Eribe	Internal revision and comments
3.3	30/11/2018	F. Bava	Update based on internal revision
3.4	05/12/2018	S. Stark, F. Bava	Update of Alpha Ventus case and finalization of deliverable
3.5	07/12/2018	S. Stark	Update of Alpha Ventus case
3.6	10/12/2018	C. Pascual	Minor changes
3.7	12/12/2018	S. Alonso	Final revision

Contents

List of Figures

List of Tables

Glossary, Abbreviations and Acronyms

CHEST	Compressed Heat Energy STorage
COP	Coefficient of Performance
DH	District Heating
DLR	Deutsches Zentrum für Luft- und Raumfahrt (German Aerospace Center)
HP	Heat Pump
HT	High Temperature
HX	Heat Exchanger
LT	Low Temperature
PCM	Phase Change Material
PLF	Partial Load Factor
PTES	Pit Thermal Energy Storage
PuTES	Pumped Thermal Energy Storage
P2P	Power-to-power
ORC	Organic Rankine Cycle
RES	Renewable Energy Source
TES	Thermal Energy Storage
TRNSYS	Transient System Simulation (software)

1. Introduction

1.1. Purpose and Scope

This deliverable describes a preliminary simulation model of the CHEST system, useful to identify general specifications and requirements of the overall system and partly of the individual components. Additionally, the deliverable presents the results of different parametric simulations carried out with the model for two of the seven case studies described in the deliverable D2.1, i.e. Aalborg and Alpha Ventus. The remaining case studies will be analysed in the deliverable D2.3.

The simulation model is developed in TRNSYS, using as starting point a previously developed model developed by DLR, partner of the CHESTER Consortium. While the DLR model only focuses on the CHEST components and evaluates their performance under a variety of boundary conditions, the TRNSYS model does a step further, by integrating the CHEST system in real-world scenarios, where the boundary conditions are set by actual requirements of existing energy systems.

The tasks carried out within Task 2.2 of the CHESTER project, whose main outcomes are presented in this deliverable, are:

- Update of the CHEST model from DLR and definition of performance maps of the CHEST components, to be used by the TRNSYS model;
- Development of a TRNSYS simulation model of the CHEST system integrated into the energy system;
- Simulations of the CHEST system through the TRNSYS model using as boundary conditions the requirements and specifications of the case studies treated in the deliverable D2.1 of the CHESTER project;
- Presentation and discussion of the results.

1.2. Structure of the document

This document is divided in three main sections.

Section 2 describes the basis and the development of the CHEST simulations model and is divided in two subsections. Subsection 2.1 describes the CHEST concept from a thermodynamic point of view and the results of simulation model as developed by DLR. These results are in the form of performance maps of the main components of the CHEST system, i.e. the high-temperature heat pump and the Organic Rankine Cycle engine. Subsection 2.2 describes the TRNSYS model, which has been developed to integrate the CHEST model as developed by DLR into the energy system.

Section 3 presents the simulation results which are obtained when applying to the TRNSYS model the boundary conditions of the energy systems of Aalborg case study (Section 3.1) and of Alpha Ventus case study (Section 3.2).

Finally, Section 4 summarizes the conclusions of the two case studies analysed in previous sections of this document.

2. Methodology

The main objective of the CHESTER project is the development and validation of an innovative system that allows energy management, storage and dispatchable supply of many different RES, by combining the electricity and the heat sector. This is done by combining an innovative power-to-heat-to-power energy storage system, the so-called CHEST (Compressed Heat Energy Storage) system with smart district heating, thus leading to a very flexible renewable energy management system (Figure 1).

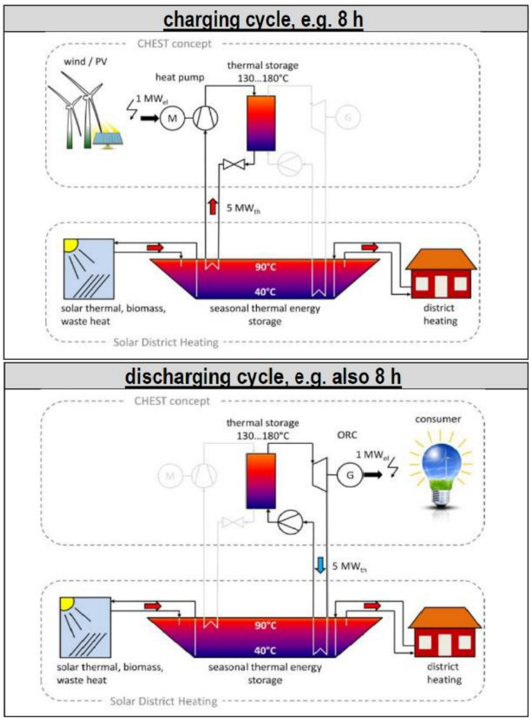

Figure 1: Principle scheme of a CHEST system integrated in DH system equipped with water pit storage.

The CHEST system is based on existing technologies (heat pump, HP; thermal storage, TES; Organic Rankine Cycle, ORC), but ground-breaking advancements are necessary to ensure high-efficiency and cost-competitiveness.

In the CHEST system, the HP consumes the electricity surplus from the grid to transfer heat from a low temperature heat source to a high temperature level (130-180°C), at which heat is stored in a high temperature thermal energy storage (HT-TES). The HT-TES is based on PCMs and needs to follow the temperatures of the heat transfer fluids of the HP (condenser) and the ORC (evaporator), so to lose as little exergy as possible. When electricity is needed, the HT-TES can be discharged, working as heat source for an ORC cycle.

Connected to a smart DH system, the CHEST system uses the seasonal TES as low-temperature heat source for the HP. In addition, the waste heat of the ORC is fed back to the seasonal TES. In the power range up to about 10 MW a high technological potential is ascribed to simple ORC engines and corresponding temperature levels between 130 °C and 180 °C in the high-temperature storage. The integration of the CHEST concept into an application with two different temperature levels in the low-temperature heat source or sink (here: approx. 90 °C and 40 °C) theoretically compensates for any irreversibility within the energy conversion. This is done by extracting of exergy from the seasonal TES which gives the possibility of achieving a real round-trip efficiency for the electric energy storage of 100 % or higher.

The principle scheme of a CHEST system, using the TES of a DH network as heat source for the HP and heat sink for the ORC, can be seen in Figure 1.

2.1. Model of the CHEST system by DLR

The CHEST system with thermal energy integration as described in [Jockenhöfer, 2018] is based on a subcritical pumped thermal energy storage (PuTES) with an organic working fluid. As depicted in Figure 2, it consists of three main components: a high-temperature heat pump (HT-HP), a high-temperature thermal energy storage (HT-TES) system and a power cycle (Organic Rankine Cycle, ORC).

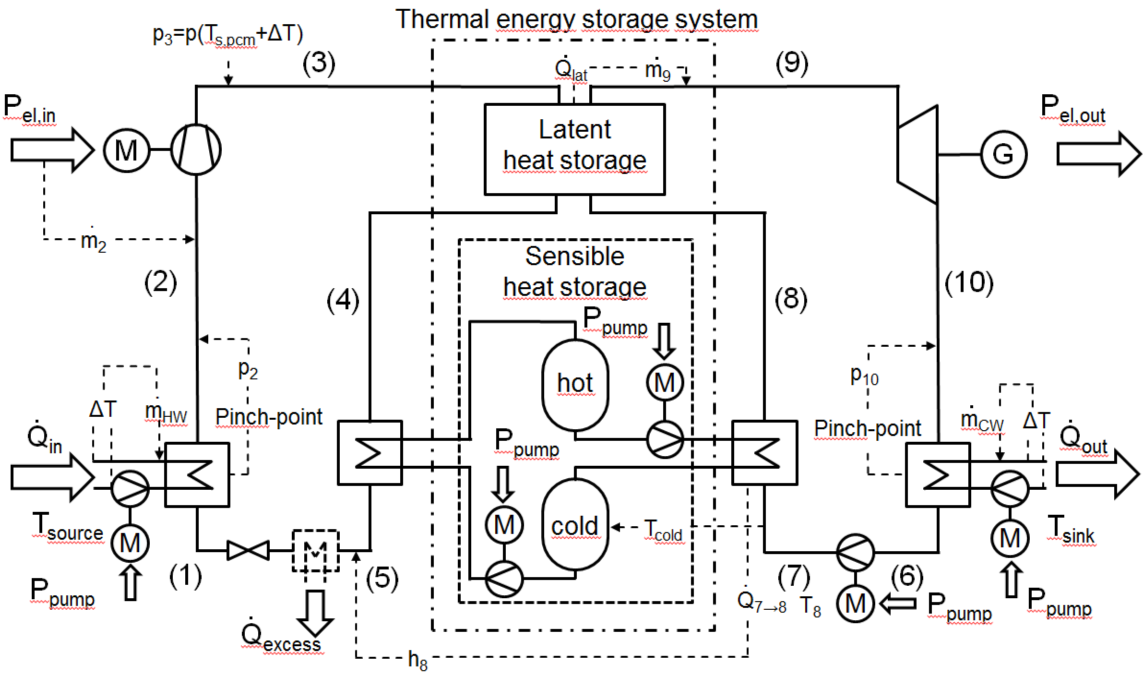

Figure 2: Process diagram of the CHEST system. The broken lines represent dependencies and control circuits. An explanation is given in Section 2.1.3.

2.1.1. Thermodynamic cycle

The thermodynamic cycle is a combination of the charging and discharging cycle parts and can best be shown in a temperature-entropy (*T, s*) diagram (Figure 3). In the diagram the charging cycle (HT-HP operation) is represented by the red curve, while the discharging cycle (ORC operation) is represented by the blue curve. The description of the charging and discharging cycles in the following sections refer to the numbering used in this diagram (Figure 3) as well as in the process flow diagram in Figure 2.

Charging

The charging cycle is a multi-step process designed to convert electrical energy and low-temperature heat into high-temperature heat, which is then transferred to the HT-TES system.

Low-temperature heat is used to evaporate the working fluid at low pressure between 40 °C and 100 °C (from point (1) to point (2) in Figure 2 and Figure 3). An electrically-driven compressor brings the gaseous working fluid to a high pressure and temperature ((2) → (3)). As the saturation temperature depends on the pressure, the working fluid is condensed in the latent heat storage at 138 °C ((3) → (4)). The working fluid exits the latent heat storage unit as a saturated liquid, still containing sensible heat. The sensible heat is transferred to a sensible two-tank pressurized water storage ((4) → (5)). Before entering the evaporator again, the working fluid is throttled to the evaporation pressure ((5) → (1)). Depending on the temperatures of the heat source and heat sink, an additional heat exchanger between the sensible heat storage and the throttling valve may be necessary to keep the ratio of sensible and latent thermal energy constant during the charging and discharging cycles. This is discussed in detail in Section 2.1.3.

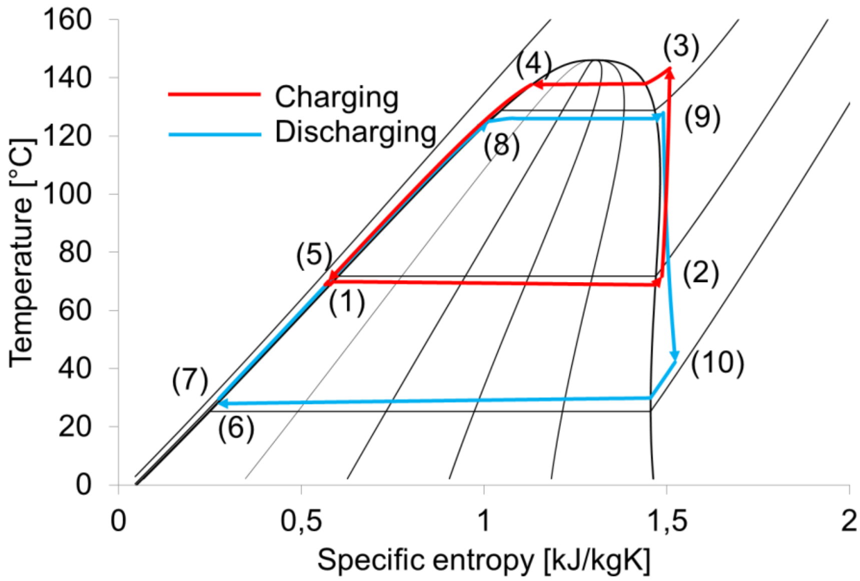

Figure 3: T, s-diagram of the CHEST cycle with Butene operating with a source temperature of 80 °C and a sink temperature of 20 °C [Jockenhöfer, 2018].

Discharging

The discharging cycle is a conventional Organic Rankine Cycle (ORC), which converts the stored high-temperature heat into electricity plus low-temperature heat.

After being compressed to the evaporation pressure ((6) → (7)), the working fluid is preheated using the sensible heat from the pressurized water storage ((7) → (8)). The latent heat storage provides heat for the evaporation of the working fluid ((8) → (9)). The enthalpy of the working fluid is converted back into electrical energy in an expander ((9) → (10)). The expanded vapor is then condensed to close the thermodynamic cycle ((10) → (6)).

2.1.2. Working fluid and storage materials

Both the working fluid and the storage materials affect the system performance. The choice of the working fluid is crucial. The focus is laid on the shape of the two-phase area. An anterograde or wet fluid, e.g. water, requires multiple inter-stage cooling, additional thermal energy storage and a wet steam expansion. Hence, matching the charging and discharging cycles is challenging. A dry fluid with a retrograde dew line requires recuperation during charging and discharging. As any additional heat transfer increases entropy, this should be avoided. Consequently, a working fluid with an isentropic dew line is favourable. Another key parameter is a reasonable steam pressure at low temperatures to avoid a high specific volume in the evaporator of the HT-HP and in the condenser of the ORC.

Finally, a suitable combination of the working fluid and the phase change material (PCM) for the latent heat thermal energy storage must be found. Potential PCMs are listed in Table 1. First, the phase change temperature, an inherent property of the PCMs, must be sufficiently lower compared to the critical temperature of the working fluid. Secondly, the phase change enthalpy should be as high as possible, in order to obtain a high energy density of the latent heat storage system.

Table 1: Properties of potential PCMs [Bauer, 2012].

PCM	Phase change temperature [°C]	Phase change enthalpy [J/kg]
KNO_3-$NaNO_2$-$NaNO_3$ (eu)	142	80
KNO_3-$LiNO_3$(eu)	133	170
$LiNO_3$-$NaNO_3$(eu)	194	265

Screening a number of working fluids, Butene in combination with a eutectic mixture of potassium nitrate and lithium nitrate (KNO_3-$LiNO_3$(eu), see Table 1) as PCM is identified as promising. However, it should be noted that Butene is a highly flammable hydrocarbon, so it would impose additional safety considerations to a CHEST system, increasing both capital cost (non-explosive components and instrumentation) and operational costs, due to additional safety features required. While the flammability and the additional safety measure to implement might not be a critical issue for large-scale CHEST system, these were regarded as little feasible for the laboratory-scale prototype. Hence, other refrigerants were considered too. The refrigerant hydrofluoroolefin (HFO) R1233zd(E) was one of these, because of its low flammability and low toxicity (class A1 according to the ISO 817 Refrigerant Classification Scheme). It would also be more suitable for the realization of the laboratory-scale prototype in terms of compatibility with the lubricant for the compressor and the volumetric expander. Additionally, it has a higher critical temperature allowing for a safer operation.

Table 2: Critical properties of potential working fluids [NIST, 2018].

Fluid	Critical temperature [°C]	Critical pressure [bar]
Butene	146.14	40.05
R1233zd(E)	165.6	35.726

Table 2 shows the critical properties of the above-mentioned fluids. Most of the simulations performed with the TRNSYS model and presented in this deliverable are carried out assuming Butene as refrigerant. Parallel simulations with R1233zd(E) are performed for some specific cases to compare the performance of the two fluids.

Other refrigerants are also considered, e.g. R1234ze(Z). A different approach consists of using two different refrigerants, one in the HT-HP and one in the ORC. Studies and investigations on the most appropriate fluids to be used as refrigerant are still ongoing and more information will be presented in future deliverables of the CHESTER project.

2.1.3. EBSILON Professional® Model of the CHEST System with thermal energy integration

Ebsilon Professional is a software that allows for detailed modelling of thermodynamic cycles [STEAG, 2018]. The software considers irreversibilities resulting from the necessary temperature differences for heat transfer, isentropic, mechanic and electric efficiency of machinery as well as pressure losses in the heat exchangers.

Heat source and heat pump evaporator

The ideal coefficient of performance (COP) of a HP is a function of the thermodynamic mean temperature of the heat supply $T_{m,source}$ and of the mean temperature of the heat transfer to the storage system $T_{m,storage}$, as shown by the following equation (1):

$$COP = \frac{T_{m,storage}}{T_{m,storage} - T_{m,source}} \quad (1)$$

In order to maximize the COP, the temperature difference between the heat source and the storage needs to be minimized. As water is used as the heat transfer fluid from the heat source to the evaporator, the thermodynamic mean temperature in the HP evaporator ((1) → (2)) is determined by the pinch-point between the Q-T (transferred heat-fluid temperature) line of the heating water and the isothermal Q-T line of the working fluid (Figure 4). While the inlet temperature of the heating water is a fixed parameter, the water outlet temperature is a function of the water mass flow. Decreasing the water mass flow leads to a lower outlet temperature. As the pinch point has to be maintained, a reduction of the mass flow leads to a lower evaporation pressure, reducing the COP. To obtain a high mean temperature of the heat supply, the water mass flow is controlled to maintain a temperature difference of 5 K between water inlet and water outlet, to minimize the entropy production.

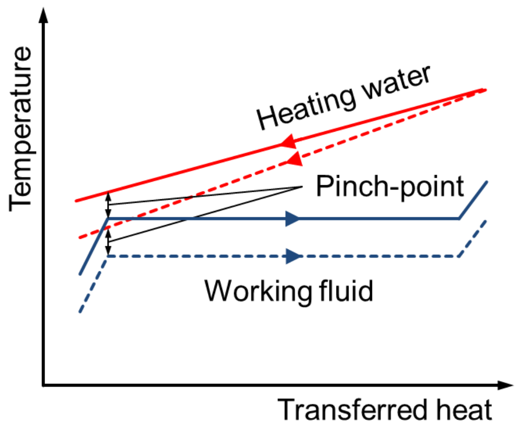

Figure 4: Q-T diagram of HP evaporator.

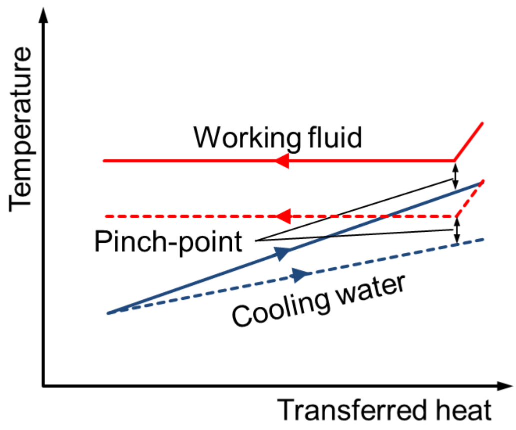

Figure 5: Q-T diagram of ORC condenser.

Electrical power input and mass flow of working fluid

The electrical input power to the compressor is set to 1000 kW, which was initially estimated by DLR to be a suitable value for the integration in a smart DH system. A controller calculates the respective mass flow of the working fluid.

Condensation pressure in latent heat storage

In the latent heat storage, the working fluid is condensed at constant temperature. The temperature difference for the heat transfer between the condensation temperature of the working fluid and the PCM is set to 5 K. Consequently, the condensation pressure is a function of the phase change temperature and the temperature difference in the latent heat storage, according to the equation (2):

$$p_3 = p_{s,pcm}\left(T_{s,pcm} + \Delta T\right) \quad (2)$$

It is assumed that the working fluid exits the latent heat storage as a saturated liquid.

Heat sink and ORC-condenser

The power output of the ORC depends, amongst other parameters, on the pressure in the condenser. Here a low pressure, resulting in a low thermodynamic mean temperature, is favourable. As shown in Figure 5, the minimal condensation pressure is determined by the pinch point between heat capacity fluxes of the working fluid and the cooling water. The inlet temperature is again a fixed parameter, so the outlet temperature is given by the cooling water mass flow. Although a high mass flow results in a low temperature difference and therefore a low condensation pressure, the temperature difference between cooling water inlet and outlet is set to 10 K to allow for a more usable outlet temperature level for DH.

Mass flow of ORC

Analogue to HP cycle, the mass flow in the ORC during discharging is calculated by a controller, in order to obtain an electrical power output from the generator of 1000 kW.

Temperature of cold sensible storage tank

Figure 6 shows the Q-T diagram of the sensible heat storage in an exaggerated sketch to allow for improved perceptibility. In general, the temperature of the sensible heat storage cannot be lower than the condensation temperature of the ORC (T_7). Hence, the temperature of the sensible heat storage is also defined by the temperature of the heat sink. In case of Butene and R1233zd(E), the curvature of the isobars causes the pinch point to be located between T_7 and T_8, so the temperature of the sensible heat storage must be set relatively high (about 60 °C), to allow for operation within the desired range of source and sink temperatures.

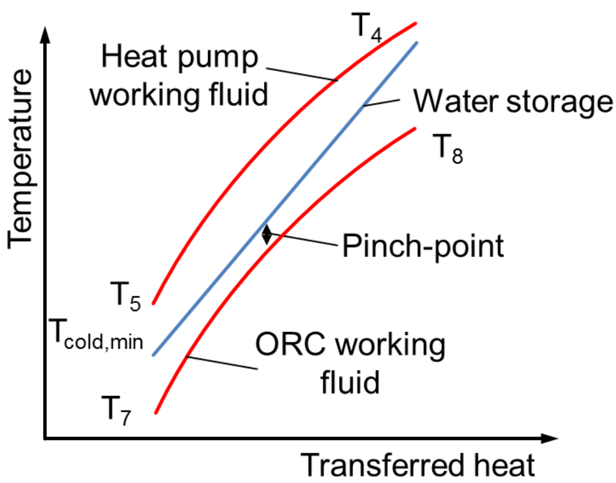

Figure 6: Q-T diagram of the sensible heat storage system

Matching of latent and sensible heat

One of the challenges in the design of a PuTES system is the difference in temperature of the thermal energy transferred between the two half-cycles via the TES system. Figure 7 compares the *T, s*-diagrams of the charging and discharging cycles for the simplest case of identical source and sink temperatures. As the evaporation temperature of the HT-HP is lower than the condensation temperature of the ORC, the HT-HP provides more sensible heat during aftercooling than needed for the preheating in the ORC. This excess heat must be rejected from the system because the temperature of the excess heat is lower than the required temperature for the sensible heat storage. In the model, the excess heat is extracted by an additional heat exchanger placed between the aftercooler and the throttling valve (Figure 2). Depending on the temperature levels, the excess heat can be supplied to a DH network or to a low-temperature TES (LT-TES).

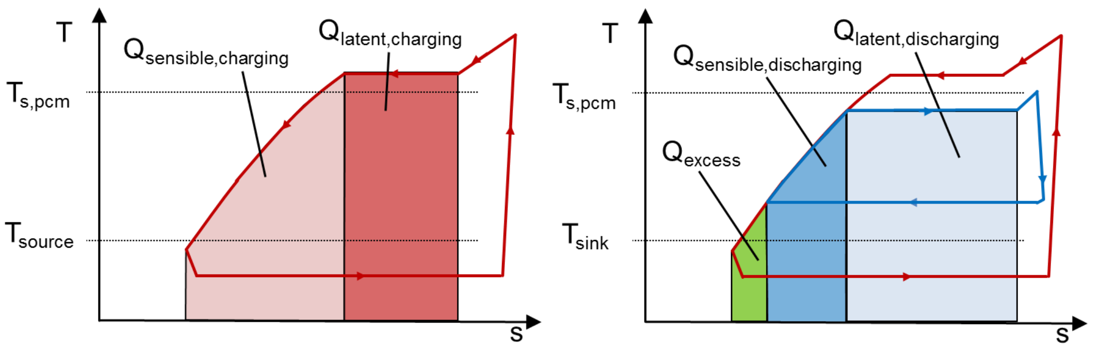

Figure 7: T, s-diagrams of the charging and discharging cycles, highlighting the transferred heat.

Conversely, if the temperature of the heat sink is sufficiently low with respect to the temperature of the heat source, there is a deficit in sensible heat, which can partly be compensated for, by using heat from the latent heat storage. In this case, the additional heat exchanger does not operate.

These constraints apply to all types of PuTES systems, regardless of the technological concept. In case of a subcritical Rankine-cycle-based concept such as CHEST, the ratio of latent and sensible heat should be constant during charging and discharging (3):

$$\left|\frac{Q_{latent}}{Q_{sensible}}\right|_{charging} = \left|\frac{Q_{latent}}{Q_{sensible}}\right|_{discharging} \tag{3}$$

The constant ratio ensures the energy balances as well as the mass balance of the sensible heat storage. If the ratio is not constant, the sensible and the latent part of the HT-TES would be charged and discharged unevenly, resulting in a discharged part of the storage, while the other part still contains energy. As described in 2.2.3 this boundary condition is neglected, and uneven charging and discharging is allowed. The excess thermal energy is transferred back to the heat source.

2.1.4. Inputs and outputs of the Ebsilon model

Table 3 summarizes the parameters used in the Ebsilon model simulation.

Table 3: Inputs parameters used for the simulation in the Ebsilon Professional model.

Parameter	Symbol	Value	Unit
isentropic efficiency compressor	$\eta_{is,compressor}$	0.8	-
isentropic efficiency expander	$\eta_{is,expander}$	0.88	-
Isentropic efficiency pumps	$\eta_{is,pump}$	0.8	-
mechanical efficiency compressor	$\eta_{mech,compressor}$	0.99	-
mechanical efficiency expander	$\eta_{mech,expander}$	0.99	-
mechanical efficiency pumps	$\eta_{mech,pumps}$	0.99	-
mechanical efficiency motors	$\eta_{mech,motors}$	0.99	-
electrical efficiency motor	$\eta_{el,motor}$	0.95	-
electrical efficiency generator	$\eta_{mech,generator}$	0.98	-
pressure loss heat exchangers	Δp_{htx}	0.5	bar
melting temperature of PCM	T_{PCM}	133	°C
heat source temperature	T_{source}	40-100	°C
heat sink temperature	T_{sink}	15-40	°C
temperature difference PCM-working fluid	ΔT_{PCM}	5	K
pinch point evaporator	$\Delta T_{evaporator}$	5	K
pinch point condenser	$\Delta T_{condenser}$	5	K

The outputs of the model of the CHEST system developed in the Ebsilon Professional software are the performance maps reported in Appendix A (Table 24-Table 27).

In the tables, the independent variables are the inlet temperatures of heat source $T_{source,in}$ and of the heat sink $T_{sink,in}$, while the following dependent variables are returned by the model:

- the outlet temperatures of the heat source $T_{source,out}$ and heat sink $T_{sink,out}$;
- the water flow rate at the heat source (m'_{HW}) and at the heat sink (m'_{CW});
- the thermal power Q'_{in} absorbed by the HP evaporator and the thermal power Q'_{out} rejected at the ORC condenser;
- the total electrical power absorbed by the HT-HP and its auxiliaries during charging (P'_{in}), and the net power output from the ORC during discharging (P'_{out});
- the thermal power Q'_{latent} and $Q'_{sensible}$ transferred to the latent heat part and to the sensible heat part of the HT-TES;
- the thermal power Q'_{excess} and the inlet and outlet temperatures of the refrigerant ($T_{excess,in}$ and $T_{excess,out}$ respectively).
- the water mass flow of the sensible heat part of the HT-TES ($m'_{sensible}$).

The apostrophe following flow rates, thermal and electric power quantities denotes that these quantities refer to a constant electrical power of 1 MW absorbed by the compressor of the HT-HP.

2.2. Description of the TRNSYS model

Figure 8 shows a screenshot of the TRNSYS model of the CHEST system integrated into the energy system. The components can be grouped in different blocks, depending on the subsystem they are part of. The following subsections describe the different subsystems in which the model is divided, and each subsection presents the function of the different components. In Figure 8, the purple frame denotes the input files to the TRNSYS model, such as availability and demand of electricity and heat as well as DH temperatures. The orange frame denotes the supply and demand side of the heat load assumed by the model, i.e. a DH network. The green frame denotes the performance maps used to calculate the behaviour of the HT-HP (divided in two parts HP-map and Excess) and ORC. The red frame denotes the HT-HP loop, representing the charging side of the CHEST system. The blue frame denotes the ORC loop, representing the discharging side of the CHEST system. The grey frame denotes the HT-TES.

On one hand, the HT-HP will start operation, when there is an electricity surplus in the grid, i.e. when the electricity generation (assumed as non-dispatchable) is higher than the simultaneous electricity demand. Other requirements for the HT-HP's operation are that: 1) the HT-TES has available storage capacity; 2) there is availability of heat at a temperature equal to or higher than the minimum temperature accepted at the entrance of the evaporator of the HT-HP. Hence, the HT-HP will start and continue operation as long as all the three above-mentioned conditions are met.

On the other hand, the ORC will start and continue operation as long as both the following conditions are met: 1) presence of an electricity deficit in the grid (Section 2.2.1) and 2) availability of heat in both the latent and sensible heat part of the HT-TES.

For a detailed description of the control of the different components in the TRNSYS model, the reader should refer to the relevant subsections below.

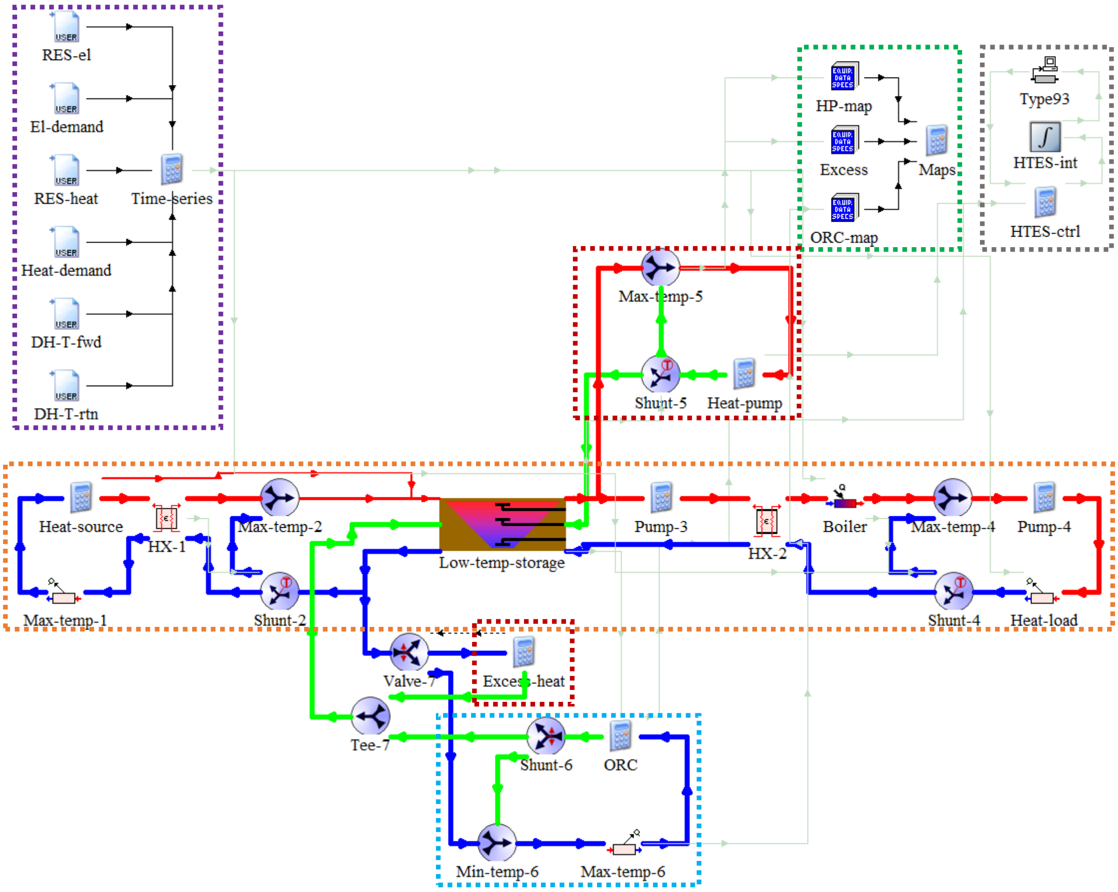

Figure 8: TRNSYS model of the CHEST system integrated into the energy system.

2.2.1. Boundary conditions

Input files

In the top left corner of the scheme (purple frame in Figure 8), data reader components (Type 9) load into TRNSYS the boundary conditions used for the simulation. These include yearly profiles with 1-hour timestep of the following quantities:

- *RES-el*: RES electricity production [MW];
- *El-demand*: Electricity demand [MW];
- *RES-heat*: RES heat production [MW], which may be solar thermal output or waste heat from industrial processes;
- *Heat-demand*: Heat demand [MW] from the load, e.g. a DH network or an industrial process;
- *DH-T-fwd*: Supply temperature of the heat demand [°C];
- *DH-T-rtn*: Return temperature of the heat demand [°C].

Different input files can be given as input to the data readers. To avoid errors during the simulation, each file should contain a single data series of 8,760 + 1 data points, one for each hour of the year and one as starting condition for the simulation.

Depending on the availability of the data, the RES electricity production profile and the electricity demand profile are likely to refer to different geographical scale. For example, the RES electricity production may be the electricity output of a local PV field and/or wind farm, while the electricity demand may refer to a regional or national level. Therefore, both profiles can be made comparable by scaling them in the equation block *Time-series* through scaling factors, defined in the Control Cards tab. In the same equation block the electricity surplus ($El_{surplus}$) and electricity deficit ($El_{deficit}$), i.e. the positive differences between the RES electricity production and the electricity demand, is calculated.

Control cards: general constants

In the control cards of the TRNSYS model the global constants which are used as boundary conditions for the simulation are specified. These are listed in Table 4. The unit of measure of each parameter is denoted in the parameter name as suffix.

Table 4: General constants listed in the Control cards of the TRNSYS model.

Variable name	Description
CHEST_ON	Parameter determining if the CHEST system is on (= 1) or off (= 0)
TS_RES_el_factor	Scaling factor for RES electricity production
TS_el_demand_factor	Scaling factor for electricity demand
TS_RES_heat_factor	Scaling factor for RES heat production
TS_heatdemand_factor	Scaling factor for RES heat demand
HP_el_capacity_MW	Nominal capacity of the installed HT-HP in the CHEST system
ORC_el_capacity_MW	Nominal capacity of the installed ORC the CHEST system
Latent_capacity_MWh	Energy content of the latent heat part of the HT-TES
Sensible_cap_MWh	Energy content of the sensible heat part of the HT-TES
PTES_volume_m3	Volume of the LT-TES
PTES_height_m	Height of the LT-TES
PTES_segments	Number of isothermal layers the LT-TES is divided in

PTES_T_in_C_max	Maximum temperature allowed at the inlet of the LT-TES
RES_heat_T_in_C_max	Maximum temperature allowed at the inlet of RES heat source (Section 2.2.2)
RES_heat_T_out_C	Expected outlet temperature from the RES heat source (Section 2.2.2)
Pump3_T_C_max	Minimum temperature required for the operation of the pump *Pump-3* (Section 2.2.2)
Pump3_T_C_min	Temperature required for the full-load operation of the pump *Pump-3* (Section 2.2.2)
HP_T_in_C_min	Minimum temperature allowed at the inlet of the evaporator of the HT-HP (minimum $T_{source,in}$ in Table 5)
HP_T_in_C_max	Maximum temperature allowed at the inlet of the evaporator of the HT-HP (minimum $T_{source,in}$ in Table 5)
ORC_T_in_C_min	Minimum temperature allowed at the inlet of the condenser of the ORC (minimum $T_{sink,in}$ in Table 6)
ORC_T_in_C_max	Maximum temperature allowed at the inlet of the condenser of the ORC (minimum $T_{sink,in}$ in Table 6)
Excess_DT_K	Temperature difference between the two sides of the heat exchanger for excess heat (Section 2.2.5)
cp_water	Specific heat of water
rho_water	Density of water

2.2.2. Heat supply and demand

The components horizontally aligned in the middle of the scheme (orange frame in Figure 8) make up the supply and demand side of the heat load considered in the case study, such as a DH network.

RES-heat supply loop

On the most left-hand side of this block, there are the components which make up the RES-heat supply loop, which consists of the equation block *Heat source*, the heat exchanger *HX-1* (Type 91) and the auxiliary cooling device *Max-temp-1* (Type 92).

The flow rate in the loop is calculated in the equation block *Heat-source*, based on the available thermal power *RES-heat*, defined by the boundary condition input file (Section 2.2.1) and the temperature difference across the RES heat source. The temperature difference is the difference between the expected outlet temperature from the RES heat source and the actual temperature at the inlet of the equation block, i.e. at the outlet of the auxiliary cooling device. In this way the outlet temperature from the heat source is always the one expected according to the boundary conditions.

The auxiliary cooling device *Max-temp-1* sets an upper limit to the temperature entering the heat source. This assures that the available thermal power from the RES heat source can be withdrawn. The use of the auxiliary cooling device is necessary when the low-temperature storage is fully charged, but heat must still be taken away from the RES heat source. For example, if the RES heat source is a waste incineration plant or a solar collector field, the heat production cannot be stopped, hence heat must be dissipated to the environment.

The RES-heat supply loop is hydraulically separated from the rest of the system by the heat exchanger *HX-1* (Type 91). In the real-world operation, the hydraulic separation allows the two interfacing loops to operate with different fluids (or different qualities of the same fluid) and different pressure levels. Additionally, the loop separation provides more flexibility and protection, as it avoids that failures in one loop directly affect the other.

Loops of the Low-Temperature Thermal Energy Storage (LT-TES)

In the central part of the block there are the charging and discharging loops integrating the LT-TES in the overall system. The thermal stratified LT-TES is modelled through the non-standard component Type 342, which simulates the behaviour of a large-scale water pit TES. Type 342 considers many aspects of large-scale TES whose description is out of the scope of this deliverable. For a detailed presentation of Type 342 the reader should refer to the official user manual [Mazzarella, 1992].

Besides the LT-TES, the charging loop of the LT-TES (on the left-hand side of the LT-TES) includes the heat exchanger *HX-1*, the converging tee junction *Max-temp-2* (Type 11h) and the tempering valve *Shunt-2* (Type 11b).

The flow rate in the loop is the same as in the RES-heat supply loop, which guarantees the same heat capacity rate at the two sides of the heat exchanger *HX-1*, thus optimizing its performance. The flow circulating in the loop is drawn from the bottom of the LT-TES, is heated up by the heat exchanger *HX-1* and is supplied back to the LT-TES in its upper part. The inlet to the LT-TES has a variable position, so that the flow is injected in the LT-TES layer with the closer temperature to improve the thermal stratification.

The converging tee junction *Max-temp-2* and the tempering valve *Shunt-2* are used to mix the flow at the exit of the heat exchanger *HX-1* with part of the flow drawn from the bottom of the LT-TES, therefore, limiting the temperature entering LT-TES to a fixed upper value (e.g. 90 °C). For example, if the LT-TES is water pit TES of the same type as those built in Denmark for seasonal storage, there are limits on the temperature that the liner material can withstand. In case of other types of LT-TES, other temperature constraints may exist.

The discharging side of the LT-TES (on the right-hand side of the LT-TES) includes the equation block *Pump-3*, the heat exchanger *HX-2* (Type 91) and the LT-TES.

Fluid at high temperature is drawn from the top of the LT-TES, pumped through the heat exchanger *HX-2* and then back into LT-TES. The inlet to the LT-TES has a variable position, consequently the return flow is injected in the LT-TES layer with the closer temperature.

The equation block *Pump-3* determines the flow $\dot{m}_{P3}$ circulating in the loop according to the following relation (4):

$$\dot{m}_{P3} = \dot{m}_{P4} \cdot \left[\max\left(0, \min\left(1, \left(T_{P3,in} - T_{P3,min}\right)/\left(T_{P3,max} - T_{P3,min}\right)\right)\right)\right] \qquad (4)$$

where $\dot{m}_{P4}$ is the flow rate of the pump *Pump-4*;
$T_{P3,in}$ is the temperature at the inlet of *Pump-3*, i.e. the temperature from the top layer of the LT-TES;
$T_{P3,min}$ is the minimum temperature required for the operation of the pump *Pump-3*;
$T_{P3,max}$ is the temperature required for the full-load operation of the pump *Pump-3*;
The term in square brackets is always between 0 and 1, hence the flow $\dot{m}_{P3}$ can vary between 0 and $\dot{m}_{P4}$. The dependence of the factor on the pump inlet temperature $T_{in,P3}$ implies that the pump *Pump-3* will not operate, if the

temperature $T_{in,P3}$ is lower than or equal to $T_{P3,min}$; it will operate at full capacity, if the temperature $T_{in,P3}$ is at least equal to $T_{P3,max}$; for intermediate values of the temperature $T_{in,P3}$, the flow rate $\dot{m}_{P3}$ will be linearly proportional to the temperature between the two above-mentioned temperatures.

The mathematical definition of the flow $\dot{m}_{P3}$ implies that the LT-TES is used to supply heat to the heat load (heat demand loop), as long as the temperature in the top layer of the LT-TES is sufficiently high ($> T_{P3,min}$). When the temperature falls below this threshold, the LT-TES can only be used to feed the HT-HP. This constraint ensures higher inlet temperatures for the evaporator of the HT-HP favouring its performance.

As for the RES-heat supply loop, the presence of a heat exchanger is required to hydraulically separate the LT-TES and the heat demand loop. In fact, both water quality and pressure are likely to be different between the LT-TES and the heat load (e.g. DH network).

Heat demand loop

On the right-hand side of the heat exchanger *HX-2* there is the heat demand loop, e.g. a DH network, which includes the heat exchanger *HX-2*, the auxiliary heater component *Boiler* (Type 6), the equation block *Pump-4*, the auxiliary cooling device *Heat-load* (Type 92), the converging tee junction *Max-temp-4* (Type 11h) and the tempering valve *Shunt-4* (Type 11b).

The pump *Pump-4* drives the flow in the loop, directly calculated from the heat demand profile, supply and return temperature profiles of the load defined by the boundary condition input files (Section 2.2.1).

The heat demand loop has as energy inputs the heat exchanger *HX-2* and the *Boiler.* The boiler is assumed to use fossil fuel as energy source, hence its operation should be minimized both for economic and environmental reasons. The boiler will only turn on, if its inlet temperature is lower than the supply temperature expected by the heat load (*DH-T-fwd*). On the other hand, if the temperature from the boiler (due to the temperature from *HX-2*) is higher than the required one, a converging tee junction *Tee-4* and a tempering valve *Shunt-4* are used to mix the flow at the exit of the boiler with part of the return flow from the heat load. The set point temperature of the tempering valve is therefore the supply temperature to the heat load (*DH-T-fwd*).

The *Heat-load*, represented by the auxiliary cooling device, removes the necessary thermal power from the supplied flow lowering its temperature to the return temperature inputted as a boundary condition (*DH-T-rtn*).

The system described so far does not present unusual characteristics. Indeed, it resembles closely a DH system equipped with a large solar collector field and a seasonal storage. Hence, the results obtained by running this part of the TRNSYS model (without activating the components of the CHEST system) could be used as a benchmark for an alternative case, where the CHEST system is implemented on top of this conventional system. The following sections describe the different blocks which build up the CHEST system.

2.2.3. Performance maps for CHEST components

The three components (Type 42) in the top-right corner of the model (green frame in Figure 8) perform linear interpolation over a set of data depending on one (or possibly more) dependent variable. The three components contain the performance maps used to calculate the behaviour of the HT-HP (divided in two parts *HP-map* and *Excess*) and ORC. The performance maps used in the TRNSYS model are shown in Table 5 and Table 6 for Butene and in Table 7 and Table 8 for R1233zd(E).

The listed data are taken from Table 24-Table 27(in Appendix A). The apostrophe following flow rates, thermal and electric power quantities denotes that these quantities refer to a specific nominal power of the machine. For the HT-HP (Table 5), the specific nominal power referred to is 1 MW electrical power absorbed by the compressor. For the ORC (Table 6), the table refers to 1 MW power output from the expander.

Table 5: Performance map used in the TRNSYS model for the HT-HP, using Butene as refrigerant.

$T_{source,in}$ [°C]	$T_{source,out}$ [°C]	Q'_{in} [kW]	P'_{in} [kW]	Q'_{excess} [kW]	$T_{excess,in}$ [°C]	$T_{excess,out}$ [°C]	Q'_{latent} [kW]	$Q'_{sensible}$ [kW]
40	35	3051	1039	889	70	27	1339	1799
50	45	3396	1044	781	70	37	1525	2070
60	55	3798	1049	621	70	48	1762	2401
70	65	4279	1056	388	70	58	2066	2817
80	75	4872	1064	46	70	69	2468	3356
90	85	6146	1081	0	70	70	3043	4119
100	95	8071	1107	0	70	70	3881	5230

Table 6: Performance map used in the TRNSYS model for the ORC, using Butene as refrigerant.

$T_{sink,in}$ [°C]	$T_{sink,out}$ [°C]	Q'_{latent} [kW]	$Q'_{sensible}$ [kW]	P'_{out} [kW]	Q'_{out} [kW]
15	25	2568	3491	913	5117
20	30	2761	3577	907	5402
30	40	3226	3764	895	6063
40	50	3829	3968	880	6884
50	60	4643	4192	862	7937

Table 7: Performance map used in the TRNSYS model for the HT-HP, using R1233zd(E) as refrigerant.

$T_{source,in}$ [°C]	$T_{source,out}$ [°C]	Q'_{in} [kW]	P'_{in} [kW]	Q'_{excess} [kW]	$T_{excess,in}$ [°C]	$T_{excess,out}$ [°C]	Q'_{latent} [kW]	$Q'_{sensible}$ [kW]
40	35	3007	1039	992	75	25	1591	1399
50	45	3363	1043	895	75	36	1834	1614
60	55	3776	1049	754	75	47	2135	1873
70	65	4272	1056	553	75	57	2517	2193
80	75	4887	1064	265	75	68	3016	2605
90	85	5859	1077	0	75	75	3704	3166
100	95	7678	1101	0	75	75	4721	3991

Table 8: Performance map used in the TRNSYS model for the ORC, using R1233zd(E) as refrigerant.

$T_{sink,in}$ [°C]	$T_{sink,out}$ [°C]	Q'_{latent} [kW]	$Q'_{sensible}$ [kW]	P'_{out} [kW]	Q'_{out} [kW]
15	25	2897	3246	947	5170
20	30	3112	3307	944	5448
30	40	3626	3438	936	6098
40	50	4290	3583	927	6915
50	60	5178	3741	916	7970

The nomenclature used in Table 5 and Table 6, which is in agreement with the one used in Figure 2, is as follows:

- $T_{source,in}$ is the water temperature at the inlet of the evaporator of the HT-HP. This temperature is the only independent variable in the performance map of the HT-HP;
- $T_{source,out}$ is the water temperature at the outlet of the evaporator of the HT-HP;
- Q'_{in} is the thermal power exchanged at the evaporator of the HT-HP;
- P'_{in} is the power absorbed by the different electric components of the HT-HP. The main contribution comes from the compressor (constant nominal power of 1 MW), while the rest is consumed by circulation pumps;
- Q'_{excess} is the thermal power that is removed from the refrigerant of the HT-HP after this exits the sensible part of the HT-TES and before it passes through the throttling valve (Figure 2);
- $T_{excess,in}$ and $T_{excess,out}$ are respectively the temperatures of the refrigerant at the inlet and at the outlet of the cooling circuit located after the sensible part of the HT-TES (Figure 2);
- Q'_{latent} is the thermal power exchanged with the latent heat part of the HT-TES. In Table 5 this thermal power is that transferred from the hot side of the HT-HP to the HT-TES, while in Table 6 it is that transferred from the HT-TES to the hot side of the ORC;
- $Q'_{sensible}$ is the thermal power exchanged with the sensible heat part of the HT-TES. In Table 5 this thermal power is transferred from the hot side of the HT-HP to the HT-TES, while in Table 6 it is transferred from the HT-TES to the hot side of the ORC;
- $T_{sink,in}$ is the water temperature at the inlet of the condenser of the ORC. This temperature is the only independent variable in the performance map of the ORC;
- $T_{sink,out}$ is the water temperature at the outlet of the condenser of the ORC;
- Q'_{out} is the thermal power exchanged at the condenser of the ORC;
- P'_{out} is the net power output from the ORC, i.e. the difference between the power output of the expander and the power absorbed by the other components of the ORC, such as circulation pumps.

It should be noted that, depending on the temperature levels used for the operation of the HT-HP and the ORC, charging and discharging may occur at different ratio between the thermal power exchanged with the sensible heat part of the TES and the one exchanged with the latent heat part. In most cases non-uniform charging/discharging of the HT-TES is to be avoided to have both the latent and the sensible heat part of the HT-TES charged at a similar level. In the TRNSYS model this is achieved by removing possible excess heat remaining in either part of the HT-TES and adding it to the Heat-source (Section 2.2.6).

When the power absorbed by the compressor is different from the nominal power of 1 MW, it is assumed that the variables such as flow rates, electric and thermal powers are linearly proportional with the compressor power.

2.2.4. High Temperature Heat Pump (HT-HP)

The components above the LT-TES (red frame in Figure 8) make up the HT-HP loop, representing the charging side of the CHEST system. This loop includes the equation block *Heat-pump*, the converging tee junction (*Max-temp-5*, Type 11h) and a tempering valve (*Shunt-5*, Type 11b).

The outputs of the equation block *Heat-pump*, i.e. the performance of the HT-HP, are determined by the performance map of the HT-HP (components *HP-map* and *Maps*; see also Section 2.2.3).

A condition which is necessary for the HT-HP's operation is the presence of an electricity surplus in the grid (Section 2.2.1). Other requirements which must be fulfilled in order for the HT-HP to operate are that: 1) the HT-TES has available storage capacity in both its latent and sensible heat part and 2) there is availability of heat at a temperature equal to or higher than the minimum temperature accepted at the entrance of the evaporator of the HT-HP.

On the one hand, the HT-HP loop draws fluid at high temperature from the top of the LT-TES and supplies it to the evaporator of the HT-HP. As the performance map for the operation of the HT-HP is defined over a limited range of temperatures, it is important that the fluid temperature at the inlet of the evaporator of the HT-HP is lower than the maximum temperature defined in the performance map. To ensure this condition, the tee junction *Max-temp-5* and the tempering valve *Shunt-5* are used to temper down the flow from the LT-TES, by mixing it with part of the flow at the outlet of the evaporator of the HT-HP. The set point temperature of the tempering valve is, therefore, the maximum evaporator inlet temperature defined in the performance map of the HT-HP ($T_{source,in}$ in Section 2.2.3).

On the other hand, if the temperature at the top of the LT-TES is lower than the minimum temperature for the evaporator inlet defined in the performance map, then the flow in the loop will be zero and the HT-HP will not operate.

The water flow entering the evaporator of the HT-HP is here cooled down and injected back into the LT-TES. The inlet to the LT-TES has a variable position, hence the return flow from the HT-HP is injected into the LT-TES layer with the closer temperature. Furthermore, the condenser side of the HT-HP, i.e. the heat sink of the HP cycle, interfaces with the HT-TES (Section 2.2.6).

The flow rate $\dot{m}_{HW}$ circulating on the water side of the evaporator of the HT-HP is calculated in the equation block *Heat-pump* as follows (5):

$$\dot{m}_{HW} = {Q_{in}}/{c_p \cdot (T_{source,in} - T_{source,out})} \tag{5}$$

where $T_{source,in}$ is the actual temperature at the inlet of the evaporator of the HT-HP;
$T_{source,out}$ is the temperature at the outlet of the evaporator of the HT-HP, calculated from the performance map (Table 5), as function of the actual temperature at the inlet of the evaporator $T_{source,in}$;
c_p is the specific heat of water;
Q_{in} is the actual thermal power exchanged at the evaporator of the HT-HP, calculated as (6):

$$Q_{in} = Q'_{in} \cdot W_{p,HP} \cdot PLF_{HP} \tag{6}$$

where Q'_{in} is the thermal power exchanged at the evaporator of a HT-HP with nominal capacity of 1 MW, calculated from the performance map (Table 5), as function of the actual temperature at the inlet of the evaporator $T_{source,in}$;
$W_{p,HP}$ is the nominal capacity of the HT-HP (in MW);
PLF_{HP} is the dimensionless partial load factor of the HT-HP, which denotes the fraction of full-load capacity that the HT-HP operates at.

The partial load factor PLF_{HP} is bounded between 0 and 1, and within this range it is given by (7):

$$PLF_{HP} = \min\left(PLF_{surplus}, PLF_{temp}, PLF_{latent,HP}, PLF_{sensible,HP}\right) \qquad (7)$$

where $PLF_{surplus}$ is the partial load factor determined by the availability of excess RES electricity. It implies that the total power absorbed by the HT-HP is at most equal to the excess RES electricity available. Hence, the factor is given by the ratio (8):

$$PLF_{surplus} = {El_{surplus}} \Big/ \left(P'_{in} \cdot W_{p,HP}\right) \qquad (8)$$

where $El_{surplus}$ (in MW) is the positive difference between the RES electricity production and the electricity demand (Section 2.2.1);
P'_{in} is the total power absorbed by a HT-HP with a nominal capacity of 1 MW, calculated from the performance map (Table 5), as function of the actual temperature at the inlet of the evaporator $T_{source,in}$;
$W_{p,HP}$ is the nominal capacity of the HT-HP (in MW).

PLF_{temp} is the partial load factor determined by the temperature at the inlet of the evaporator of the HT-HP and is given by (9):

$$PLF_{temp} = 0.5 \cdot \left(T_{source,in} - \min\left(T_{source,in}\right)\right) \qquad (9)$$

where $T_{source,in}$ is the actual temperature at the inlet of the evaporator of the HT-HP;
$\min\left(T_{source,in}\right)$ is minimum water temperature allowed at the inlet of the evaporator (40 °C in Table 5).

The definition of PLF_{temp} implies that the HT-HP will not operate, if the temperature at the inlet of the evaporator $T_{source,in}$ is lower than or equal to the minimum temperature of the temperature range of the performance map of the HT-HP; it will operate at full capacity, if the temperature $T_{source,in}$ is at least 2 °C higher than the temperature min($T_{source,in}$); for intermediate values of the temperature $T_{source,in}$, the partial load factor will be linearly proportional to the temperature. This ramp control condition is inserted to avoid unstable on/off operation, which would compromise the convergence of the TRNSYS model.

$PLF_{latent,HP}$ and $PLF_{sensible,HP}$ are the partial load factor respectively determined by the state of charge of the latent heat part and of the sensible heat part of the HT-TES. They are the ratios between the heat, which can still be fed into the latent/sensible heat part of the HT-TES, and the heat that would be transferred to it by the HT-HP in a simulation timestep. These factors assure that the HT-HP operation is limited during each timestep, not delivering to the HT-TES more heat than the one that can still be stored.

Because of the overall partial load factor PLF_{HP} is defined as the minimum of the above-described partial load factors, the most stringent condition determines the operation of the HT-HP.

It should be noted that, according to the way Q_{in} is determined (see equation above), the model assumes a perfect linearity between the electric power absorbed by the HT-HP and the thermal power at the evaporator. This is a simplification which is introduced in the model, due to the absence of more detailed information on the behaviour of the CHEST components in partial load conditions. In the real world, partial load operation in unlikely to show such a linearity. Hence, future analyses within the CHESTER project will investigate and clarify how the different components work in partial load conditions.

The HT-HP loop includes also the equation block *Excess-heat* (red frame, below the LT-TES). The reason the *Excess-heat* block appears separated from the other components of the HT-HP loop is that, due to simulation reasons, this must share the hydraulic connection to the LT-TES with the ORC loop. This can be done because the ORC and the HT-HP will never operate simultaneously, so the controlled flow diverter *Valve-7* (Type 11f) and the converging tee junction *Tee-7* (Type 11h) will allow flow through either leg of the tee junction. This excess heat represents the thermal power that must be removed from the refrigerant of the HT-HP after this exits the sensible part of the HT-TES and before it passes through the throttling valve (see Q_{excess} in Figure 2 and in Section 2.2.3). Depending on the temperature levels of the excess heat and of the LT-TES, part of the excess heat may be exploited and stored in the LT-TES.

The equation block *Excess-heat* takes input from the performance map *Excess* to evaluate the amount and the temperature level of excess heat available depending on the operating conditions (Table 5). The water flow rate $\dot{m}_{excess}$, which can extract useful heat from the cooling circuit of the excess heat, is calculated in the equation block *Excess-heat* as follows (10):

$$\dot{m}_{excess} = {Q_{excess,stored}} \Big/ {c_p \cdot (T_{w,out} - T_{w,in})} \tag{10}$$

where $Q_{excess,stored}$ is the excess heat which can be stored in the LT-TES because it is available at a sufficiently high temperature;
c_p is the specific heat of water;
$T_{w,out}$ is the water outlet temperature from the cooling circuit of excess heat. Assuming a temperature difference $\Delta T_{HX,excess}$ between the two sides of the heat exchanger, $T_{w,out}$ is assumed equal to $T_{excess,in}$ - $\Delta T_{HX,excess}$ (Table 6);
$T_{w,in}$ is the water inlet temperature to the cooling circuit of excess heat, which corresponds to the temperature at the bottom of the LT-TES.

The amount of useful excess heat $Q_{excess,stored}$ which can be stored in the LT-TES is given by (11):

$$Q_{excess,stored} = Q_{excess} \cdot \left(\left(T_{excess,in} - T_{excess,mid}\right) \Big/ \left(T_{excess,in} - T_{excess,out}\right) \right) \tag{11}$$

where $T_{excess,in}$ and $T_{excess,out}$ are respectively the temperatures of the refrigerant at the inlet and at the outlet of the cooling circuit of excess heat (Table 6);

$T_{excess,mid}$ is calculated as the maximum value between the water inlet temperature to the cooling circuit $T_{w,in}$ increased by $\Delta T_{HX,excess}$ and the temperature of the refrigerant at the outlet of the cooling circuit $T_{excess,out}$.

Q_{excess} is the total excess heat available, calculated as (12):

$$Q_{excess} = Q'_{excess} \cdot W_{p,HP} \cdot PLF_{HP} \tag{12}$$

where all parameters have been previously defined.

2.2.5. Organic Rankine Cycle (ORC)

The components below the LT-TES (blue frame in Figure 8) make up the ORC loop, representing the discharging side of the CHEST system. This loop includes the equation block *ORC*, the converging tee junction *Min-temp-6* (Type 11h), the controlled flow diverter *Shunt-6* (Type 11f) and the auxiliary cooling device *Max-temp-6* (Type 92).

The outputs of the equation block *ORC*, i.e. the performance of the ORC, are determined by the performance map of the ORC (components *ORC-map* and *Maps*; see also Section 2.2.3).

The conditions which must be both met in order for the ORC to operate are: 1) the presence of electricity deficit in the grid (Section 2.2.1) and the availability of heat in both the latent and sensible heat part of the HT-TES.

The ORC loop draws fluid at low temperature from the bottom of the LT-TES and supplies it to the condenser of the ORC. As the performance map for the operation of the ORC is defined over a limited range of temperatures, it is important that the fluid temperature at the inlet of the condenser of the ORC is higher than the minimum temperature and lower than the maximum temperature defined in the performance map ($T_{sink,in}$). The first condition is ensured by the tee junction *Min-temp-6* and the flow diverter *Shunt-6*, which are used to recirculate part of the warmer flow at the outlet of the condenser of the ORC and mix it with the colder flow from the LT-TES. The reason a controlled flow diverter is used instead of a tempering valve is that the tempering valve Type 11b in TRNSYS only works for setting an upper limit to a flow temperature, but not a lower limit. However, the working principle of the two components is the same. Besides, if the temperature at the exit of tee junction *Min-temp-6* is higher than the maximum temperature allowed to enter the condenser of the ORC, then the auxiliary cooling device *Max-temp-6* removes the necessary thermal power from the supplied flow to meet the temperature constraint.

The water flow entering the condenser of the ORC is here heated up and injected back into the LT-TES. The inlet to the LT-TES has a variable position, so that the return flow is injected into the LT-TES layer with the closer temperature. Likewise, the evaporator side of the ORC, i.e. the heat source of the ORC cycle, interfaces with the HT-TES.

The flow rate $\dot{m}_{CW}$ circulating in the loop on the water side of the condenser of the ORC is calculated in the equation block *ORC* as follows (13):

$$\dot{m}_{CW} = {Q_{out}}\Big/{c_p \cdot \left(T_{sink,out} - T_{sink,in}\right)} \tag{13}$$

where $T_{sink,in}$ is the actual temperature at the inlet of the condenser of the ORC;
$T_{sink,out}$ is the temperature at the outlet of the condenser of the ORC, calculated from the performance map (Table 6), as function of the actual temperature at the inlet of the condenser $T_{sink,in}$;
c_p is the specific heat of water;
Q_{out} is the actual thermal power exchanged at the condenser of the ORC, calculated as (14):

$$Q_{out} = Q'_{out} \cdot W_{p,ORC} \cdot PLF_{ORC} \tag{14}$$

where Q'_{out} is the thermal power exchanged at condenser of an ORC with nominal capacity of 1 MW, calculated from the performance map (Table 6), as function of the actual temperature at the inlet of the condenser $T_{sink,in}$;
$W_{p,ORC}$ is the nominal capacity of the ORC (in MW);
PLF_{ORC} is the dimensionless partial load factor of the ORC, which denotes the fraction of full-load capacity that the ORC operates at.

The partial load factor PLF_{ORC} is bounded between 0 and 1, and within this range it is given by (15):

$$PLF_{ORC} = \min\left(PLF_{deficit}, PLF_{latent,ORC}, PLF_{sensible,ORC}\right) \tag{15}$$

where $PLF_{deficit}$ is the partial load factor determined by the uncovered electricity demand. It implies that the net power output of the ORC is at most equal to the uncovered electricity demand. The factor is hence given by the ratio (16):

$$PLF_{deficit} = {El_{deficit}}\Big/{\left(P'_{out} \cdot W_{p,ORC}\right)} \tag{16}$$

where $El_{deficit}$ (in MW) is the positive difference between the electricity demand and the RES electricity production (Section 2.2.1);
P'_{out} is the net power output (in MW) of an ORC with nominal capacity of 1 MW;
$W_{p,ORC}$ is the corresponding nominal power of the ORC (in MW).
$PLF_{latent,ORC}$ and $PLF_{sensible,ORC}$ are the partial load factor respectively determined by the state of charge of the latent heat part and of the sensible heat part of the HT-TES. They are the ratio between the heat content of the latent/sensible heat part of the HT-TES and the heat that would be drawn by the ORC in a simulation timestep. These factors assure that the ORC operation is limited during in each timestep, so not to draw from the HT-TES more heat than that which is stored.

Due to the overall partial load factor PLF_{ORC} defined as the minimum of the above-described partial load factors, the most stringent condition determines the operation of the ORC.

As mentioned in Section 2.2.4 regarding the HT-HP, the correlations used by the model in case of partial load entail linearity in the performance of the ORC with respect to the full-load conditions. This may not be necessarily true in the real world and future investigations should clarify the actual performance in case of partial load.

2.2.6. High-Temperature Thermal Energy Storage (HT-TES)

In the top-right corner of the model (grey frame in Figure 8) there are the components simulating the HT-TES, which consists of the integrator *HTES-int* (Type 24), the equation block *HTES-ctrl* and the input value recall block (Type93). In the real world, the HT-TES of the CHEST system will consist of a PCM storage for the latent heat part, and a pressurized hot water tank for the sensible heat part. Hence, the integrator has two inputs, one being the thermal power exchanged with the latent heat part of the HT-TES and the other one being the thermal power exchanged with the sensible heat part. The reason for using the integrator is that in the model the focus is mainly in the state of charge of the HT-TES, which is perfectly interpreted by the integrator. Additionally, the use of the integrator is compatible with the performance maps available for the operation of the HT-HP and of the ORC, where the interaction between these components and the HT-TES is expressed in terms of transferred power and not of temperature levels. It is noted that thermal losses from the two TESs are not included in the model. A more detailed model of the CHEST system is planned to be developed within the CHESTER project: at that stage thermal losses from the HT-TES will also be considered.

The thermal powers, which are passed as inputs to the integrator, are the net thermal power exchanged with the two parts (latent and sensible) of the HT-TES. These are calculated in the equation block *HTES-ctrl*. For the latent heat part of the storage the net thermal power exchanged $Q_{net,latent}$ (in MW) is given by (17):

$$Q_{net,latent} = Q_{HP,latent} - Q_{ORC,latent} - Q_{latent,reset} \tag{17}$$

where $Q_{HP,latent}$ (in MW) is the thermal power transferred from the condenser of the HT-HP to the latent heat part of the HT-TES, calculated based on the performance maps and actual operating conditions (Section 2.2.3);

$Q_{ORC,latent}$ (in MW) is the thermal power transferred from the latent heat part of the HT-TES to the evaporator of the ORC, calculated based on the performance maps and actual operating conditions;

$Q_{latent,reset}$ (in MW) is the thermal power dissipated from the latent heat part of the HT-TES in case of uneven state of the charge between the two parts of the HT-TES (see below).

The mathematical definition of net thermal power exchanged with the sensible heat part of the HT-TES $Q_{net,sensible}$ is given by the same expression as of $Q_{net,latent}$, simply replacing the subscript *latent* with the subscript *sensible*.

Depending on the operating conditions of the HT-HP and the ORC, charging and discharging may occur at different ratio between the thermal power exchanged with the sensible heat part of the HT-TES and that exchanged with the latent heat part. In most cases non-uniform charging/discharging of the HT-TES is unwanted, because, for example, if either part of the HT-TES is fully charged, the HT-HP will not be able to run, although the other part of the HT-TES may be able to store additional heat. Furthermore, a fully discharged part of the HT-TES would prevent the ORC operation, regardless of the amount of heat stored in the other part. In the

TRNSYS model a fairly uniform state of charge of the HT-TES is achieved by removing possible excess heat in either part of the HT-TES, that cannot be used in the ORC, and adding it to the Heat-source (Section 2.2.6). However, in WP3, different system configurations are being analysed and evaluated to prevent this unwanted behaviour.

In the model, the monitoring of the state of charge of the two parts of the HT-TES is carried out in equation block *HTES-ctrl*. The ratios R_{latent} and $R_{sensible}$ between the state of charge of the latent heat part and of the sensible heat part are calculated as (18):

$$R_{latent} = (R_{sensible})^{-1} = {}^{E_{latent}}/_{E_{sensible}} \tag{18}$$

where E_{latent} and $E_{sensible}$ are the amount of heat (in MWh) stored respectively in the latent heat part and in the sensible heat part of the HT-TES.

If the amount of heat stored in the latent heat part of the HT-TES is significantly higher than in the sensible heat part, the thermal power $Q_{latent,cleanup}$ (in MW) which is dissipated during one timestep from the latent heat part of the HT-TES is given by (19):

$$Q_{latent,cleanup} = [\max(0, \min(1, R_{latent} - 2))] \cdot {}^{E_{latent}}/_{10\ \mathrm{h}} \tag{19}$$

where the all parameters have been previously defined.

Conversely, if the amount of heat is higher in the sensible heat part of the HT-TES, the thermal power $Q_{sensible,cleanup}$ is dissipated. Its mathematical definition is given by the same expression as of $Q_{latent,cleanup}$, simply replacing the subscript *latent* with the subscript *sensible*.

The mathematical definition of $Q_{latent,cleanup}$ and $Q_{sensible,cleanup}$ implies that, if the energy content of either part of the HT-TES is no higher than twice the energy content of the other part, the thermal power to be dissipated from the HT-TES is zero. On the contrary, if the energy contents of the two parts of the HT-TES differ more than twice, the term in square bracket will be larger than 0, and lower than or equal to 1. The thermal power dissipated in one timestep is then proportional to this term. The fraction on the right side of the term in square bracket represents the maximum thermal power which is dissipated in one timestep from the more charged part of the HT-TES. This thermal power is taken to be 1/10 of the heat content of the considered part of the HT-TES.

Finally, the input value recall block (Type93) is used to freeze during a timestep the value of the state of charge of the two parts of the HT-TES at the beginning of the timestep. If Type93 is not used, there could be the risk that the state of charge of the HT-TES would be continuously updated during the different iterations of the same timestep, so affecting the transferred power to the HT-TES itself in a circular loop —e.g. through the partial load factors or $Q_{cleanup}$—, possibly causing convergence issues and errors in the energy balance.

3. Case Studies

3.1. Case Study #2: Aalborg, Denmark

The implementation of a CHEST system in the Aalborg case study (see Deliverable D2.1 of the CHESTER project) is investigated through TRNSYS simulations under different boundary conditions.

The CHEST system is integrated in the TRNSYS model considering the current structure and the energy demands of the energy system in Aalborg and the plans for implementing a 1,000,000 m^3 water pit thermal energy storage (PTES) in the near future (see CHESTER deliverable D2.1).

The following inputs are used as input files required by the TRNSYS model (Section 2.2.1):

- *RES-el*: the electricity production profile from fluctuating RES (i.e. onshore wind, offshore wind and PV) in West Denmark (DK 1 grid) is used. This is appropriately scaled so that the yearly integral of the profile is equal to the yearly electricity consumption of Aalborg. The only exceptions are the cases presented in Section 3.1.6, for which a different scaling is used.
- *El-demand*: the electricity load profile of the electric grid in West Denmark is used. This is appropriately scaled in such a way that the yearly integral of the profile is equal to the yearly electricity consumption of Aalborg.
- *RES-heat*: the profile of waste heat from Portland cement factory and from the incineration plant in Aalborg is used. No scaling is applied, so the profile corresponding to the actual heat is available from these sources. The outlet temperature from the RES heat source is set to 90 °C. The maximum temperature at the inlet of the RES-heat source is 60 °C (Section 2.2.2).
- *Heat-demand*: the load profile from Aalborg DH network is used. No scaling is applied.
- *DH-T-fwd*: a constant supply temperature of 90°C for the DH network is used.
- *DH-T-rtn*: a return temperature of 40 °C and 50 °C is assumed for winter and summer respectively. In spring/autumn months, the return temperature is linearly interpolated between these two values.

The profiles of electricity production from RES, electricity demand, DH heat demand, availability of waste heat (*RES-heat*) and the temperatures of the DH network used as input in the TRNSYS model for the Aalborg case are shown in Figure 9 and Figure 10. The scaling of the profiles (as described in the bullet list above) is implemented in the figures.

Regarding the performance maps, Butene is assumed as working fluid in all the presented scenarios, with the only exceptions of the cases presented in Section 3.1.5.

The temperatures $T_{P3,min}$ and $T_{P3,max}$, which regulate the operation of the pump *Pump-3* and hence the discharging of the LT-TES, are 70 °C and 85 °C respectively in all the presented scenarios (Section 2.2.2). As a reference scenario, a TRNSYS simulation is performed without the CHEST system, to identify the performance of the DH system itself.

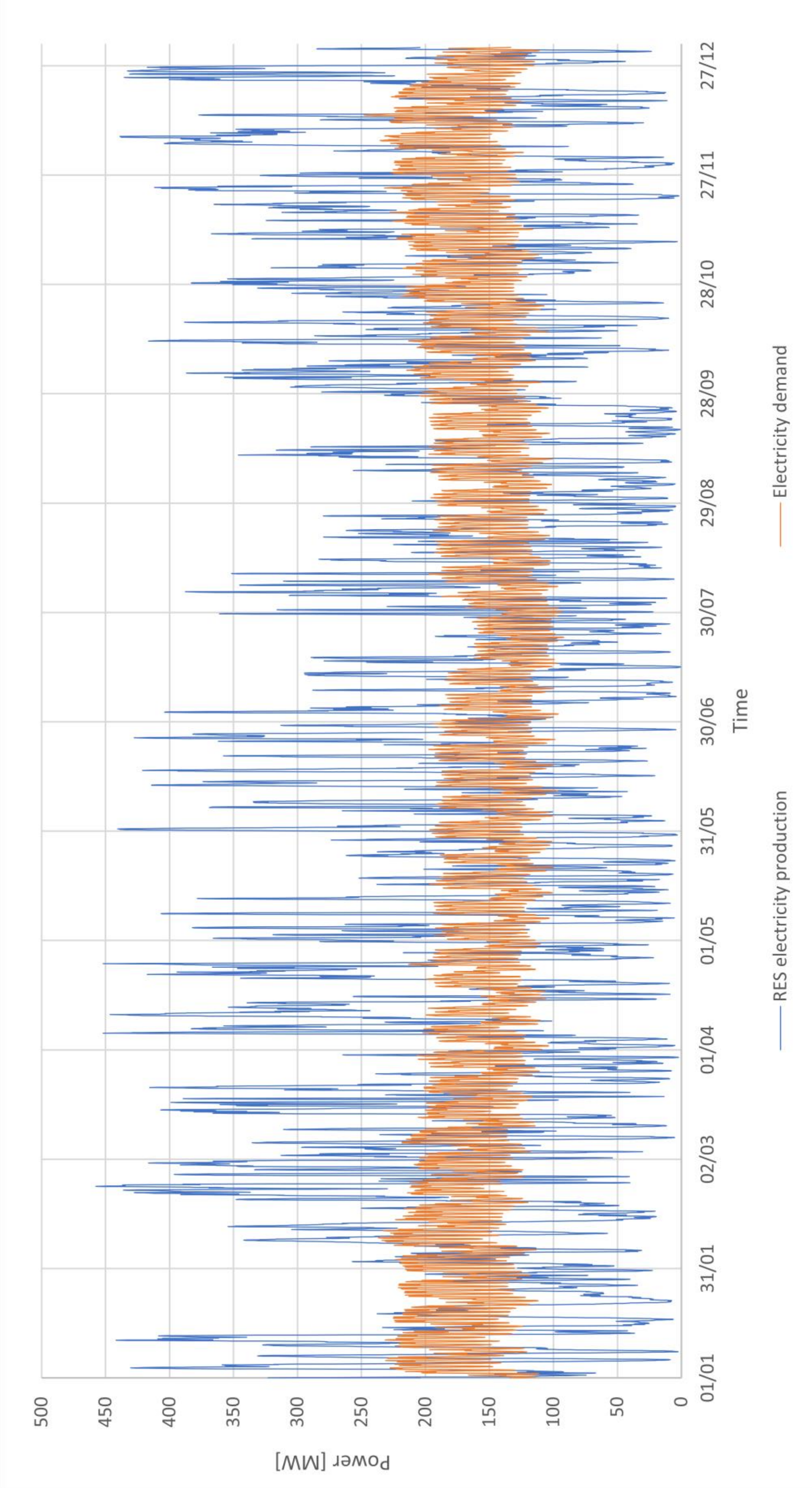

Figure 9: Profiles of electricity production and electricity demand used in Aalborg case.

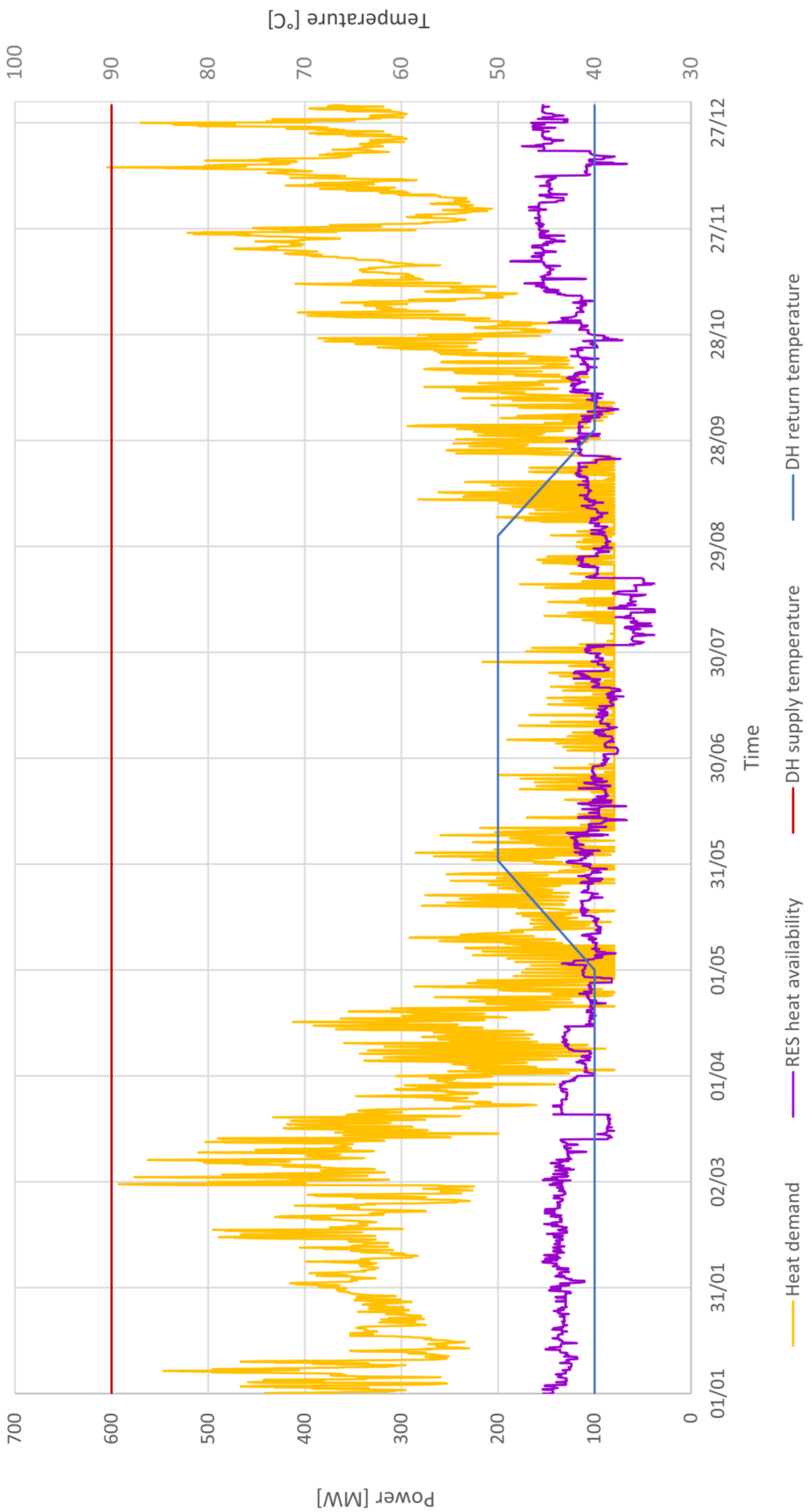

Figure 10: Profiles of DH demand, RES heat availability and DH temperatures used in Aalborg case.

Under the above-mentioned boundary conditions and energy profiles, the parameters listed in Table 9 are constant in all the presented scenarios, unless otherwise specified.

Table 9: General parameters for used in the simulations.

	Energy [MWh]
RES electricity production	1.40E+06
Electricity demand	1.40E+06
RES-heat available	9.98E+05
DH heat demand	1.93E+06
Electricity surplus	3.97E+05
Electricity deficit	3.97E+05
RES electricity directly used	1.00E+06

An overview of the parameters which are varied in the parametric analyses is presented in Table 10.

Table 10: Overview of the main parameters varied in the different parametric analyses presented in the following sections (Section 3.1.1-3.1.6) of this deliverable.

Section number		3.1.1 - Constant ratio	3.1.1 - Variable ratio	3.1.2	3.1.3
RES-electricity / Electricity demand	[-]	1.0	1.0	1.0	1.0
Capacity of HT-TES, Δt	[h]	Infinite	Infinite	72	2 - 96
Latent-to-sensible ratio of HT-TES	[-]	-	-	0.74	0.74
Fluid		Butene	Butene	Butene	Butene
HP capacity	[MW]	1 - 200	1 - 100	10	1 - 100
ORC capacity / HP capacity	[-]	1.00	0.25 - 1.00	1.00	1.00
Section number		**3.1.4**	**3.1.5**		**3.1.6**
RES-electricity / Electricity demand	[-]	1.0	1.0	1.0	0.5, 1, 1.5
Capacity of HT-TES, Δt	[h]	12, 24	12, 24	12, 24	12, 24
Latent-to-sensible ratio of HT-TES	[-]	0.74	1.14	0.74	0.74
Fluid		Butene	R1233zd(E)	Butene	Butene
HP capacity	[MW]	1, 10	1, 10	1, 10	1 - 75
ORC capacity / HP capacity	[-]	0.25 - 1.10	0.25 - 1.10	0.25 - 1.10	0.25 - 1.10

3.1.1. HP and ORC capacity with infinite HT-TES

Constant ratio between HP and ORC capacity

First, the size of the HP and of the ORC of the CHEST system are varied to identify which range of capacities is most relevant to be investigated in connection to Aalborg case. The capacity of the HP and ORC is varied in the range 1 MW-200 MW, keeping constant the ratio between the HP capacity and the ORC capacity. This range is chosen based on the maximum value assumed by the electricity surplus and electricity deficit over the year (Figure 11), calculated as the difference between the RES electricity production and the electricity demand. Due to the highest electricity surplus being about 300 MW and the highest electricity deficit being about 200 MW, the latter is chosen as upper value of the investigated range.

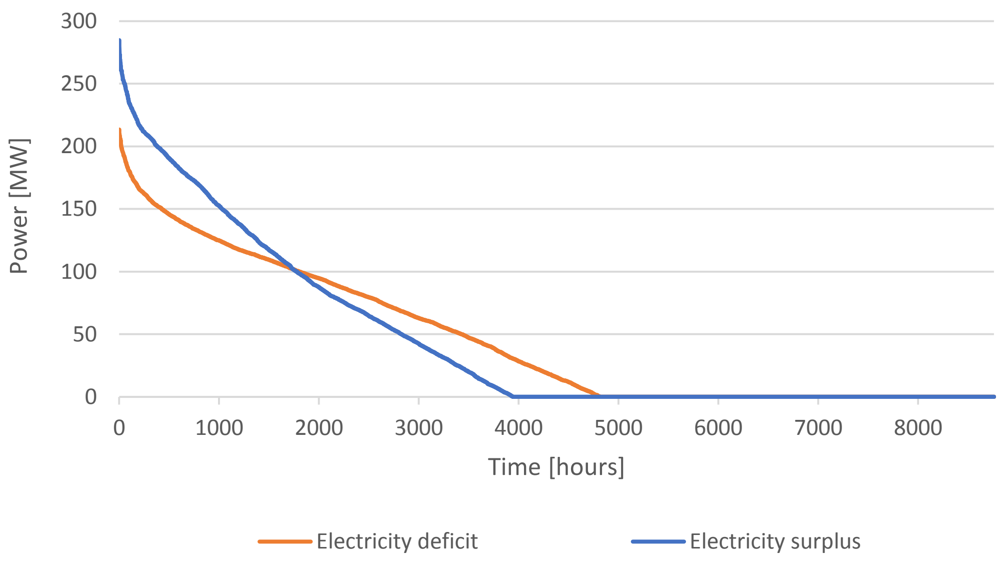

Figure 11: Distribution of electric surplus and electric deficit in Aalborg case during the year (8760 hours).

In this set of simulations, the storage capacity of the HT-TES is assumed infinite to limit the number of parameters affecting the results. Assuming an infinite storage capacity for the HT-TES entails that the most appropriate range of HP and ORC capacities identified is affected by the surplus/deficit of electricity and by the availability of RES heat. In real world applications the HT-TES will have a finite size, which is likely to further decrease the range of appropriate capacities for the HP and ORC components.

The size of the LT-TES is kept constant and equal to 1,000,000 m^3.

Figure 12, Figure 13 and Figure 14 show the effect of the HP and ORC capacity on some performance indicators of the CHEST system.

Figure 12 shows the electricity absorbed by the HP and produced by the ORC over the year. When increasing the capacity of the HP and of the ORC, the electricity absorbed by the HP and that produced by the ORC increased. However, the increase is less than the proportional to the installed capacity and it presents asymptotic behaviour at large capacities.

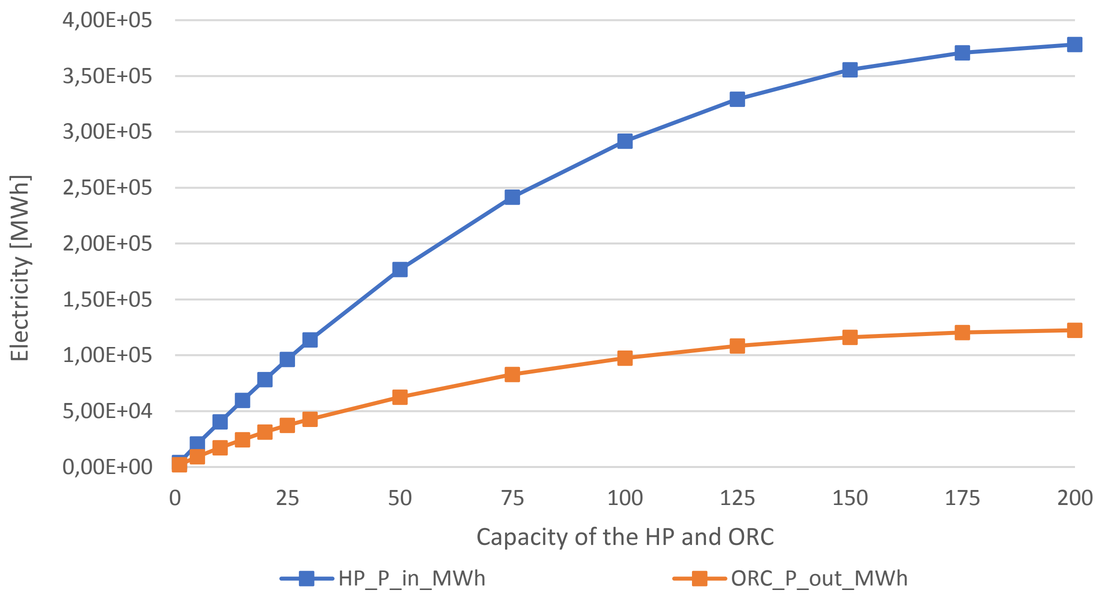

Figure 12: Electricity absorbed by the HP and produced by the ORC as function of the HP and ORC capacity (infinite HT-TES size).

The amount of electricity absorbed by the HP shows an asymptotic behaviour for a HP capacity of 200 MW, which is explained by the distribution of the electricity surplus (Figure 11). Since most of the electricity surplus occurs at powers lower than 200 MW, HP capacities larger than this value would be strongly under-used and would give a very modest increase in electricity use. Figure 12 shows that the increase in absorbed electricity is approximately linear for HP capacities in the range 1 MW-50 MW. At higher capacities the slope of the curve becomes progressively milder. This is caused partly by the increasingly steeper slope of the electricity surplus curve (Figure 11) and partly by the fact that increasing HP capacities entail lower temperatures in the top of the LT-TES. As seen in Figure 10, the amount of high temperature RES-heat is limited to a power of about 100-150 MW during the year. For each MW of absorbed electricity, the evaporator of the HP absorbs between 3 MW and 6 MW of heat, depending on the temperature at the inlet of the evaporator. The performance map for the HP using Butene (Table 5) shows that the peak electricity absorbed by HP decreases with the temperature at the inlet of the evaporator. Hence, lower temperatures in the top of the PTES entail a lower amount of absorbed electricity.

The ORC shows an asymptotic behaviour for an installed capacity of 150 MW, which is explained by the distribution of the electricity deficit shown in Figure 11. As most of the electricity deficit occurs at powers lower than 150 MW, ORC capacities larger than this value are strongly under-used and give modest significant increase in electricity production. At lower ORC capacities, the trend of the curve of the produced electricity in Figure 12 reflects the amount of heat stored in the HT-TES, which is determined by the HP operation. Hence, the two curves show a similar trend in this range of capacity. However, it can be noted that the curve of the ORC-produced electricity increases less steeply than that of the HP-absorbed electricity. The reason for this is that the COP of the HP decreases at larger HP capacities (Figure 14) for the same reason of the lower inlet temperatures at the evaporator of the HP described above. A lower COP means that for the same amount of electricity absorbed by the HP, a lower amount of heat is transferred to the HT-TES, hence, a lower amount of heat is available for the ORC.

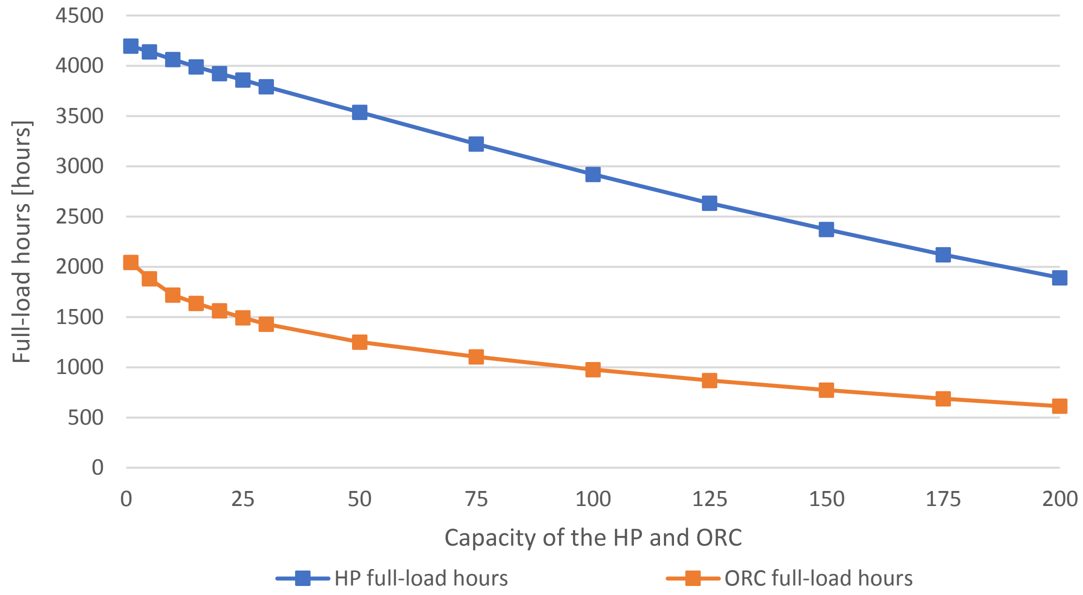

Figure 13: Full-load hours of the HP and of the ORC as function of their capacity (infinite HT-TES size).

Figure 13 shows the full-load hours of operation for both the HP and the ORC, defined as the ratio between the electricity absorbed by the HP/produced by the ORC and the HP/ORC capacity respectively. The full-load hours of the HP and of the ORC decrease almost linearly with the increase of the installed capacity of the component. This is an immediate consequence of the curves of the absorbed/produced electricity shown in Figure 12, once they are normalized to the installed capacity of the HP/ORC.

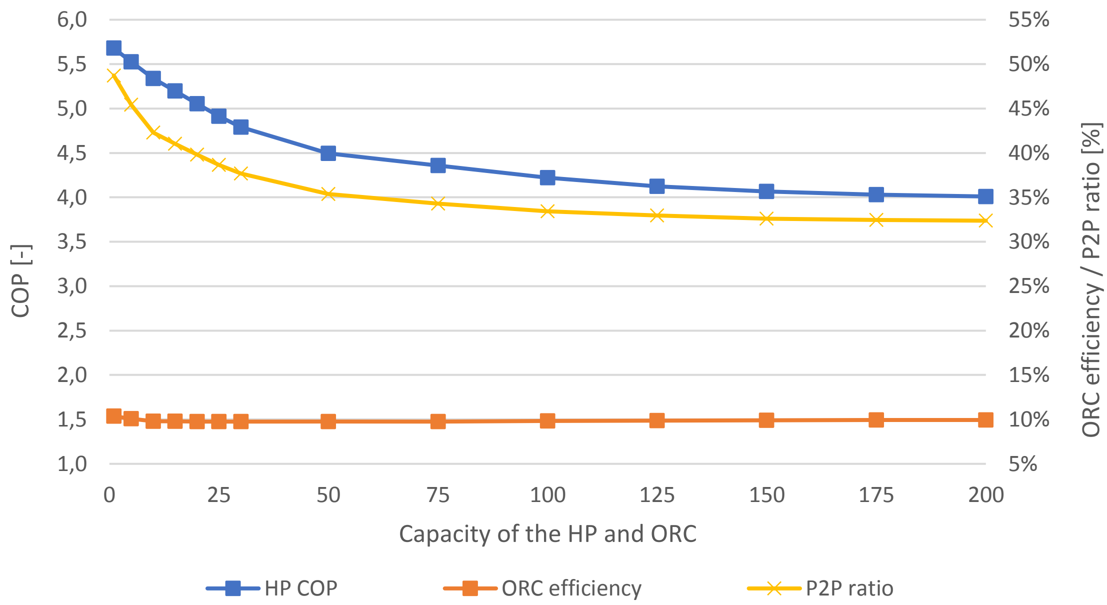

Figure 14: COP of the HP, efficiency of the ORC and power-to-power (P2P) ratio ORC as function of the HP and ORC capacity (infinite HT-TES size).

Figure 14 shows the COP of the HP, the efficiency of the ORC and the power-to-power ratio of the CHEST system, which is defined as the ratio between the electricity produced by the ORC and that absorbed by the HP. The reason for the lower COP at increasing HP capacity has already been explained above.

The efficiency of the ORC is roughly constant. This is due to the almost constant temperature supplied at the condenser of the ORC, which directly determines its efficiency. The inlet temperature at the condenser of the ORC is primarily determined by the return temperature of the DH network (40-50 °C, see Figure 10). If, due to intense ORC operation, the temperature at the bottom of the PTES increases above the maximum value allowed at the entrance of the condenser of the ORC (50 °C, see Table 6), it would be cooled down to 50 °C (Section 2.2.5) giving rise to blow-off heat dissipated to the environment (Figure 15). Hence, the ORC operates at an almost constant efficiency of about 10 %, in agreement with the performance map for this temperature level (Table 6).

Another option, currently not implemented in the TRNSYS model, would be to make the condenser of the ORC exchange heat at lower temperature (e.g. sea water, rivers, etc.). This would increase the amount of energy leaving the system (hence, the DH boiler would operate more), but at the same time it would favour the ORC electricity production improving the power-to-power ratio of the CHEST system. This possibility will be investigated in the deliverable D2.3 of the CHESTER project.

As the power-to-power ratio is determined by the combination of the performance of both HP and ORC, the almost constant ORC efficiency causes the trend of the power-to-power ratio to be similar to that of the COP of the HP.

Since some heat is dissipated to the environment to allow the operation of the ORC, the heat has to be reintegrated in the system through additional operation of the boiler of the DH system, whose output follows the same trend as the one of the dissipated heat (Figure 15).

Compared to the scenario without CHEST, the investigated scenarios with CHEST have the benefit of being able to store excess electricity and release it when needed (Figure 12), at the cost of making the central boiler operate more (Figure 15). Relevant data are listed in Table 11.

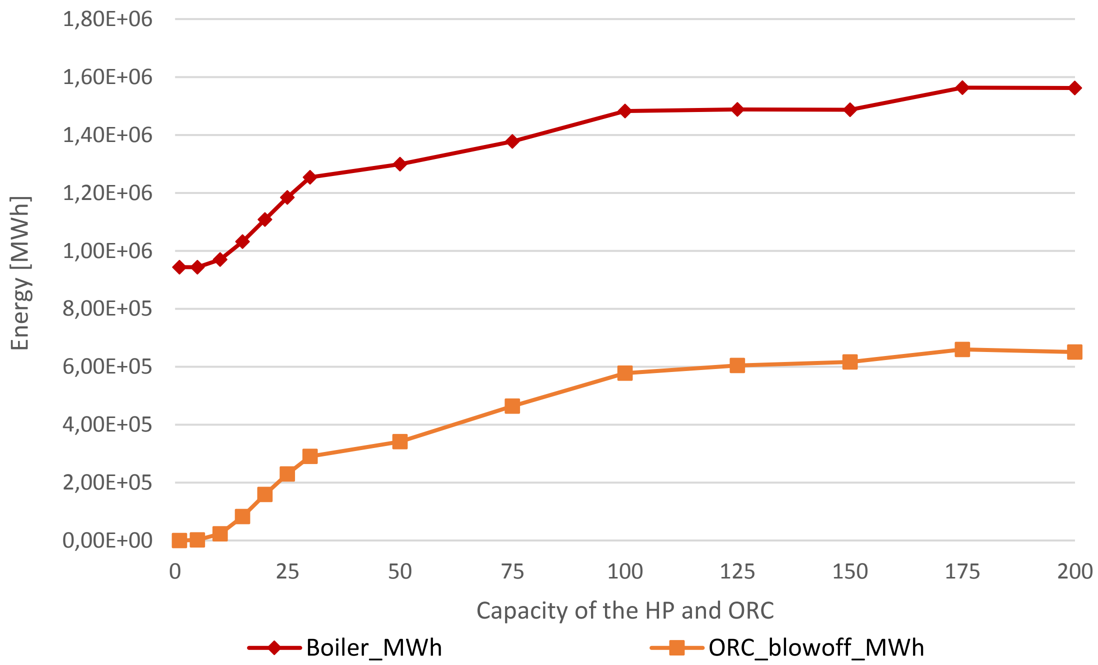

Figure 15: Heat dissipated by the auxiliary cooling device before the condenser of the ORC (see Section 2.2.5) and heat production from the DH central plant.

Table 11: Electricity absorbed by the HP and produced by the ORC, and boiler operation in the investigated scenarios.

HP and ORC capacity [MW]	Electricity absorbed by HP [MWh]	Electricity produced by ORC [MWh]	Boiler output [MWh]	Increase in boiler output compared to reference [MWh]
Reference (No CHEST)	-	-	9.44E+05	-
1	4.20E+03	2.04E+03	9.44E+05	1.54E+02
5	2.07E+04	9.40E+03	9.69E+05	2.58E+04
10	4.06E+04	1.72E+04	1.03E+06	8.76E+04
15	5.99E+04	2.46E+04	1.11E+06	1.64E+05
20	7.85E+04	3.12E+04	1.18E+06	2.40E+05
25	9.65E+04	3.73E+04	1.25E+06	3.10E+05
30	1.14E+05	4.29E+04	1.30E+06	3.55E+05
50	1.77E+05	6.25E+04	1.38E+06	4.34E+05
75	2.42E+05	8.29E+04	1.48E+06	5.39E+05
100	2.92E+05	9.76E+04	1.49E+06	5.44E+05
125	3.29E+05	1.09E+05	1.49E+06	5.43E+05
150	3.56E+05	1.16E+05	1.56E+06	6.19E+05
175	3.71E+05	1.20E+05	1.56E+06	6.19E+05
200	3.78E+05	1.22E+05	1.56E+06	6.18E+05

Variable ratio between HP and ORC capacity

In previous sections, the capacity of the HP and the capacity of the ORC is arbitrarily chosen to be the same. However, there is no specific reason this should always be the case. Hence, in this subsection different ratios between HP and ORC capacities are simulated, while keeping all other boundary conditions the same as in the previous subsection.

Given the asymptotic behaviour for HP capacities larger than 100 MW (Figure 12), a smaller range of HP capacities is selected for these simulations, having 100 MW as upper limit. Additionally, given the linearity at capacities lower than 30 MW, fewer points are chosen. For each value of HP capacity within this new range, the ORC capacity is varied so to assume different relative sizes compared to the HP capacity.

A first round of simulations is performed using ratios between ORC and HP capacities both higher and lower than 1. Since ratios higher than 1 did not have any effect on the electricity production from the ORC, its efficiency or other relevant parameters, a second round of simulations has been performed focusing only on ratios lower than 1.

On the one hand, the simulations results show that varying the ORC relative capacity has a negligible impact on the performance indicators of the HP, such as COP, absorbed electricity, amount of heat exchanged by the HP with the other components of the systems. In fact, in presence of an infinite HT-TES capacity, the capacity the ORC has no relevant effect on the operation of the HP. Also, the efficiency of the ORC is not significantly affected in the different scenarios, for the same reasons described in the previous subsection.

On the other hand, the electricity production from the ORC is the parameter that is mostly affected by the variation in ORC capacity. Table 12 lists the electricity produced by the ORC in the different investigated scenarios. In general, an ORC having a relative capacity of 0.5 compared to the HP capacity, performs as well as an ORC having the same capacity as the HP (ratio=1). In case of infinite HT-TES size, the limiting factor for the ORC operation is the profile of electricity deficit and the amount of heat rejected at the condenser of the HP.

Figure 14 shows that in the range 1-100 MW the HP has a minimum COP of 4.2 (for 100 MW HP), while the ORC has a fairly constant efficiency of 10 %. This means that for each MWh of absorbed electricity the HP stores about 4.2 MWh of high-temperature heat. Even assuming that this entire amount of heat is exploited by the ORC (despite not being so because of the different latent/sensible ratio of the HP and ORC, see Sections 2.1.3 and 2.2.3), the ORC electricity production would be about 0.42 MWh. Therefore, it can be concluded that, under the assumed electricity profiles and the hypothesis of infinite HT-TES, the ORC can be sized down to 0.4 times the size of the HP, without affecting its yearly performance.

At low HP capacities (1-10 MW), characterized by a higher COP, the ORC electricity output starts decreasing for ORC relative capacities lower than 0.5, when the limiting factor for the ORC production is the number of hours with electricity deficit. In the range of ORC relative capacities between 0.25 and 0.40, the electricity production decreases roughly proportionally to the ORC capacity.

For a 100 MW HP, characterized by a lower COP, the main limiting factor for the ORC production is mainly the amount of heat available in the HT-TES and not the number of hours of electricity deficit. Hence, the size of the ORC does not have an impact on the electricity production.

At intermediate HP capacities, an intermediate behaviour is observed, with fairly constant ORC electricity production for the higher ORC relative capacities (when the limiting factor is the amount of high-temperature heat available) and a decreasing production for the lower ORC capacities (when the limiting factor is the number of hours of ORC operation).

The resulting power-to-power ratios in the different scenarios are listed in Table 13 and are coherent with the results presented in Table 12 and those in the previous subsection. Finally, the additional heat output from the boiler compared to reference scenario without CHEST system is given in Table 14.

Table 12: Electricity production from the ORC for different HP capacities and ORC/HP capacity ratios.

		HP capacity [MW]					
		1	10	30	50	75	100
ORC capacity relative to HP capacity [-]	0.25	1.05E+03	1.04E+04	3.06E+04	5.04E+04	7.44E+04	9.71E+04
	0.30	1.25E+03	1.24E+04	3.66E+04	6.01E+04	8.32E+04	9.76E+04
	0.40	1.67E+03	1.65E+04	4.32E+04	6.30E+04	8.33E+04	9.78E+04
	0.50	2.02E+03	1.73E+04	4.32E+04	6.30E+04	8.32E+04	9.77E+04
	1.00	2.04E+03	1.72E+04	4.29E+04	6.25E+04	8.29E+04	9.76E+04

Table 13: Power-to-power ratio of the system for different HP capacities and ORC/HP capacity ratios.

		HP capacity [MW]					
		1	10	30	50	75	100
ORC capacity relative to HP capacity [-]	0.25	24.9%	25.5%	26.9%	28.5%	30.8%	33.3%
	0.30	29.9%	30.6%	32.2%	34.0%	34.4%	33.4%
	0.40	39.9%	40.6%	37.9%	35.6%	34.5%	33.5%
	0.50	48.2%	42.5%	37.9%	35.6%	34.4%	33.5%
	1.00	48.7%	42.3%	37.7%	35.4%	34.3%	33.4%

Table 14: Additional heat output from the boiler compared to reference scenario without CHEST for different HP capacities and ORC/HP capacity ratios.

		HP capacity [MW]					
		1	10	30	50	75	100
ORC capacity relative to HP capacity [-]	0.25	1.22E+04	1.42E+05	3.90E+05	4.63E+05	5.81E+05	5.74E+05
	0.30	1.05E+04	1.26E+05	3.59E+05	4.26E+05	5.44E+05	5.47E+05
	0.40	5.36E+03	8.91E+04	3.17E+05	4.06E+05	5.40E+05	5.53E+05
	0.50	1.07E+03	7.15E+04	3.26E+05	4.18E+05	5.43E+05	5.52E+05
	1.00	1.54E+02	8.76E+04	3.55E+05	4.34E+05	5.39E+05	5.44E+05

3.1.2. Finite size of HT-TES: ratio between latent and sensible part

The performance map of the HP when using Butene (Table 5) shows that the ratio between the heat transfer to the latent and sensible part of the HT-TES is approximately 0.74, regardless of the heat source temperature. This may suggest sizing the HT-TES in such a way that the heat capacity of the latent part is 0.74 times that of the sensible part.

The performance map of the ORC for the same fluid shows that the ratio between the heat transfer from the latent and sensible part varies between 0.74 and 1.11 for inlet temperatures to the condenser between 15 °C and 50 °C. However, the stable inlet temperatures to the ORC (Section 3.1.1) causes the ORC to operate with an almost constant latent-to-sensible ratio of about 1.1.

Due to the difference in the latent-to-sensible ratio between the HP and the ORC, the sensible part of the HT-TES has some excess heat which cannot be used by the ORC and which must be discharged to allow a cyclic operation of the HT-TES (Section 2.2.6). This is done in the TRNSYS model according to the strategy described in Section 2.2.6. However, in WP3 different system configurations are being analysed to prevent this behaviour. Figure 16 shows the effect of this strategy on the state of charge of the latent and sensible part of the HT-TES during a period characterized by different charging and discharging phases. The state of charge is expressed in relative terms, as the ratio between the actual heat content of the storage and its maximum capacity. A ratio of 0.74 between the heat capacity of the latent and sensible part of the HT-TES is assumed.

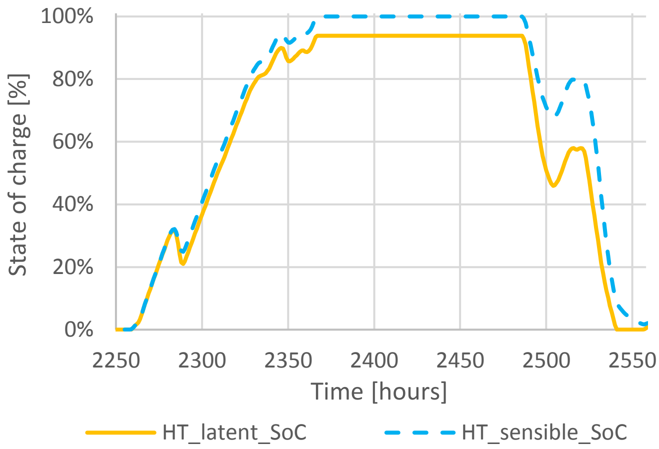

Figure 16: State of charge in the latent and sensible part of the HT-TES according to the clean-up strategy described in Section 2.2.6.

Figure 16 shows that, when both parts of the HT-TES are empty, the HP charges them uniformly, as the latent-to-sensible ratio of the HP is equal to the latent-to-sensible ratio of the HT-TES, i.e. 0.74. Intermediate discharges occur with a latent-to-sensible ratio of about 1.1, which causes a gap between the curves of state of charge of the two parts of the HT-TES. Since the latent-to-sensible ratio of the ORC is higher than the HP one and of the HT-TES one, the latent part of the HT-TES is discharged more (in relative terms) than the sensible part. If another charging phase occurs, the sensible part of the HT-TES, having a higher state of charge, will reach its full capacity sooner and will stop the HP operation. Although the latent part of the HT-TES is smaller than the sensible part, it cannot be fully charged, and it could have been sized smaller. In fact, simulations using latent-to-sensible ratios of the HT-TES equal to 0.70 and 0.65 give almost identical performances compared to scenarios using 0.74. For ratios equal to or lower than 0.60, the latent part of the HT-TES has proved to be small and it has acted like the limiting factor for the CHEST operation.

The clean-up strategy of the HT-TES as described in Section 2.2.6 is not completely effective in removing the excess heat from the sensible part of the HT-TES. Therefore, a new strategy has being developed, based on the specific boundary conditions of Aalborg case. To ensure an even state of charge of the two parts of the HT-TES, heat is removed from the sensible part of the HT-TES according to the following relation (20):

$$Q_{sensible,cleanup} = \min\left[E_{sensible}, E_{latent} \cdot \left(\frac{E_{sensible}}{E_{latent}} - \frac{1}{0.74}\right)\right] \qquad (20)$$

where $E_{sensible}$ and E_{latent} are the amount of heat (in MWh) stored respectively in the sensible heat part an in the latent heat part of the HT-TES.

The effect of the new clean-up strategy is shown in Figure 17.

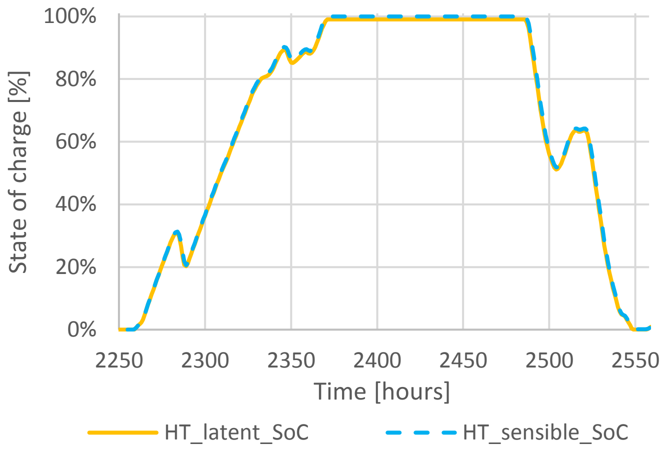

Figure 17: State of charge in the latent and sensible part of the HT-TES according to the new clean-up strategy.

The effect on the overall system of the new clean-up strategy is a better utilization of the HT-TES, which appears to have a larger capacity compared to a HT-TES having the same volume of the latent and sensible parts and implementing the old clean-up strategy. Hence, a CHEST system using this clean-up strategy would have a longer HP and ORC operation and a higher number of HT-TES cycles. This effect is even more notable at low HT-TES capacities, where the HT-TES capacity is more likely to act as a limiting factor for the HP operation. For example, for the scenarios shown in Section 3.1.3, the old clean-up strategy reduces the electricity consumption of the HP by 9 % and 5 % compared to the new clean-up strategy in case of the smallest HT-TES capacity (Δt=2 hours, see Section 3.1.3), varying the HP capacity between 1 MW and 100 MW. For larger HT-TES capacities (Δt=72 hours), this reduction is between -2 % and -1 %, depending on the HP capacity. The ORC electricity production presents almost identical relative variations.

Given the better performance of the new strategy compared to the previous one, it is used in all other studied scenarios for a finite size of the HT-TES.

3.1.3. Storage capacity of HT-TES

In this Section the effect of introducing a finite HT-TES is investigated. Different sizes of the HT-TES are considered, according to the following relation (21):

$$C_{HT\text{-}TES} = W_{p,HP} \cdot COP_{ref} \cdot \Delta t \tag{21}$$

where $C_{HT\text{-}TES}$ is the overall storage capacity of the HT-TES (in MWh);
$W_{p,HP}$ is the nominal capacity of the HT-HP (in MW);
COP_{ref} is a fixed COP assumed for the HP. A value of 6 is taken;
Δt is the time (in hours) that a HP with capacity $W_{p,HP}$ and COP COP_{ref} would need to completely fill the HT-TES, when operating at full load.

In the investigated scenarios presented in this section, the parameter Δt is varied between 2 and 96 hours. The overall storage capacity of the HT-TES is divided between latent and sensible part, hence, the storage capacity of the latent part is 0.74 times that of the sensible part. The capacity of the HP is varied in the same range 1-100 MW seen above and the relative ORC capacity is kept to 1.

The effect of a finite HT-TES capacity on the full-load hours of the HP and of the ORC is shown in Figure 18 and Figure 19. The legend denotes that the different curves refer to different HP (and ORC) capacities (in MW). In both figures the isolate data points on the right side of the diagram denote the number of full-load hours that the system would have in case of infinite storage (Section 3.1.1).

Figure 18 and Figure 19 show that the number of full-load hours increases for larger HP and ORC capacities, as explained in Section 3.1.1. Additionally, the number of full-load hours increases, when increasing the HT-TES capacity, even though with a progressively milder slope. This is explained by the fact that for small HT-TES the HT-TES capacity is the major limiting factor for the operation of the HP and of the ORC. Hence, enlarging the HT-TES entails an almost proportional increase of the HP and the ORC operation. However, for larger HT-TES capacities, other limiting factors, such as the electricity surplus and electricity deficit, occur. In this context enlarging the HT-TES has a progressively smaller impact. The same reason explains why the larger the HP and ORC are, the smaller the HT-TES needs the system to approach its asymptotic performance. The larger HP and ORC tend to be more limited in their operation due to the availability of electricity surplus, which increases the HT-TES size, since certain threshold has smaller effect.

It can also be observed that, for the same HT-TES size, the number of full-load hours of the ORC are more affected by the HP capacity compared to the HP (i.e. the curves are more spread in Figure 19 than in Figure 18). This is caused by the different COP at different HP capacities. As explained in Section 3.1.1 and seen in Figure 22, lower HP capacities are characterized by higher COPs. Accordingly, for the same amount of electricity absorbed by the HP, more heat is transferred to the HT-TES. Because the HT-TES is calculated in relation to the HP capacity and assuming a constant COP (see relation above), the HP that has higher capacities and lower COP transfers relatively less heat to the HT-TES compared to an HP smaller. Since this heat is the energy input to the ORC, its operation is directly affected, resulting in a significantly lower number of full-load hours at high HP capacities.

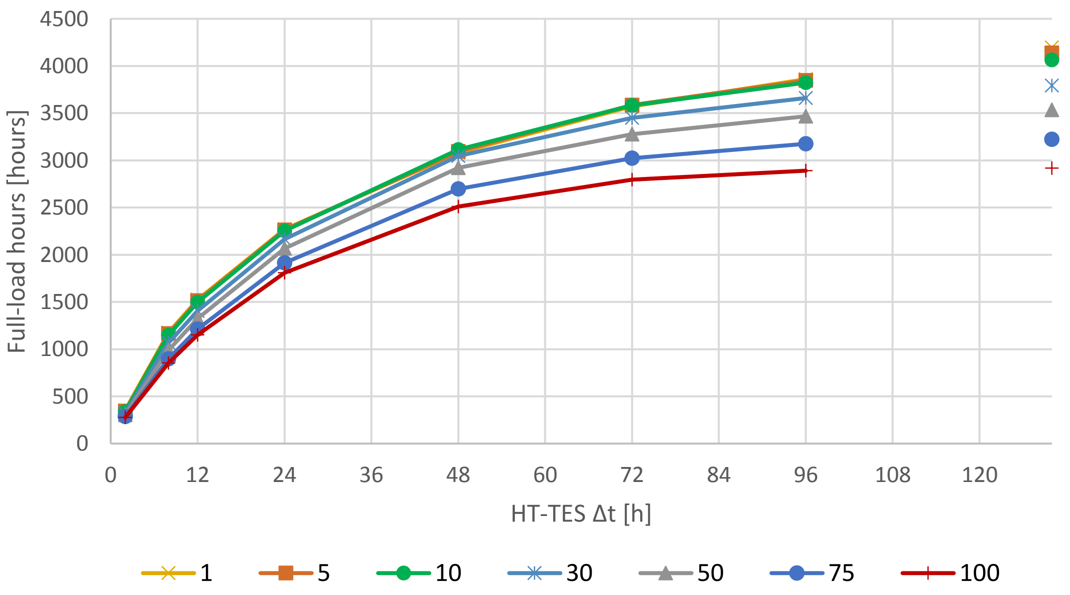

Figure 18: Full-load hours of the HP as function of the HT-TES capacity for different HP (and ORC) capacities.

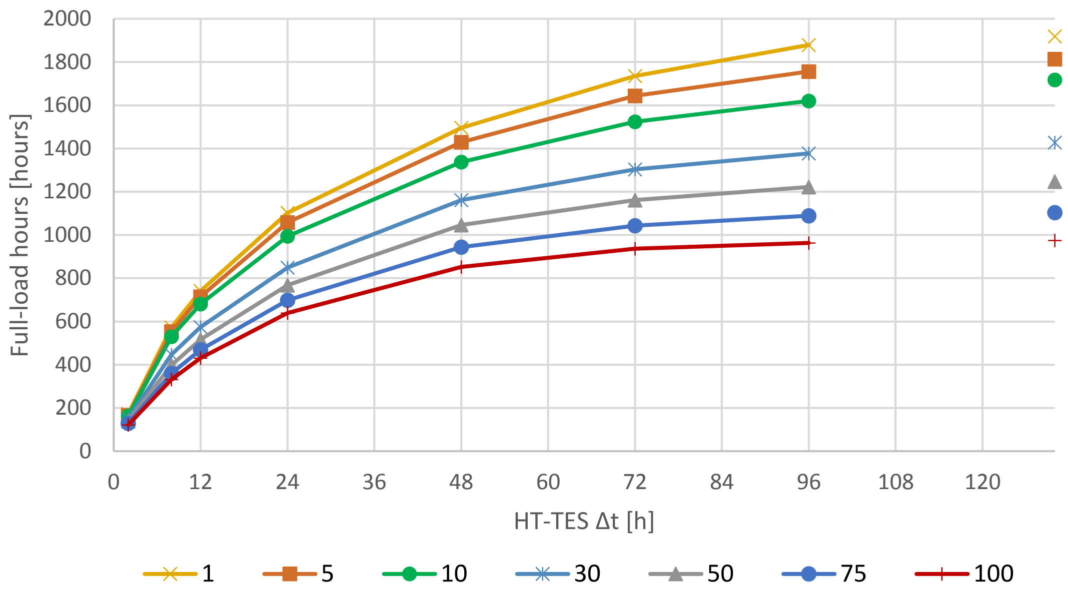

Figure 19: Full-load hours of the ORC as function of the HT-TES capacity for different HP (and ORC) capacities.

The greater operation of the HP and of the ORC at higher capacities and in larger HT-TES sizes has an additional operation cost of the DH boiler. Figure 20 shows the additional heat output from the DH boiler compared to reference scenario without CHEST as function of the HT-TES capacity.

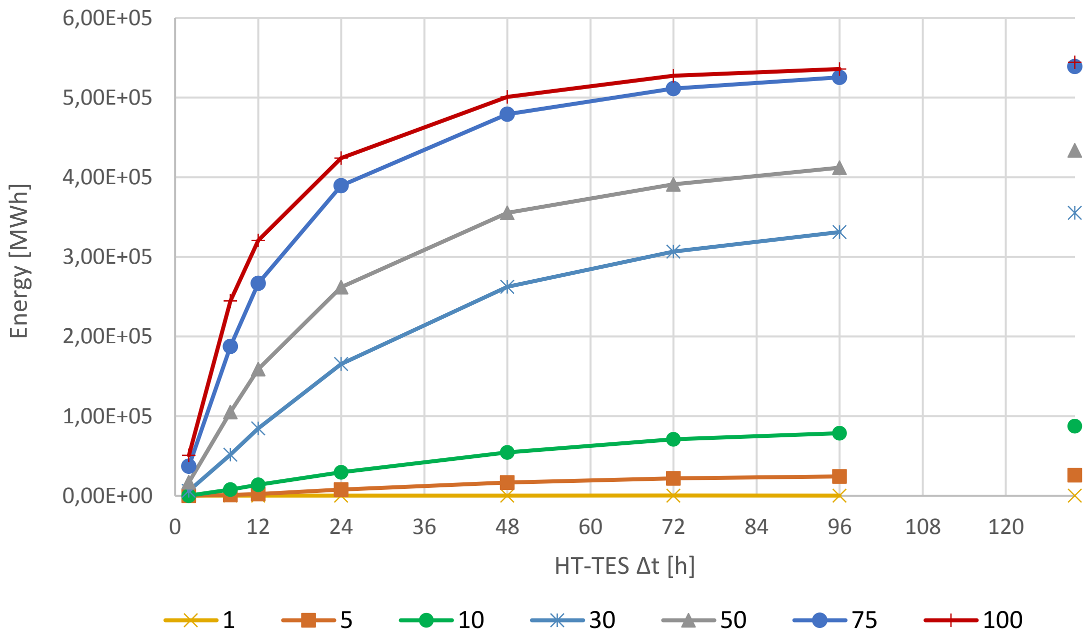

Figure 20: Additional heat output from the boiler compared to reference scenario without CHEST as function of the HT-TES capacity for different HP (and ORC) capacities.

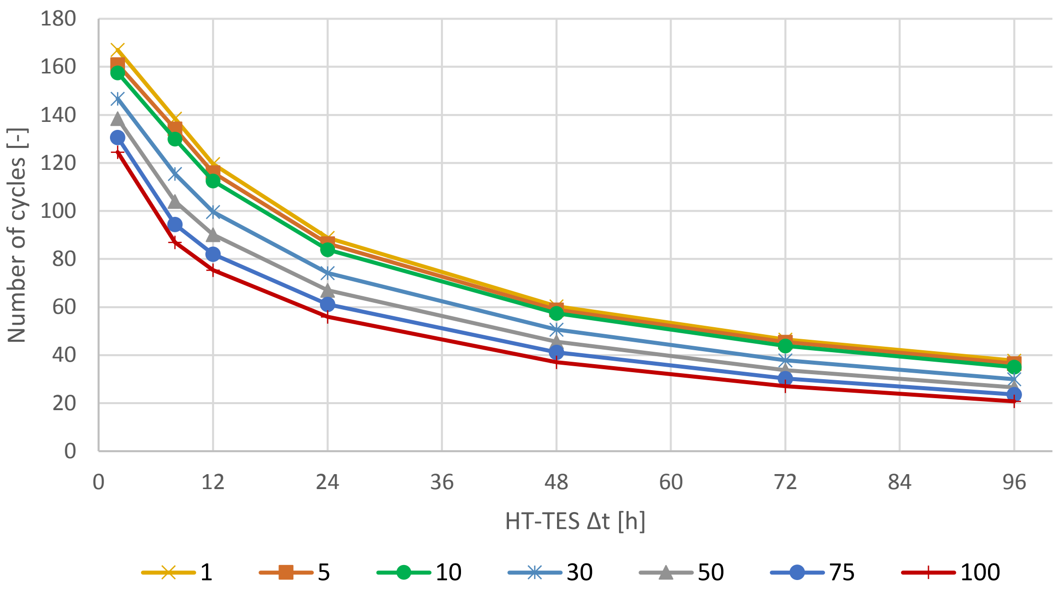

Figure 21: Number of cycles of the latent part of the HT-TES as function of the HT-TES capacity for different HP (and ORC) capacities.

Figure 21 shows the number of cycles of the latent part of the HT-TES as function of the HT-TES capacity for different HP and ORC capacities. The number of cycles for the latent part of the HT-TES is calculated as (22):

$$\#cycles_{latent} = \frac{E_{latent,ORC} + E_{latent,cleanup}}{C_{HT\text{-}TES,latent}} \tag{22}$$

where $E_{latent,ORC}$ (in MWh) is the yearly heat transferred from the latent part of the HT-TES to the evaporator of the ORC;

$Q_{latent,cleanup}$ (in MWh) is the yearly heat dissipated from the latent heat part of the HT-TES in case of uneven state of the charge between the two parts of the HT-TES (Section 2.2.6);

$C_{HT\text{-}TES,latent}$ is the storage capacity of the latent part of the HT-TES (in MWh).

The mathematical definition of number of cycles for the sensible part of the HT-TES is given by the same expression as of $\#cycles_{latent}$, simply replacing the subscript *latent* with the subscript *sensible*.

The diagram of the number of cycles of the sensible part of the HT-TES is not shown, as it is equivalent to that in Figure 21.

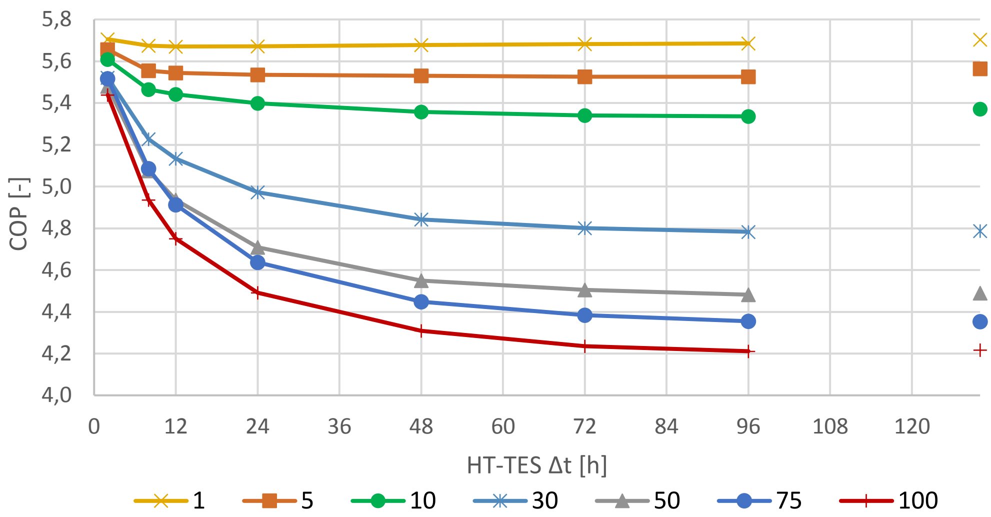

Figure 22: COP of the HP as function of the HT-TES capacity for different HP capacities.

Figure 22 shows the COP of the HP as function of the HT-TES capacity for the investigated HP capacities. When the HP absorbs more heat than the high-temperature heat stored in the PTES, it reduces the temperature at the top of the PTES, compromising its future performance. This leads to the fact that the greater the HP and the bigger the HT-TES, the more heat the HP takes from the PTES and the lower the average COP. Consequently, also the power-to-power ratio presents a similar trend (Figure 23).

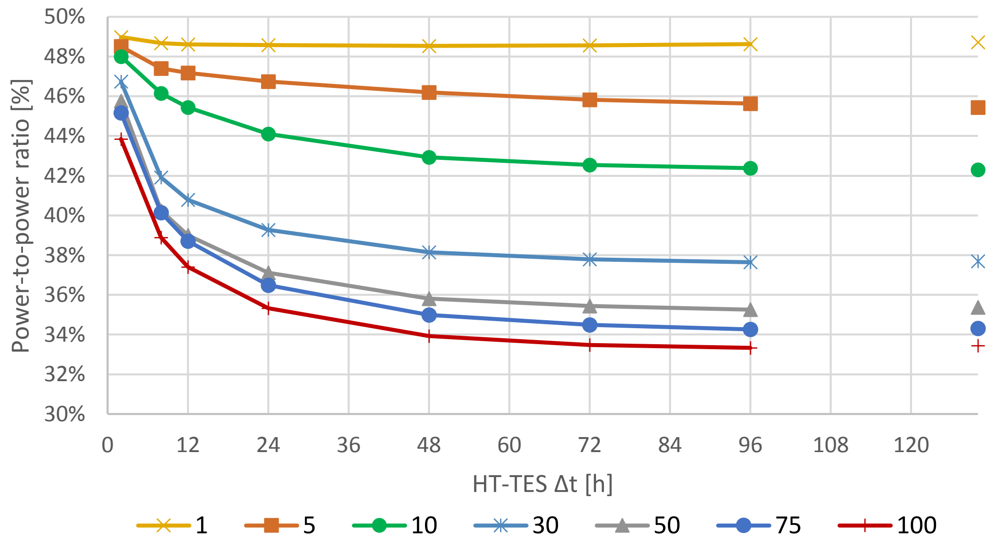

Figure 23: Power-to-power ratio of the CHEST system as function of the HT-TES capacity for different HP (and ORC) capacities.

3.1.4. Variable ratio between HP and ORC capacities

Similar to the analysis on the ratio between HP and ORC capacities presented in Section 3.1.1, the current section describes the effect of the ORC relative capacity on the performance indicators of the CHEST system. The main difference compared to the analysis in Section 3.1.1 is that in this case the HT-TES has a limited capacity. Based on the results presented in Section 3.1.3, the analysis is limited to 4 capacities of HT-TES, sized on a value of Δt of 12 hours and 24 hours respectively, and on a HP capacity of 1 MW and 10 MW. These values are chosen because of the fairly good performance they entail in terms of full-load hours of the CHEST components, COP of the HP, power-to-power ratio and cycles of the HT-TES. The values of COP_{ref} used for the sizing of the HT-TES are 5.7 and 5.4 for the HP capacities of 1 MW and 10 MW respectively, according to the results from Figure 22.

The performance of the CHEST system is evaluated as function of different ratios between ORC capacity and HP capacity. Similarly, to the analysis presented in Section 3.1.1, this ratio is varied between 0.25 and 1.1 for each of the 4 cases mentioned above.

Figure 24 and Figure 25 show the number of full-load hours of the ORC and of the HP respectively, as function of the ORC relative capacity in the 4 investigated scenarios.

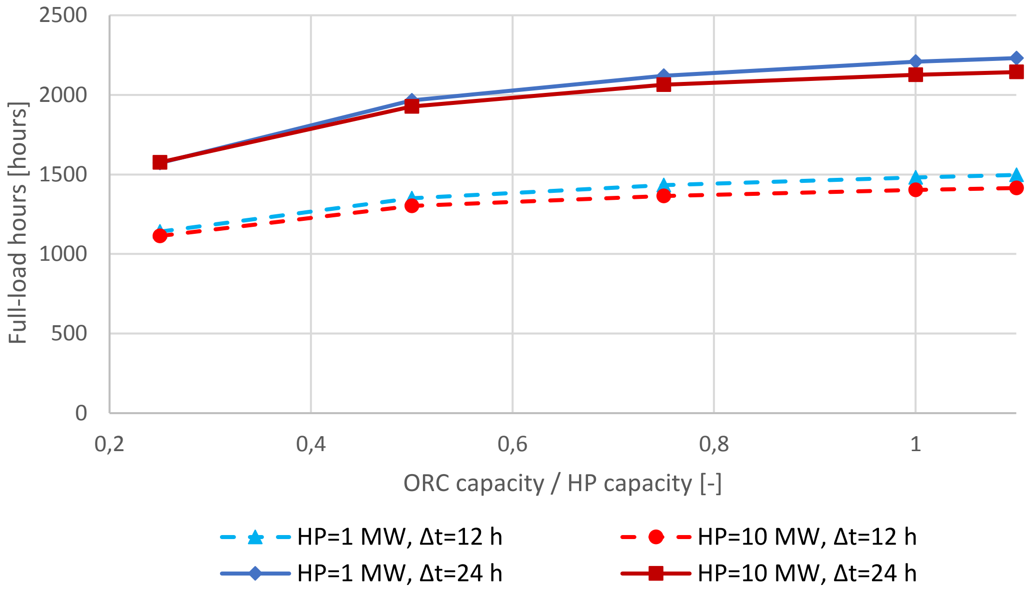

Figure 24: Full-load hours of the HP as function of the ORC relative capacity for the different HP capacities and HT-TES sizes.

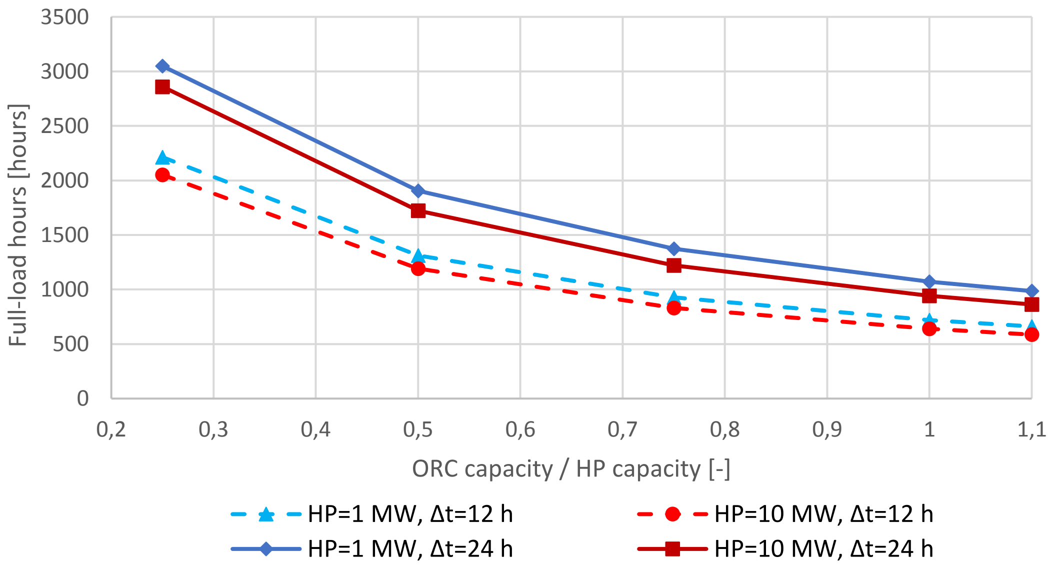

Figure 25: Full-load hours of the ORC as function of the ORC relative capacity for the different HP capacities and HT-TES sizes.

Figure 24 shows that the lower ORC relative capacities entail a lower number of full-load operation of the HP. In Section 3.1.1 it is said that relative size of the ORC does not affect the operation of the HP. This is due to the infinite size of the HT-TES. However, in presence of a finite HT-TES capacity, the operation of the HP is not independent of the ORC size any longer. In fact, if a period of electricity deficit is not sufficiently long, a smaller ORC will discharge less heat from the HT-TES. In a following period of electricity surplus, the HT-TES will still be partially charged, so it will be able to receive less energy. Hence, smaller ORC decreases the number of cycles of the HT-TES (Figure 29), the number of full-load hours of the HP (Figure 24) and consequently the amount of absorbed electricity (Figure 26).

In Section 3.1.1 is discuss that an ORC relative capacity higher than 1 has a minor impact on the full-load hours of the ORC (Figure 25), while relative capacities lower than 1 increase the number of full-load hours. Consequently, the overall electricity production underwent a minor reduction when the ORC relative capacity decreases no lower than 0.5 (Figure 27).

In Figure 24 and Figure 25 is observed that, in the considered range of HP capacities, the HP capacity does not have a major impact on the electricity absorbed and produced by the CHEST system. Obviously, larger machines exchange more electricity in absolute terms (Figure 26 and Figure 27), but when this is normalized and the number of full-load hours is considered, their values are very similar and the curves mainly aligned.

The effect of the size of the HT-TES is in agreement with the results in Section 3.1.3, therefore larger HT-TES entails a strong increase in the number of full-load hours at this range of the HT-TES sizes.

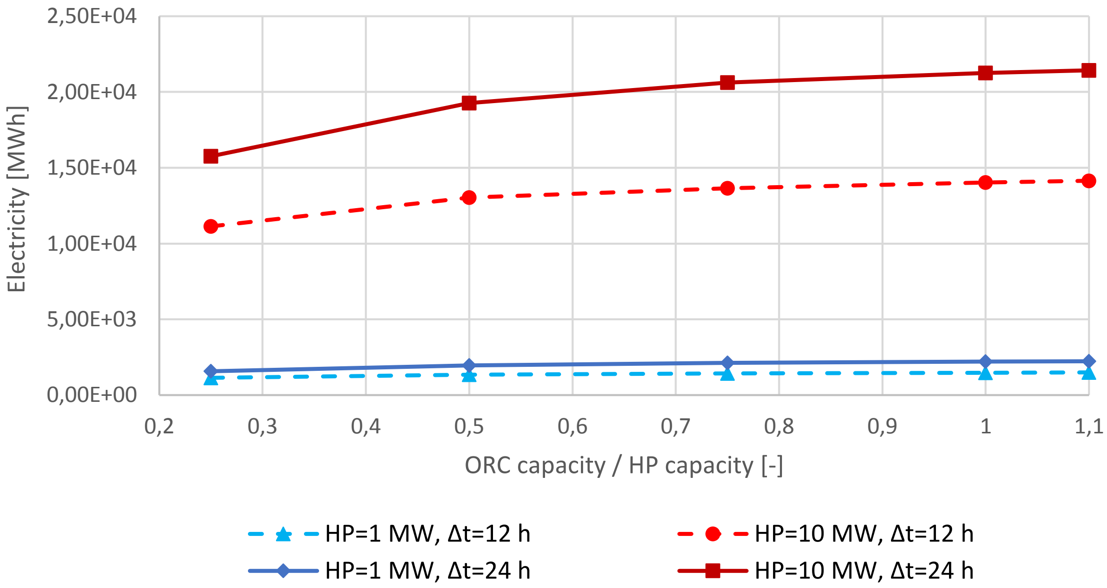

Figure 26: Electricity absorbed by the HP as function of the ORC relative capacity for the different HP capacities and HT-TES sizes.

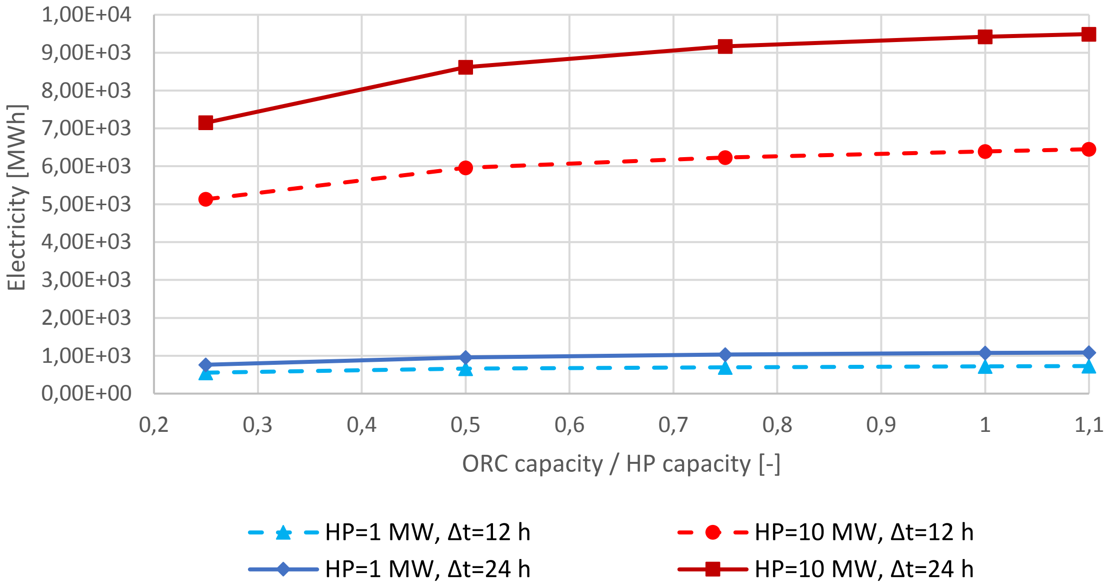

Figure 27: Electricity production from the ORC as function of the ORC relative capacity for the different HP capacities and HT-TES sizes.

The electricity absorbed by the HP and produced by the ORC affects the operation of the DH boiler, determining some additional heat output. Figure 28 shows the additional heat output from the DH boiler compared to reference scenario without CHEST as function of the ORC relative capacity for the four scenarios treated in this section.

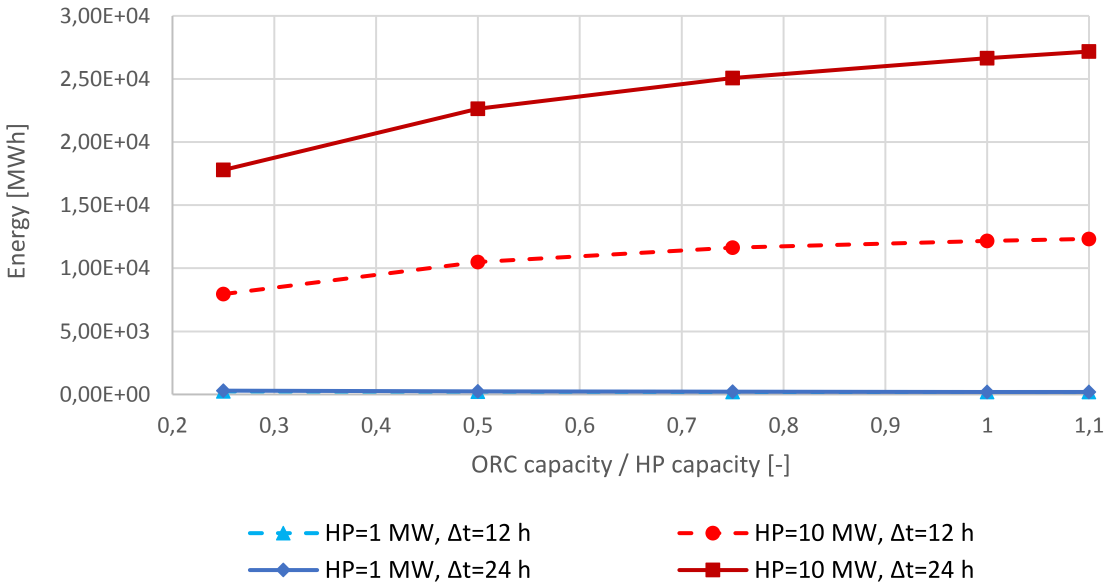

Figure 28: Additional heat output from the boiler compared to reference scenario without CHEST as function of the ORC relative capacity for the different HP capacities and HT-TES sizes.

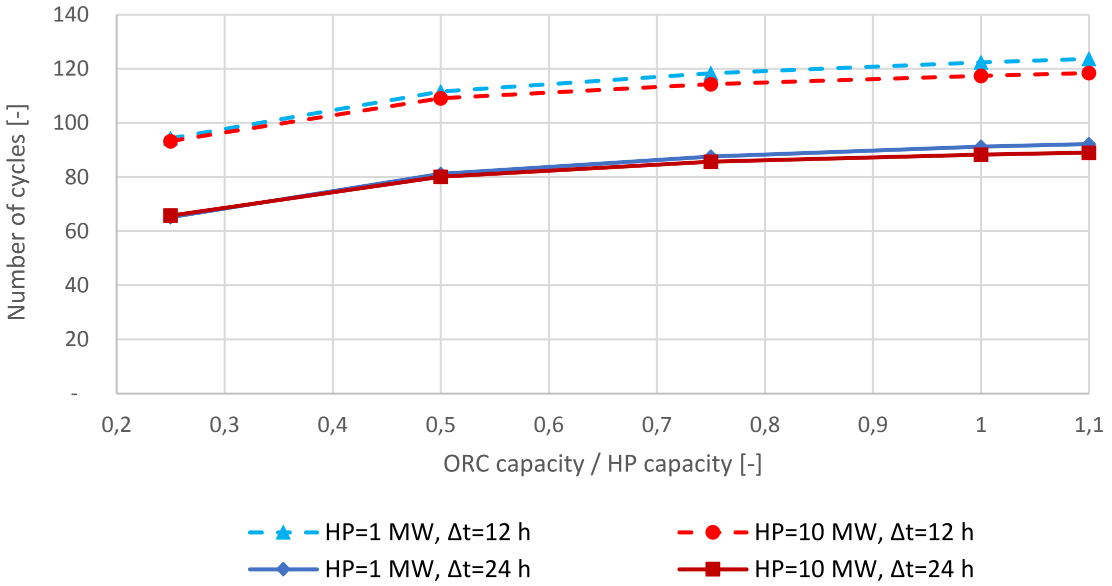

Figure 29: Number of cycles of the latent part of the HT-TES as function of the ORC relative capacity for the different HP capacities and HT-TES sizes.

The COP of the HP is mainly function of the HP capacity and its values are in agreement with those assumed for the sizing of the HT-TES (5.7 and 5.4, see above). In addition, the power-to-power ratio is mainly independent of the ORC relative capacity and the resulting values are basically identical to those presented in Section 3.1.3 for the same combinations of HT-TES size and HP capacity.

3.1.5. Working fluid: R1233zd(E) against Butene

All simulations presented in the previous sections are performed assuming Butene as working fluid in both the HP loop and in the ORC loop. In this section results based on R1233zd(E) as working fluid are presented and compared to the results previously obtained for Butene. The boundary conditions chosen for the simulations are the same as those described in Section 3.1.4, from where the results presented in this section and referring to Butene come from. Because of the similarity between the results for a HP capacity of 1 MW and for 10 MW in Section 3.1.4, only the latter is considered here.

Regarding R1233zd(E), the total capacity of the HT-TES is calculated as explained in Section 3.1.3. The assumed values of Δt are 12 and 24 hours. The value of COP_{ref} is 5.2 for R1233zd(E) for a HP capacity of 10 MW, which agrees with the results later obtained. The total capacity of the HT-TES is split between the latent and sensible part as explained in Section 3.1.2, using a ratio of 1.14 between the heat capacity of the latent and sensible part of the HT-TES, in agreement with the latent-to-sensible ratio of the HP.

The results regarding the HP operation (full-load hours and electricity use) are basically identical for Butene (Figure 24 and Figure 26) and R1233zd(E), hence are not reported here.

The number of full-load hours of the ORC and its electricity production are shown in Figure 30 and Figure 31 as function of the ORC relative capacity for both Butene and R1233zd(E) and for the two different HT-TES sizes. The trend of the curves with respect to the ORC relative capacity is the same as the described one in Section 3.1.4, so it is not further commented here.

Comparing the two fluids, it is seen that the CHEST system performs better when using R1233zd(E), producing on average 10 % more electricity compared to Butene.

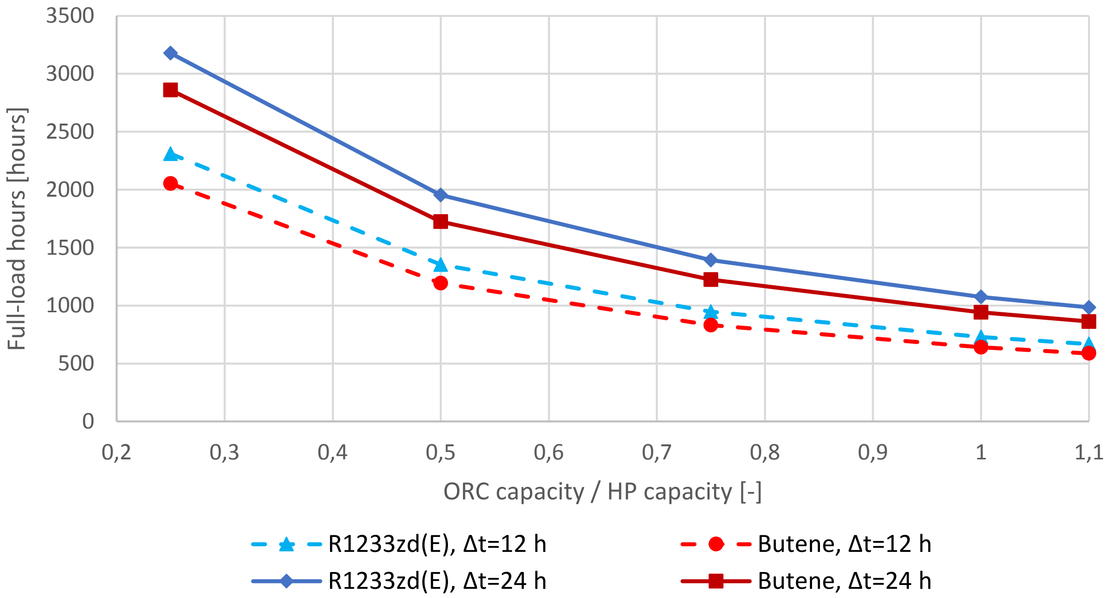

Figure 30: Full-load hours of the ORC as function of the ORC relative capacity for the different working fluids and HT-TES sizes.

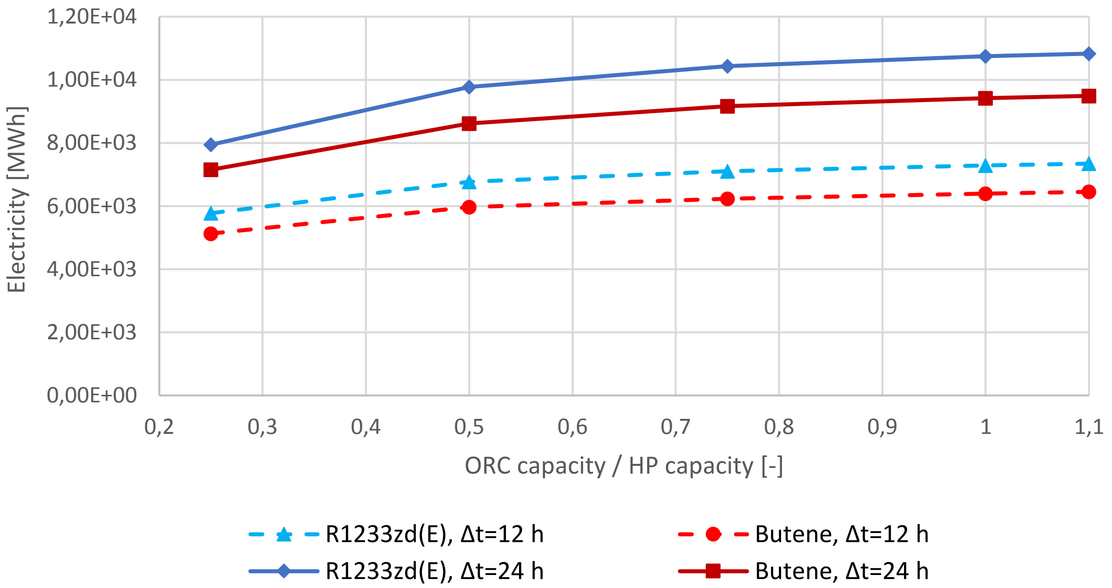

Figure 31: Electricity production from the ORC as function of the ORC relative capacity for the different working fluids and HT-TES sizes.

The better performance of the CHEST system when using R1233zd(E) might be seem in disagreement with the performance maps of the HP and of the ORC for the two different fluids, of which two extracts are presented in Table 15 and Table 16 at the relevant temperature levels (for the complete maps, refer to Section 2.2.3). The higher COP of the HP when using Butene (+4 %) is compensated by the slightly lower efficiency of the ORC (-4 %). The reason of the different performance is the different ratio between latent and sensible heat during charging and discharging. As explained in Section 3.1.2 for Butene, the large difference in latent-to-sensible ratio between the HP operation (0.74) and the ORC operation (1.1) entails that a portion of the heat stored in the sensible part of the HT-TES has to be dissipated through the clean-up procedure. Furthermore, Table 15 and Table 16 show that in case of R1233zd(E) the ratios are closer, about 1.15 in HP operation and 1.38 in ORC operation. This entails a lower amount of heat to be dissipated from the sensible heat part of the HT-TES, as can be seen in Figure 32.

Table 15: Extract of the performance maps of the HP using Butene and R1233zd(E) as working fluids.

Working fluid	$T_{source,in}$ [°C]	$T_{excess,in}$ [°C]	P'_{in} [kW]	Q'_{latent} [kW]	$Q'_{sensible}$ [kW]	$\frac{Q'_{latent}}{Q'_{sensible}}$ [-]	COP [-]
Butene	70	70	1056	2066	2817	0.73	4.62
Butene	80	70	1064	2468	3356	0.74	5.47
R1233zd(E)	70	75	1056	2517	2193	1.15	4.46
R1233zd(E)	80	75	1064	3016	2605	1.16	5.28

Table 16. Extract of the performance maps of the ORC using Butene and R1233zd(E) as working fluids.

Working fluid	$T_{sink,in}$ [°C]	Q'_{latent} [kW]	$Q'_{sensible}$ [kW]	P'_{out} [kW]	$\frac{Q'_{latent}}{Q'_{sensible}}$ [-]	η [-]
Butene	50	4643	4192	862	1.11	9.8%
R1233zd(E)	50	5178	3741	916	1.38	10.3%

This better use of the high-temperature heat stored in the HT-TES entails a higher power-to-power ratio in case of R1233zd(E), which is about 51 %-53 % in the two investigated scenarios, compared to 44 %-46 % in case of Butene.

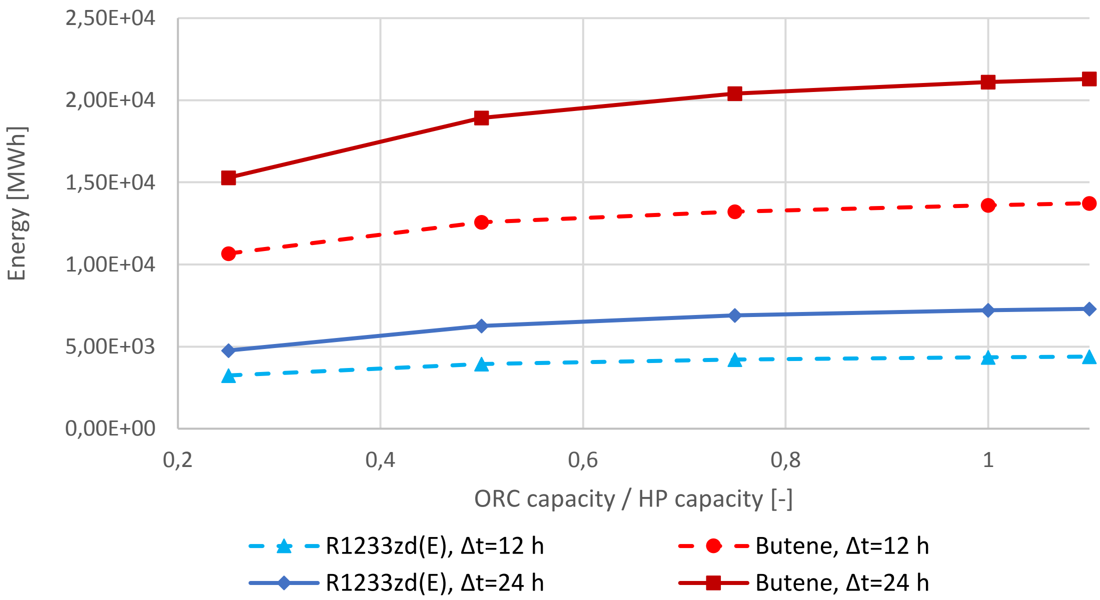

Figure 32: Heat to be dissipated from the sensible part of the HT-TES as function of the ORC relative capacity for the different working fluids and HT-TES sizes.

3.1.6. RES electricity production and electricity demand

All simulations presented in the previous sections are performed assuming a scaling of the profile of the RES electricity production such that the yearly production is equal to the yearly electricity demand of Aalborg. In this section two new scaling factors are chosen and accordingly the RES electricity production is 50 % higher and 50 % lower than the electricity demand respectively. The case with a RES electricity production equal to the electricity demand is used as reference. In every case, the hourly profiles of production and demand are the same as those shown in Figure 9 being the working fluid Butene.

Based on the above-mentioned assumptions, the values listed in Table 17 apply to the performed simulations.

Table 17: General parameters for used in the simulations. All values are expressed in MWh.

	Ratio between RES el. and el. demand		
	1.0	**1.5**	**0.5**
RES electricity production	1.40E+06	2.10E+06	6.99E+05
Electricity demand	1.40E+06	1.40E+06	1.40E+06
Electricity surplus	3.97E+05	9.67E+05	1.86E+04
Electricity deficit	3.97E+05	2.68E+05	7.18E+05
RES electricity directly used	1.00E+06	1.13E+06	6.80E+05

The three different RES penetration scenarios are simulated considering different HP capacities (ranging from 1 MW to 75 MW) and different ORC relative capacities (ranging from 0.25 to 1.10). The storage capacity of the HT-TES is calculated as explained in Section 3.1.3, assuming a value for Δt of 24 hours. The value of COP_{ref} is iteratively chosen corresponding to the actual yearly-average COP in the different scenarios.

Figure 33 shows the number of full-load hours of the HP as function of the ORC relative capacity for the different HP capacities and for the different investigated ratios between RES electricity production and electricity demand. A larger availability of RES electricity entails more full-load hours, especially for the larger HP and larger ORC. Larger HPs could better exploit the higher electricity surplus peaks, while larger ORCs are able to discharge more the HT-TES during hours of electricity deficit. However, the increase is relatively small compared to the increase in electricity surplus. This is expected, as an electricity production higher than the demand causes the system to be more often limited by the HT-TES being completely full. Conversely, a lower availability of RES electricity entails a drop in the number full-load hours, especially for the larger HP capacities, regardless of the ORC relative capacity. In fact, in this scenario most of the RES electricity could be directly use and a little amount is available as surplus (Table 17). Hence, a CHEST system with a HP capacity of 30 MW can absorb about 85 % of the entire electricity surplus. Larger systems turn out to be oversized.

The number of full-load hours of the ORC for the different combinations of HP and ORC capacities is shown in Figure 34. A larger availability of RES electricity has limited effect on the number of full-load hours for most of the combinations of HP and ORC capacities. Only at the lowest ORC relative capacity, there is a decrease in the full-load hours of the CHEST systems with the lower HP capacities, due to the lower amount of electricity which has been previously absorbed by the HP (Figure 33). However, the lower amount of electricity absorbed by the HP in case of lower availability of RES electricity also reduces the electricity production output of the ORC, which therefore presents fewer hours of full-load.

The COP of the HP is not significantly affected by the electricity availability, but mainly by the HP capacity. Since the resulting COPs are largely similar to those reported in Section 3.1.3, these are not repeated here, but can be read from Figure 22, entering the diagram with a value of Δt=24 hours on the x-axis and choosing the correct HP capacity from the legend. Similar considerations apply to the power-to-power ratio.

Overall, the higher availability of RES electricity compared to the demand seemed to favour larger CHEST systems, with HP capacities about 30 MW and ORC relative capacities about 0.2-0.5. Nevertheless, the lower availability of RES electricity seems to favour smaller systems, with HP capacities about 1-10 MW and ORC relative capacities about 0.2.

Although not shown in the report, the two scenarios with a RES electricity production 50 % higher and 50 % lower than the electricity demand are also simulated for a HT-TES storage capacity based on a value for Δt of 12 hours, instead of 24 hours. In case of a ratio between RES electricity production and electricity demand of 1.5, the smaller HT-TES causes a reduction of about 30 %-40 % in the number of full-load hours of both HP and ORC. Thus, it may be reasonable to maintain the larger HT-TES size. In case of a ratio between electricity production and demand of 0.5, the smaller HT-TES has a much smaller impact —i.e., a reduction of about 10 %-15 % in the number of full-load hours of both HP and ORC—, as in this case the electricity surplus represents the main limiting compared to the HT-TES capacity. In this case, the smaller HT-TES size seems more suitable.

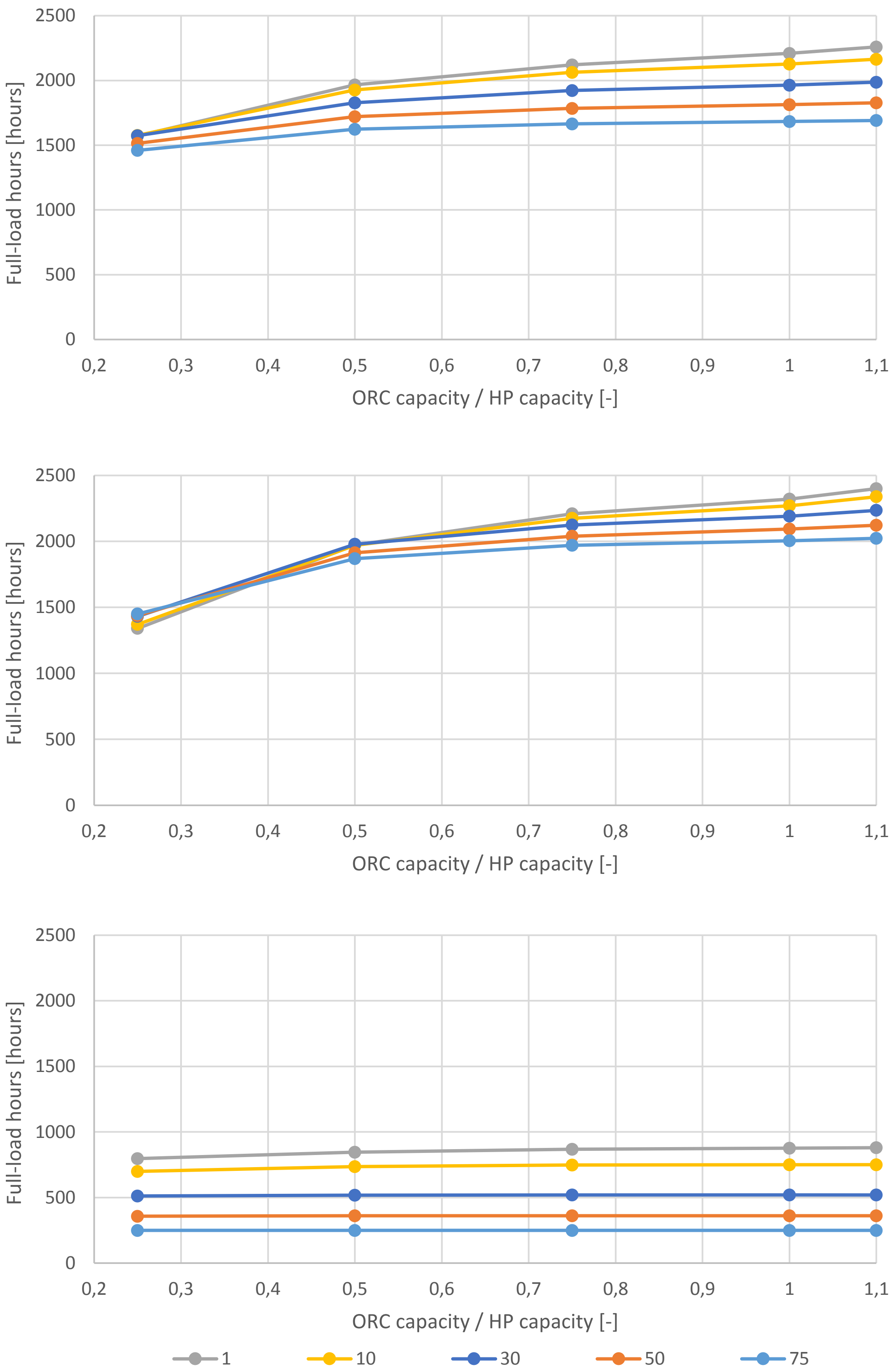

Figure 33: Full-load hours of the HP as function of the ORC relative capacity for the different HP capacities and a ratio between RES electricity production and electricity demand of 1 (top), 1.5 (middle) and 0.5 (bottom). HT-TES sized on a value of Δt=24 hours.

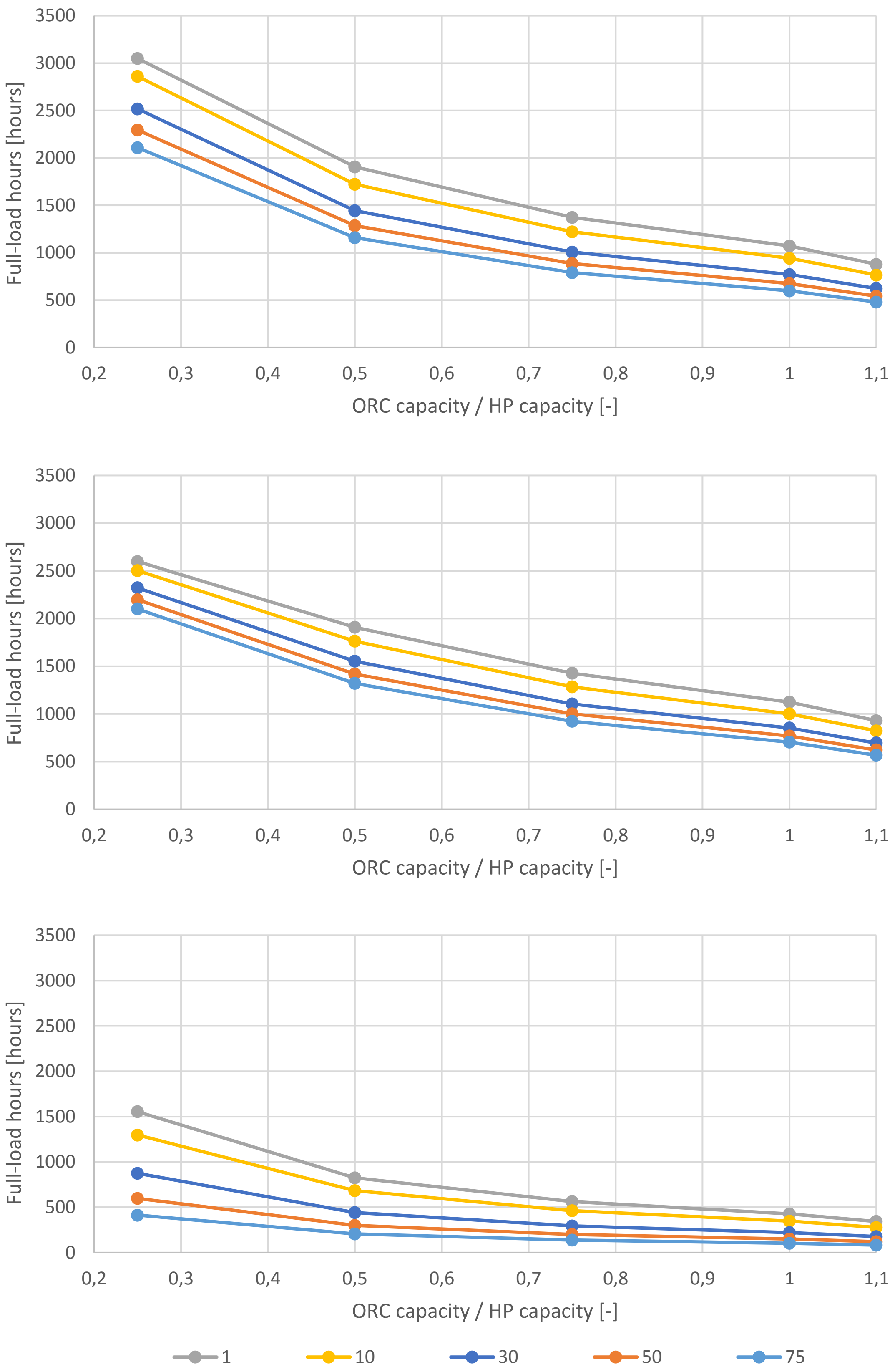

Figure 34: Full-load hours of the ORC as function of the ORC relative capacity for the different HP capacities and a ratio between RES electricity production and electricity demand of 1 (top), 1.5 (middle) and 0.5 (bottom). HT-TES sized on a value of Δt=24 hours.

3.1.7. Discussion

Based on the results presented in the previous sections, regarding the implementation of a CHEST system in the Aalborg case study, the following conclusions can be drawn.

The waste heat available (RES-heat) exceeds the DH load during summer time, thus the presence of the PTES in the TRNSYS model (which is under analysis in Aalborg) allows for this excess heat to be stored in summer and to be used later in autumn to cover the DH demand. Therefore, the system could avoid wasting this excess. The implementation of the CHEST system draws useful energy out of the PTES when in HP operation and injected it back during ORC operation. However, due to temperature constraints, not all low-temperature heat from the CHEST system could be reused within the system.

On the one hand, the system dissipates energy through the auxiliary cooling device *Max-temp-1* (Section 2.2.2), the non-reusable part of the excess heat from the HP (Q_{excess} in Section 2.2.4) and the auxiliary cooling device *Max-temp-6* (Section 2.2.5).

On the other hand, the CHEST system injects energy into the system in form of electricity absorbed by the HP (the electricity production from the ORC should be discounted, as it leaves the system). Overall, the low-temperature heat which is dissipated is higher than the net energy input coming from the absorbed electricity, so the implementation of the CHEST system entails an increase in the operation of the DH boiler.

However, it should be considered the benefit deriving from the ability to displace electricity from periods when it is in excess to periods when this lack. To quantify this benefit, it is necessary to have information on the value of the electricity in the different periods, the value of the balancing service that a CHEST system could provide to the electrical grid, the cost of the alternatives storage technologies as well as the technical and economic factors which apply to the dispatch of electricity.

The assumed boundary conditions suggest that a CHEST system implemented in the Aalborg case could have the following characteristics:

- nominal electric capacity of the HP around 10 MW,
- nominal capacity of the ORC which is around 50 % of that of the HP,
- nominal a capacity of the HT-TES able to store 12-24 hours of electricity input to the HP,
- ratio between the storage capacity of the latent heat part of the HT-TES and the sensible heat part equal to 0.74, i.e. around the latent-to-sensible ratio of the HP.

The latent-to-sensible ratio of the of the HT-TES can also be used to regulate the clean-up procedure of the sensible heat part of the HT-TES, in order to optimize the use of its storage capacity.

Regarding the working fluid, the comparison between Butene and R1233zd(E) shows that the latter gives a better performance under the assumed boundary conditions, due to the more similar latent-to-sensible ratios of the HP and of the ORC, which allow a more efficient use of the heat stored in the HT-TES. However, it should be noted that other considerations may apply when choosing the working fluid, such as safety of operation, environmental impact, compatibility with lubricants, cost, etc. The identification of the best fluid for the CHEST components is out of the scope of this analysis and will be further researched within the project in WP3 and WP4.

As for the availability of electricity surplus, its higher availability seems to favour larger CHEST systems, with larger HP capacities compared to those suggested above, and relatively similar ORC relative capacities. Nevertheless, the lower availability of RES electricity seems to favour smaller HP capacities, smaller ORC relative capacities and smaller HT-TES.

No specific recommendation on the relative size of the LT-TES capacity with respect to the HT-TES capacity can be given. As the LT-TES is used also as seasonal storage between the RES-heat source and the DH network, its sizing cannot be merely related to the CHEST system. Additionally, to keep the boundary conditions as close as possible to the realistic boundary conditions in Aalborg case, the volume of the PTES (acting as LT-TES within the CHEST system) is kept constant and equal to 1,000,000 m^3. In principle, the CHEST system can also operate in connection of a DH network without the LT-TES. During HP operation, heat could be drawn from the supply pipe before entering the DH boiler, at a temperature which has as upper limit the RES-heat temperature and as lower limit the return temperature from the DH network. The actual temperature would be determined by the relative quantities of RES-heat and DH load, as well as the control strategy. During ORC operation, the condensing heat could be injected back in the return pipe of the DH loop, pre-heating it.

3.2. Case Study #5: Alpha Ventus Wind Park, Germany

The effects of the implementation of a CHEST system in the Alpha Ventus case study (see deliverable D2.1 of the CHESTER project) are investigated through TRNSYS simulations under different boundary conditions. As was described in deliverable D2.1, in this case study the electricity production profiles are taken from the Alpha Ventus Wind Park in the North Sea. Since neither the near-by cities Emden nor Norden could provide data in the required level of detail, the other input data (electricity demand, heat production and demand, forward and return temperatures of the district heating system) come from a district in the Southern German city Crailsheim. The chosen district of the city Crailsheim fits well regarding size and structure and represents a typical district to be provided with energy from the CHEST system.

In the TRNSYS model the integration of the CHEST system is assumed, considering the current structure and the energy demands of the energy system in Crailsheim. As was said in deliverable D2.1 the currently installed borehole thermal energy storage is not suitable for being used as a PTES due to the very limited charging and discharging power. However, for taking a reasonable value for the PTES volume in the simulations, which fits to the heat supply system, this borehole thermal energy storage served as an orientation. As was mentioned in deliverable D2.1, the borehole thermal energy storage has a volume of 39,000 m^3, which is however the volume of the ground soil up to a certain distance around the boreholes. Based on the available information about density and specific heat capacity of this ground soil a volume of 26,000 m^3 has finally being chosen as the PTES volume to be used in all simulations.

A second important issue to be determined before running the simulations is about scaling of the profiles. Without scaling, the yearly electricity production from the wind park is about 227.8 GWh, while the yearly electricity consumption of the district in Crailsheim accounts for about 1.39 GWh, which is a factor of about 164 between the yearly electricity production and the yearly electricity consumption.

Scaling the wind park profile to 1/164th of its original value does not seem reasonable, because in this case the maximum electricity surplus and deficit would account for only 0.3 MW which would then be the upper value of the investigated capacity range of the CHEST system. Additionally, such scaling would not represent the actual situation of the wind farms in north Germany, whose electricity output is often higher than the electricity demand in northern Germany and must hence be transported elsewhere through the transmission lines, sometime up to their full transmission capacity. For the same reason, scaling up the electricity consumption profile by a factor of 164 is not considered. Finally, it has being decided to apply a factor of 1/16.4 to the electricity production profile and a factor of 10 to the electricity consumption profile. This results in a maximum electricity surplus of around 2.7 MW and a maximum electricity deficit of around 2.6 MW. Considering a scaling factor of 10 means that all hourly electricity consumption values are multiplied with this factor. It is not considered here that such a greater electricity consumption (resulting from a greater district of this city) would maybe show a smoothing of peaks due to simultaneity effects. All the simulations described in Sections 3.2.1 to 3.2.5 have been carried out with the above-mentioned scaling factors.

However, as the pronounced objective of this case study is to investigate the situation of decisive electricity production excess (see case study description in deliverable D2.1), some simulations have also been carried out with a ratio of the RES electricity production to electricity demand of > 1.0. The results of these simulations can be found in 3.1.6.

In all simulations, the heat side is taken in its original form, i.e. no scaling is applied to the RES heat generation and the heat demand profile and the DH supply and return temperatures are taken exactly as retrieved from the monitoring data of the DH network in Crailsheim.

To sum it up, the following inputs are used as input files required by the TRNSYS model (Section 2.2.1):

- *RES-el*: the measured electricity production profile from the wind park Alpha Ventus is used. For the first part of the simulations (Sections 3.2.1 to 3.2.5), this is appropriately scaled so that the yearly electricity production from the wind park is equal to the yearly electricity consumption of the district in Crailsheim. For the second part of the simulations (Section 3.1.6) it is scaled so that there is a considerable excess of electricity production compared to the electricity consumption in order to investigate a scenario that is quite typical or will be in the nearer future for the North of Germany.
- *El-demand*: the (synthetic) electricity load profile of the district in Crailsheim is used. Concerning scaling see the comments above.
- *RES-heat*: the measured RES heat generation profile from the DH network in Crailsheim is used. Due to data deficiencies and difficulties in directly calculating the heat generation from the solar thermal collectors, difference between the DH heat demand and the backup heating via the auxiliary heating grid (see descriptions in deliverable D2.1) is taken as the RES heat generation profile. No scaling is applied.
- *Heat-demand*: the measured load profile from the DH network in Crailsheim is used. No scaling is applied.
- *DH-T-fwd*: the measured supply temperatures of the DH network in Crailsheim are used.
- *DH-T-rtn*: the measured return temperatures of the DH network in Crailsheim are used.

The (synthetic) profile of the electricity demand is shown in Figure 35. The scaling of the profile as described above is implemented in this figure. In Figure 35 can be observed distinct steps in the profile showing differences in the electricity consumption between the several months. This is a result of the synthetic generation of the profile with defined monthly scaling factors for the electricity consumption for the different consumers like the single-family houses, the street lights, the commercial buildings and so on. The synthetic profile also contains such scaling factors for the hours of the day, however, this is not visible in Figure 35. The profile of the electricity production from RES cannot be shown here due to confidentiality reasons.

The profiles of DH heat demand, RES heat availability and the temperatures of the DH network used as input in the TRNSYS model for the Alpha Ventus case are shown in Figure 36.

Regarding the performance maps, Butene is assumed as working fluid in all presented scenarios, with the only exceptions of the cases presented in Section 3.2.5.

The temperatures $T_{P3,min}$ and $T_{P3,max}$, which regulate the operation of the pump *Pump-3* and hence the discharging of the LT-TES, are 70 °C and 85 °C respectively in all the presented scenarios (Section 2.2.2).

As a reference scenario, a TRNSYS simulation is performed without the CHEST system, to identify the performance of the DH system itself and also to compare certain results in the context of the electricity grid between the situation with and without CHEST system (Section 3.2.6).

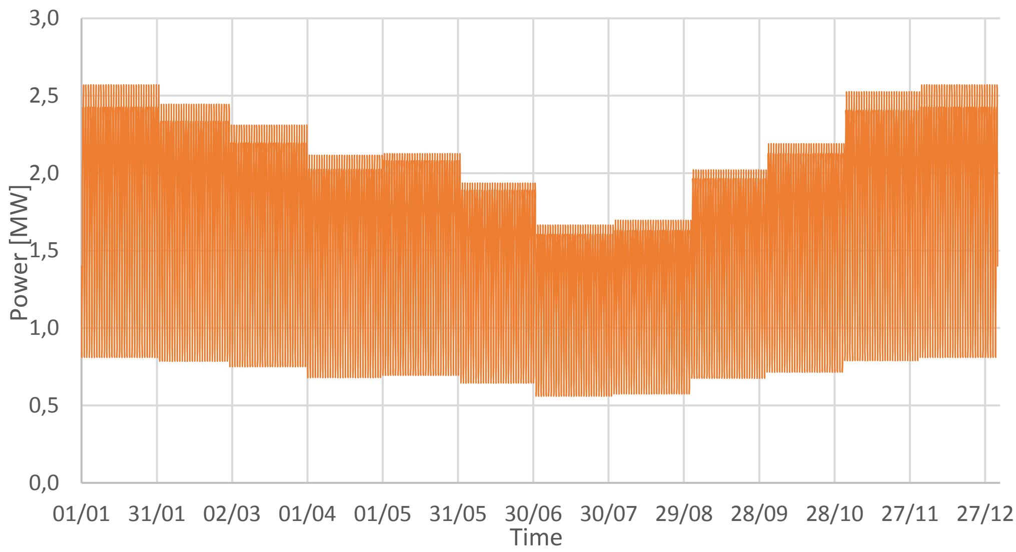

Figure 35: Profile of electricity demand used in Alpha Ventus case.

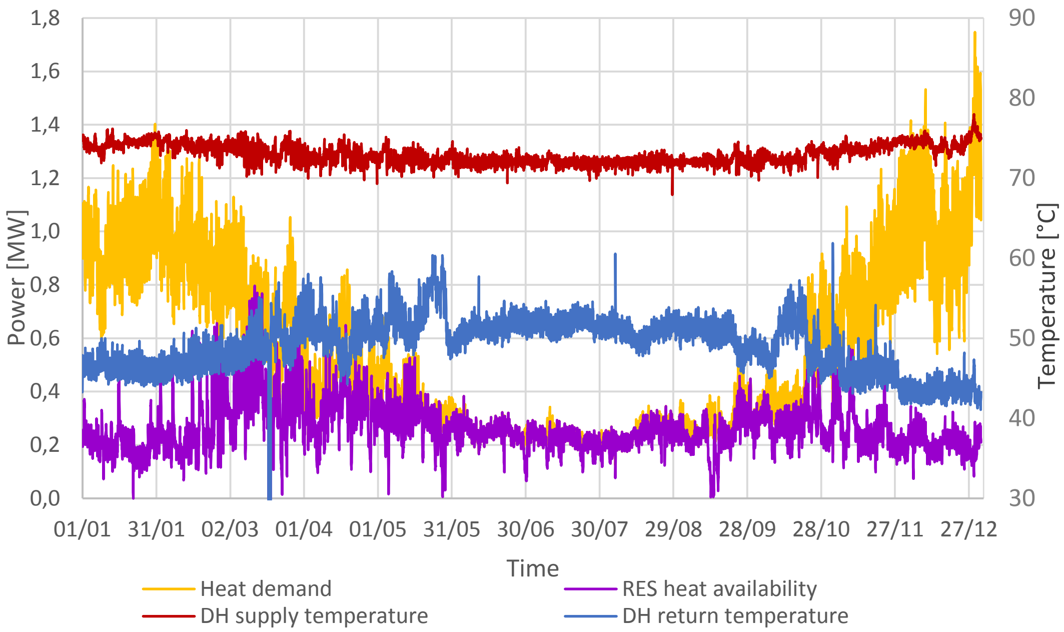

Figure 36: Profiles of DH demand, RES heat availability and DH temperatures used in Alpha Ventus case.

Under the above-mentioned boundary conditions and energy profiles, the parameters listed in Table 18 are constant in all the presented scenarios, unless otherwise specified.

Table 18: General parameters used in the simulations.

	Energy [MWh]
RES electricity production	13,892
Electricity demand	13,880
RES-heat available	2,315
DH heat demand	4,917
Electricity surplus	4,782
Electricity deficit	4,770
RES electricity directly used	9,110

An overview of the parameters which are varied in the parametric analyses is presented in Table 19.

Table 19: Overview of the main parameters varied in the different parametric analyses presented in the following sections (Section 3.2.1-3.2.6) of this deliverable.

Section number		3.2.1-Constant ratio	3.2.1-Variable ratio	3.2.2	3.2.3
RES-electricity / Electricity demand	[-]	1.0	1.0	1.0	1.0
Capacity of HT-TES, Δt	[h]	Infinite	120	40, 4	2 - 120
Latent-to-sensible ratio of HT-TES	[-]	-	0.714	0.714	0.714
Fluid		Butene	Butene	Butene	Butene
HP capacity	[MW]	0.1 – 3.0	0.1 – 3.0	0.1, 1.0	0.1 – 3.0
ORC capacity / HP capacity	[-]	1.00	0.25 - 1.00	1.00	1.00
Section number		**3.2.4**	**3.2.5**		**3.2.6**
RES-electricity / Electricity demand	[-]	1.0	1.0	1.0	1.0, 2.0, 5.0
Capacity of HT-TES, Δt	[h]	8, 24	8, 24	8, 24	40, 80, 120
Latent-to-sensible ratio of HT-TES	[-]	0.714	0.714	0.714	0.714
Fluid		Butene	R1233zd(E)	Butene	Butene
HP capacity	[MW]	0.2, 2.0	0.2, 2.0	0.2, 2.0	3.0
ORC capacity / HP capacity	[-]	0.25 - 1.20	0.25 - 1.20	0.25 - 1.20	1.00

3.2.1. HP and ORC capacity with large HT-TES

Constant ratio between HP and ORC capacity

First, the size of the HP and of the ORC of the CHEST system are varied to identify the most relevant range of capacities to be investigated in connection to Alpha Ventus case. Figure 37 shows the electricity surplus and electricity deficit over the year. As already mentioned in the introduction of this case study, the maximum electricity surplus accounts for around 2.7 MW while the maximum electricity deficit is around 2.6 MW.

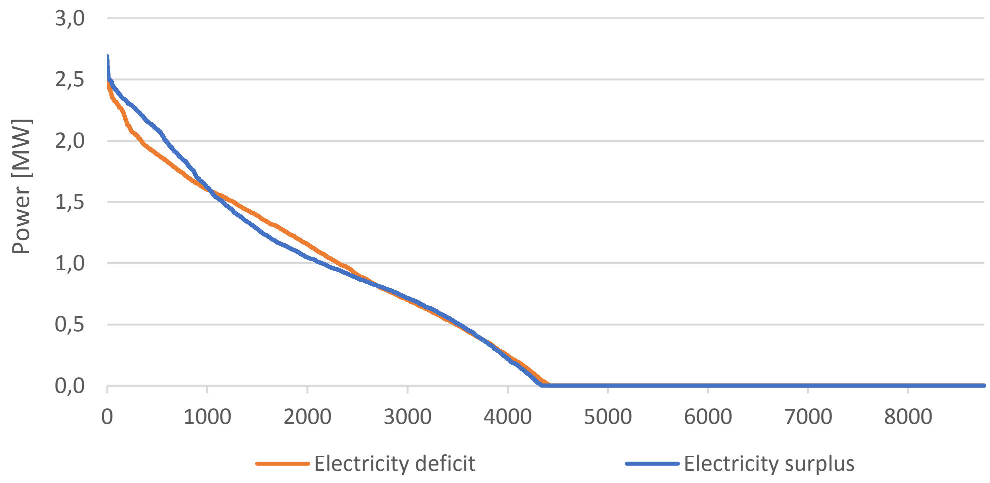

Figure 37: Distribution of electric surplus and electric deficit in Alpha Ventus case during the year (8760 hours).

Based on this it is chosen to vary the HP and ORC capacity in a range of 0.1 to 3 MW, keeping constant the ratio between the HP capacity and the ORC capacity. In this set of simulations, the storage capacity of the HT-TES is assumed so large, that it would never be get completely full. In this way, the storage capacity can be regarded as infinite.

As mentioned above, the size of the LT-TES is kept constant and equal to 26,000 m^3.

Figure 38 shows the electricity absorbed by the HP and the electricity produced by the ORC as function of the HP and ORC capacity. Increasing the capacity of the HP and of the ORC increases the electricity absorbed by the HP and that produced by the ORC. Towards large capacities again an asymptotic behaviour is visible. Especially when comparing the results of an HP and ORC capacity of 2 and 3 MW, almost no increase of the electricity absorbed by the HT-HP and the electricity produced by the ORC. This is due to the fact that electricity surplus and deficit above 2 MW is available only few hours per year as can be recognized from Figure 37. For the lower HP and ORC capacities of about 0.1 - 1 MW the slope of the electricity curves is approximately linear.

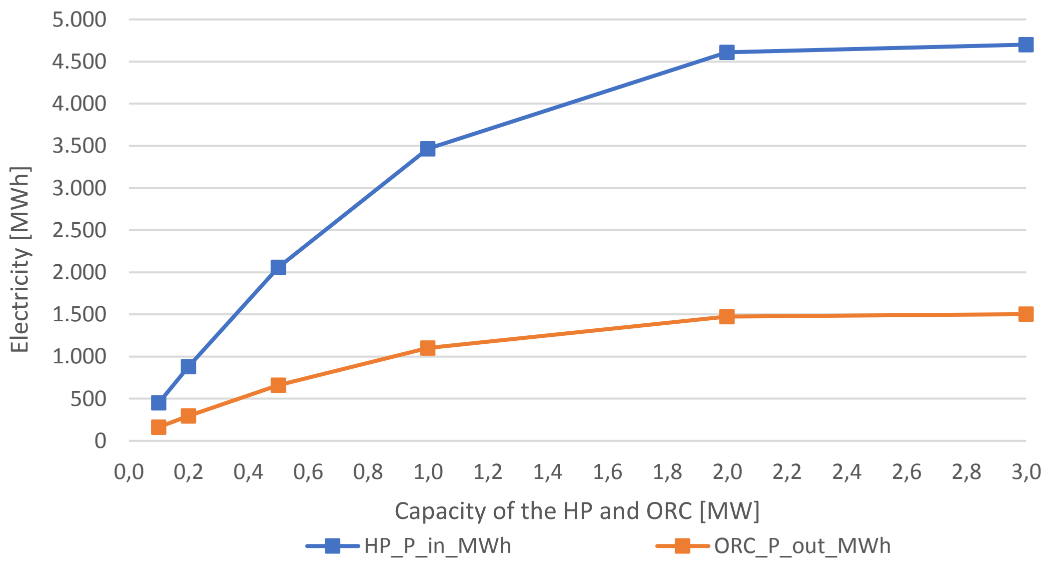

Figure 38: Electricity absorbed by the HP and produced by the ORC as function of the HP and ORC capacity (infinite HT-TES size).

In Figure 39 can be observed the effect of the HP and ORC capacity on the full-load hours of the HP and of the ORC. The diagram looks similar to the one presented for the Aalborg case, i.e. an increase of the HP and ORC capacity results in a decrease in the full-load hours for both the HP and the ORC. This is due to the fact that in Figure 38 the slope of the HP curve is also steeper, because the full load-hours are calculated by the electricity absorbed/produced divided by the HP and ORC capacity as is pointed out in Section 3.1.1.

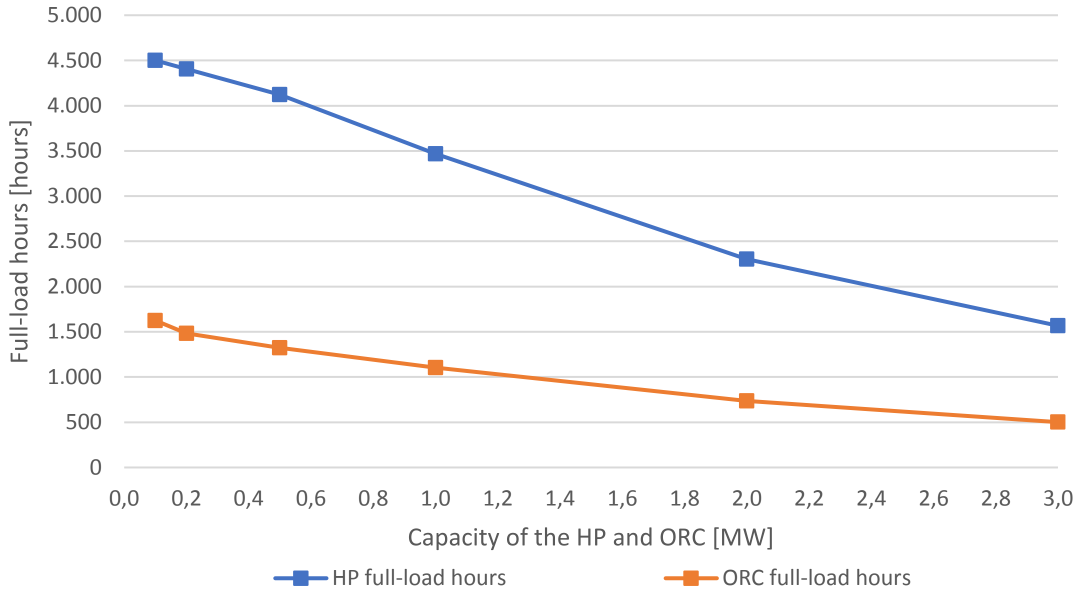

Figure 39: Full-load hours of the HP and of the ORC as function of their capacity (infinite HT-TES size).

The COP of the HP, the efficiency of the ORC and the power-to-power ratio of the CHEST system defined as the ratio between the electricity produced by the ORC and the electricity absorbed by the HP can be shown in Figure 40.

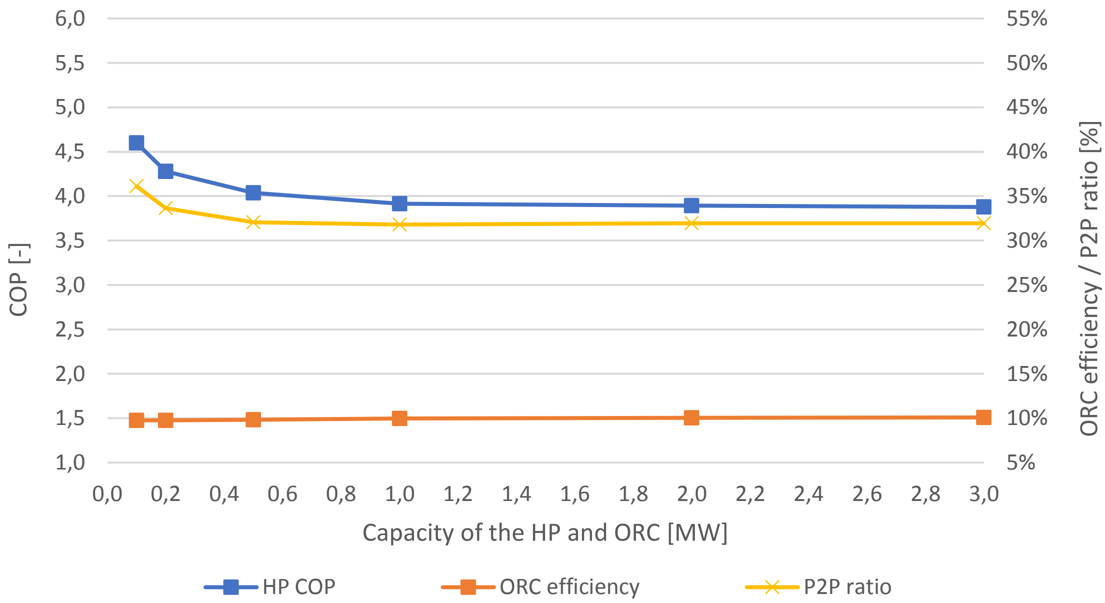

Figure 40: COP of the HP, efficiency of the ORC and power-to-power (P2P) ratio as function of the HP and ORC capacity (“infinite” HT-TES size).

The ORC efficiency is nearly constant (about 10 %), while the COP and the power-to-power ratio show a slight decrease with increasing HP and ORC capacity. As it has already been explained in Section 3.1.1, the decreasing COP with increasing HP capacity is a result of the lower temperatures in the top of the LT-TES, because the HP takes up more heat from the LT-TES. Due to the constant ORC efficiency the P2P shows the same trend as the COP.

A difference compared to the Aalborg case consists of the slightly lower COP at lower HP and ORC capacities. For the higher HP and ORC capacities where the COP is almost independent of the HP and ORC capacity, the COPs of the Aalborg and of the Alpha Ventus case are comparable showing a value of about 4.0 for Aalborg and 3.9 for Alpha Ventus case.

Due to some heat dissipation as a result of the ORC operation (ORC blow-off), this heat has to be brought back into the system, which is done by an additional boiler. Figure 41 shows the curves for both the heat of the boiler and of the ORC blow-off dependent on the HP and ORC ratio.

The figure shows that the ORC blowoff increases with increasing HP and ORC capacity, but at higher HP and ORC capacities this increase gets smaller and finally the ORC blowoff stays constant at the highest HP and ORC capacity chosen here. The boiler shows a bit different trend with also an increase at the lowest HP and ORC capacities, followed by a decreasing trend and finally also almost constant values meaning that there is almost no dependency of the boiler output on the HP and ORC capacity at a HP and ORC capacity range of 1 - 3 MW.

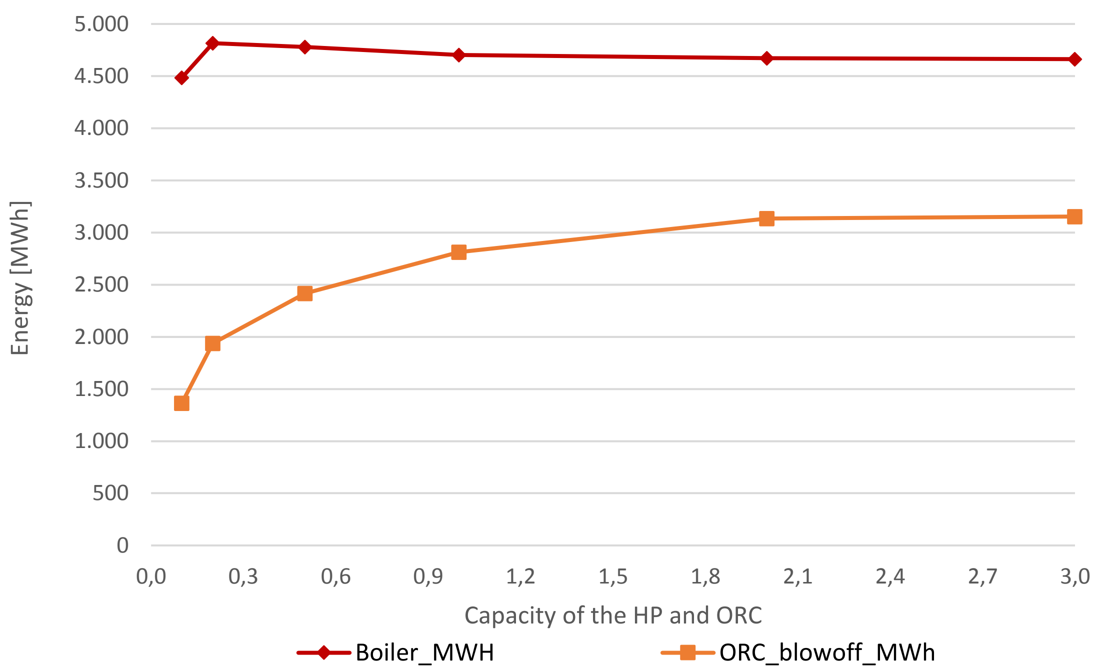

Figure 41: Heat dissipated by the auxiliary cooling device before the condenser of the ORC (Section 2.2.5) and heat production from the DH central plant.

Compared to the scenario without CHEST, the investigated scenarios with CHEST have the benefit of being able to store excess electricity and release it at times with lack of electricity in the grid (Figure 38), with a slightly higher heat demand for balancing the ORC heat blow-off (Figure 41). The relevant data are listed in Table 20.

Table 20: Electricity absorbed by the HP and electricity produced by the ORC, and boiler operation in the investigated scenarios.

HP and ORC capacity [MW]	Electricity absorbed by HP [MWh]	Electricity produced by ORC [MWh]	Boiler output [MWh]	Boiler output compared to reference [MWh]
Reference (No CHEST)	-	-	3,092	-
0.1	449	163	4,484	1,392
0.2	879	295	4,816	1,724
0.5	2,061	656	4,778	1,686
1	3,468	1,093	4,703	1,610
2	4,540	1,435	4,671	1,579
3	4,631	1,464	4,662	1,570

Variable ratio between HP and ORC capacity

In this section, different ratios between HP and ORC capacities are simulated while keeping the other boundary conditions constant. The HT-TES is sized on a Δt=120 h. This value is chosen, after observing that the results in case of a constant ratio between HP and ORC capacity (see previous subsection) does not differ significantly when assuming Δt=4000 h and Δt=120 h. Hence, a HT-TES with Δt=120 h can be regarded as having a practically "infinite" storage capacity for the chosen electricity profiles. Some selected results are shown in the following tables (Table 21, Table 22 and Table 23).

Table 21: Electricity production from the ORC in MWh for different HP capacities and ORC/HP capacity ratios.

		HP capacity [MW]					
		0.1	0.2	0.5	1	2	3
ORC capacity relative to HP capacity [-]	0.25	91	181	438	793	1,294	1,515
	0.50	129	241	544	970	1,468	1,495
	1.00	152	281	627	1,070	1,473	1,503

Table 22: Power-to-power ratio of the system for different HP capacities and ORC/HP capacity ratios.

		HP capacity [MW]					
		0.1	0.2	0.5	1	2	3
ORC capacity relative to HP capacity [-]	0.25	38.2%	35.4%	32.7%	31.9%	32.4%	32.3%
	0.50	37.2%	34.4%	32.3%	31.8%	32.1%	31.9%
	1.00	36.6%	33.9%	32.1%	31.8%	32.0%	32.0%

Table 23: COP of the HP for different HP capacities and ORC/HP capacity ratios.

		HP capacity [MW]					
		0.1	0.2	0.5	1	2	3
ORC capacity relative to HP capacity [-]	0.25	4.9	4.5	4.2	4.0	4.1	4.0
	0.50	4.7	4.4	4.1	4.0	4.0	3.9
	1.00	4.7	4.3	4.1	4.0	3.9	3.9

The simulation results first show that at high HP capacities (2 and 3 MW) the electricity absorbed by the HP and produced by the ORC, respectively, as well as the performance parameters (COP, ORC efficiency and power-to-power ratio) are nearly independent of the ratio between HP and ORC capacity. The COP does also not show this dependency on the ratio between HP and ORC at lower HP capacities, because changing the ORC capacity has in principle no effect on the performance of the HP. As the COP only shows minor changes with increasing the ratio between ORC and HP capacity, so does the power-to-power ratio, because the ORC is still on the same level of about 10 %.

Some changes in the ORC electricity production can be observed in Table 21 when the ratio between HP and ORC capacity is changed, at least at lower HP capacities. This can be explained with the behaviour shown in Figure 38. At a given HP capacity, increasing the ratio between ORC and HP, the ORC capacity increases, as well as the ORC electricity production, but the higher this ORC capacity gets the lower is the increase.

Despite of the same finding between the Aalborg and the Alpha Ventus case, i.e. the performance parameters show a small dependence on the ratio between HP and ORC capacity, the trend of this dependence is different in the two cases. In Aalborg case the COP and the power-to-power ratio increased with increasing the ORC capacity at a fixed HP capacity (Table 13). In contrast, Table 22 and Table 23 show a decrease of these two performance parameters with an increase of the ORC capacity at a fixed HP capacity.

This leads to the conclusion that a ratio of ORC to HP capacity of lower than 1 is favourable; thus, building up a smaller ORC motor compared to a ratio of 1. Looking at the ORC electricity production values in Table 21, it is reasonable to apply an ORC/HP capacity ratio of 0.5 for getting only a negligible reduction of the ORC electricity production compared to a ratio of 1. Further results and discussions on the ratio between HP and ORC capacity, with a limited size of the HT-TES, will be given in Section 3.2.4.

3.2.2. Finite size of HT-TES: ratio between latent and sensible part

All simulations performed for Alpha Ventus are performed using the standard clean-up strategy, as described in Section 2.2.6. The ratio between the capacity of the latent part and the sensible part of the HT-TES is always 5:7 (≈0.714).

The problem of a mismatch in the curves for the State of Charge (SoC) of the latent and the sensible part of the HT-TES is observed here as is shown in Figure 42 and Figure 43.

During discharging, the latent part of the HT-TES is discharged faster than the sensible part so the state of charge of the two parts is not the same anymore. Once there is a mismatch of the two curves this situation can continue for several charging and discharging cycles until both parts of the HT-TES get empty, because then the HP charges the two parts of the HT-TES uniformly again.

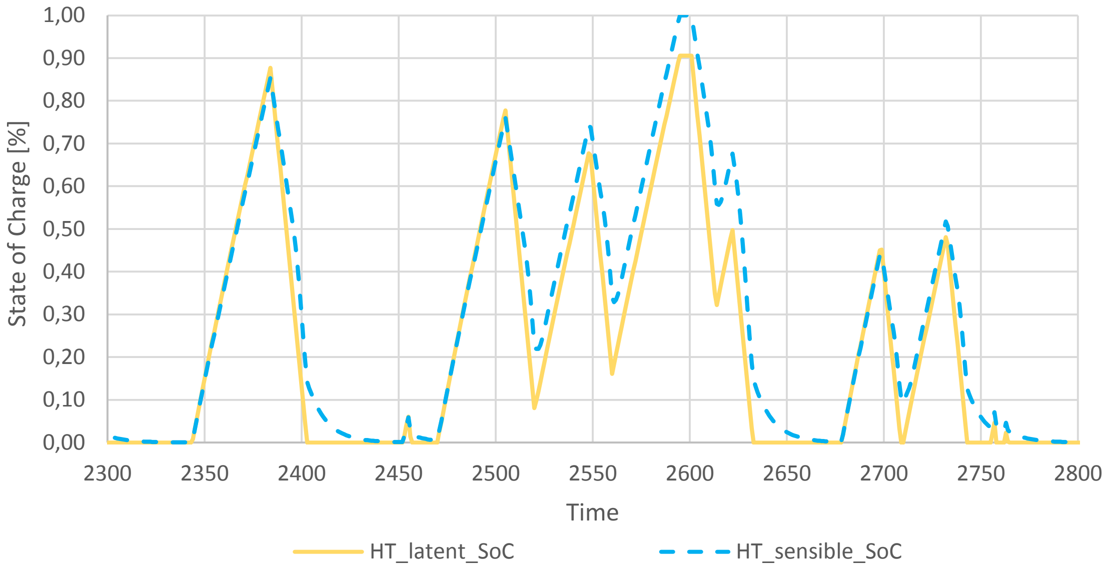

Figure 42: State of charge in the latent and sensible part of the HT-TES according to the standard clean-up strategy described in Section 2.2.6 (HP and ORC capacity of 0.1 MW, HT-TES Δt = 40 h).

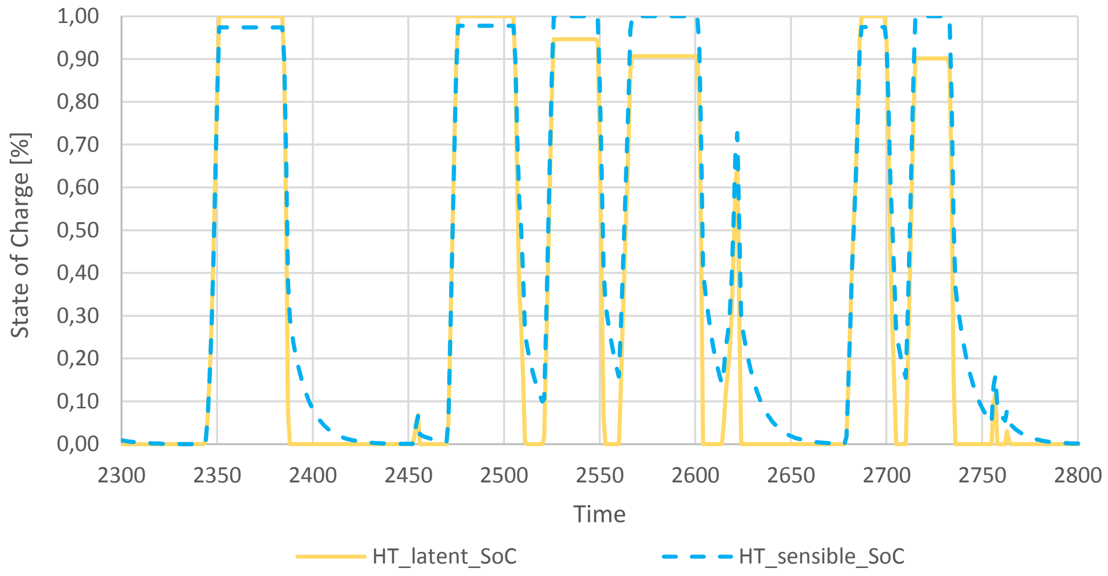

Figure 43: State of charge in the latent and sensible part of the HT-TES according to the standard clean-up strategy described in Section 2.2.6 (HP and ORC capacity of 1 MW, HT-TES Δt = 4 h).

When the latent part of the HT-TES is discharged stronger, as said above, it means that in the coming charging period the sensible part of the HT-TES will reach its full capacity sooner. This stops the HP operation, hence, the latent part is not further charged. That is why several times in Figure 43 it can be observed a fully charged sensible HT-TES and a constant, but lower SoC of the latent HT-TES in this situation.

However, Figure 43 shows the opposite case. Namely, there is a fully charged latent part and a sensible part close to, but not fully charged. This is probably due to the fact that the ratio of latent to sensible part is chosen with 0.714 here, which is slightly lower than the approximately 0.74 in the HP performance map. This means that starting from a fully empty HT-TES, it will be charged with the ratio of 0.74, but as the latent part is (relative to this) a bit smaller, it is charged sooner and when the latent part is fully charged also stops the HP operation.

The conclusion, based on the used performance map, where the factor between the heat transferred to the latent part of the HT-TES and the heat transferred to the sensible part during HP operation is nearly constant (around 0.74), is that this value should be taken as the ratio between latent and sensible part of the HT-TES. Regarding the clean-up strategy, the new strategy described in Section 3.1.2 is implemented in Alpha Ventus case, but the effect can be expected to be the same as in Aalborg case, with a better utilization of the HT-TES.

3.2.3. Storage capacity of HT-TES

Simulations with different storage capacities of the HT-TES are carried out, using different HP and ORC capacities, but with a constant ratio 1:1. As it is pointed out in the previous section, the ratio of the latent to sensible part of the HT-TES is the same for all simulations (about 0.714). According to the approach presented in Section 3.1.3, the storage capacity is also expressed in a time Δt, needed for a HP with capacity $W_{p,HP}$ and COP COP_{ref} to completely charge the HT-TES when operating at full load. A COP of 6 is assumed, while the time Δt is varied in the range 2 - 120 h.

The effect of a finite HT-TES capacity on the full-load hours of the HP and of the ORC is shown in Figure 44 and Figure 45. The legend denotes that the different curves refer to different HP (and ORC) capacities (in MW).

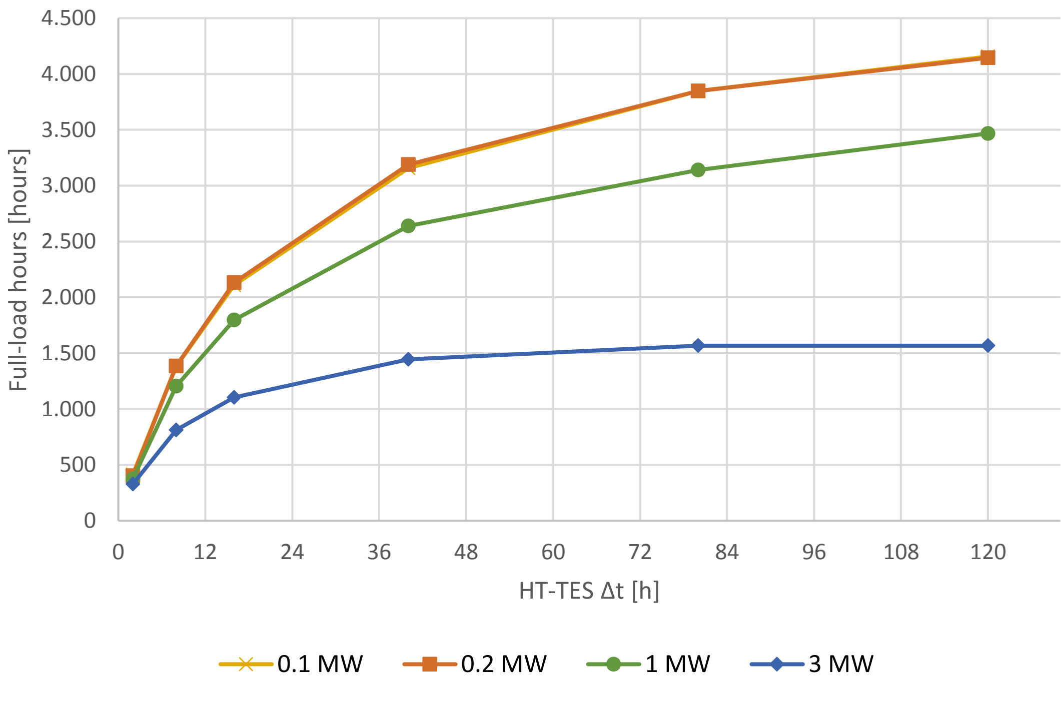

Figure 44: Full-load hours of the HP as function of the HT-TES capacity for different HP (and ORC) capacities.

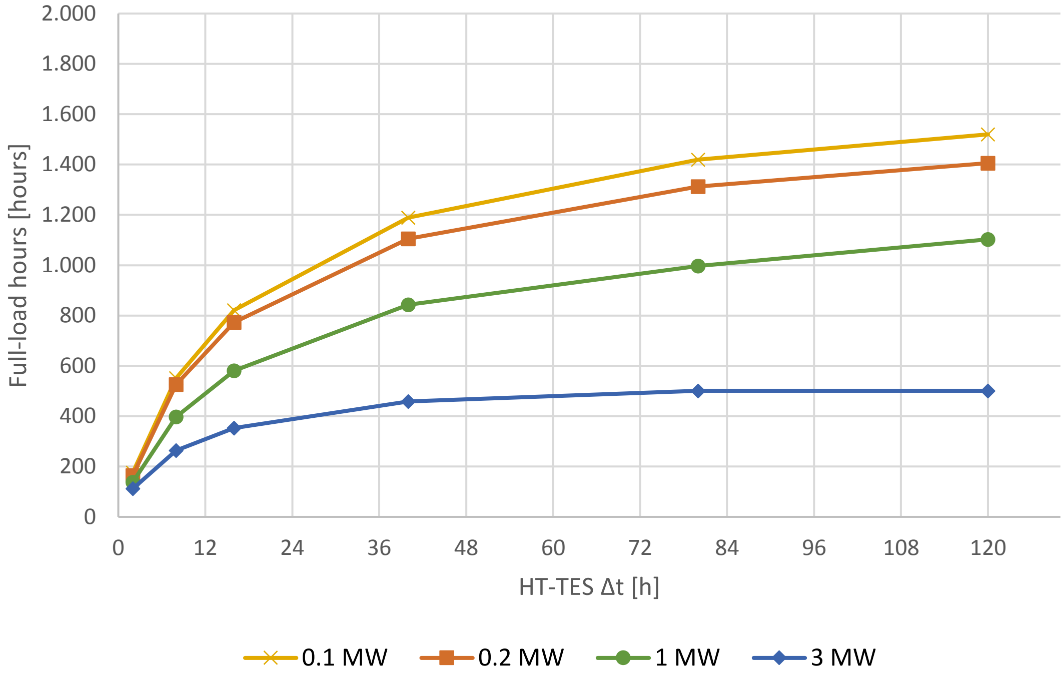

Figure 45: Full-load hours of the ORC as function of the HT-TES capacity for different HP (and ORC) capacities.

The trends of the curves shown in these two figures are quite similar to the results observed for the Aalborg case. For a given HP (and ORC) capacity, the full-load hours increase with increasing storages capacity, with a steep slope at low HT-TES capacities and a small one at high HT-TES capacities. At low HT-TES capacities, this storage capacity is the limiting factor, because it is small in comparison to the HP capacity, so is fully charged soon. However, at high storage capacities, it takes too long for the HP to fully charge the HT-TES. That is why the HT-TES is rarely fully charged and the further increase of the storage capacity only shows minor effects.

An increase of the HP capacity leads to the fact that the HT-TES is charged faster, so it takes less time until the HT-TES is fully charged, and the HP operation has to stop. Hence, at a given HT-TES capacity the increase of the HP capacity results in a decrease of HP full-load hours.

For the ORC these findings are similar to the HP because the ORC can only operate when the HP shows respective operation hours before to charge the HT-TES. The observation of the Aalborg case about the number of full-load hours of the HP that are more affected by the HP capacity compared to the ORC cannot be made here, although the reason for this – the different COPs at different HP capacities – is also valid in this case.

The number of cycles of the latent part of the HT-TES as a function of the HT-TES capacity (for the definition of cycles of the HT-TES, refer to Section 3.1.3) can be show in Figure 46. The diagram shows a decreasing number of cycles with increasing HT-TES capacity, similarly as in the Aalborg case. The diagram for the number of cycles of the sensible part of the HT-TES is not shown, as the values are almost identical.

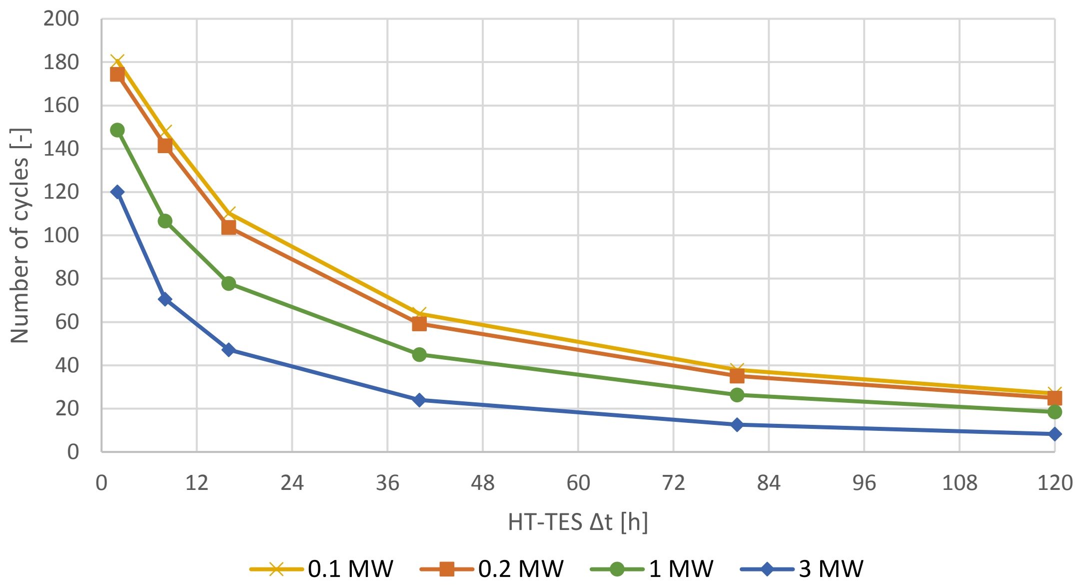

Figure 46: Number of cycles of the latent part of the HT-TES as function of the HT-TES capacity for different HP (and ORC) capacities.

Figure 47 and Figure 48 show the COP of the HP and the power-to-power ratio of the CHEST system dependent on the HT-TES capacity, respectively. The findings here are the same as for the Aalborg case. Due to the almost constant ORC efficiency the P2P curve follow the trend of the COP curves. Comparing the values of Aalborg and Alpha Ventus case it seems that in general the COPs and the power-to-power ratios are a bit smaller here.

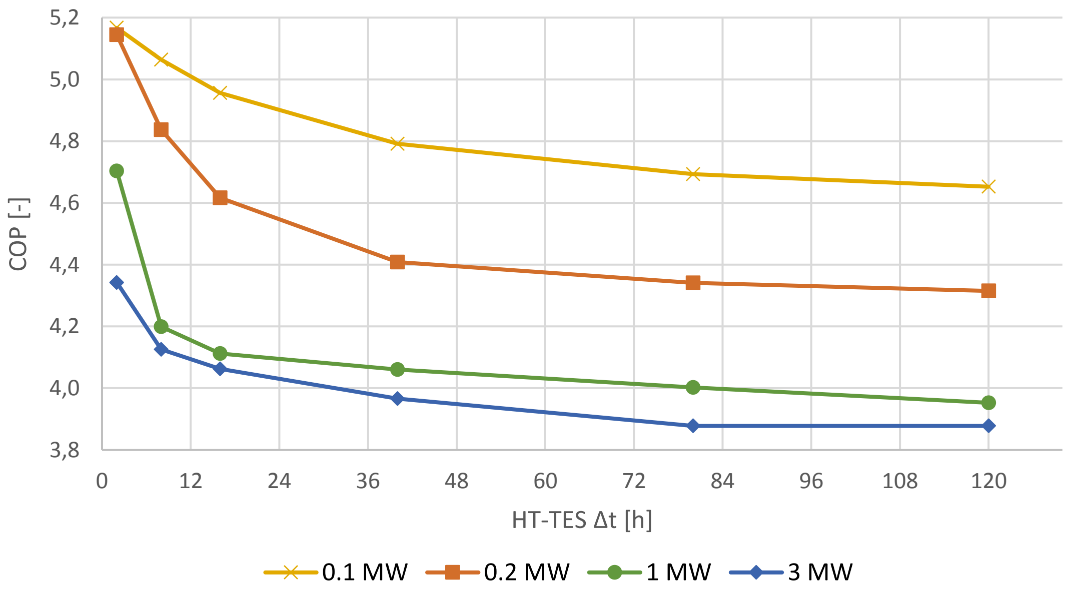

Figure 47: COP of the HP as function of the HT-TES capacity for different HP capacities.

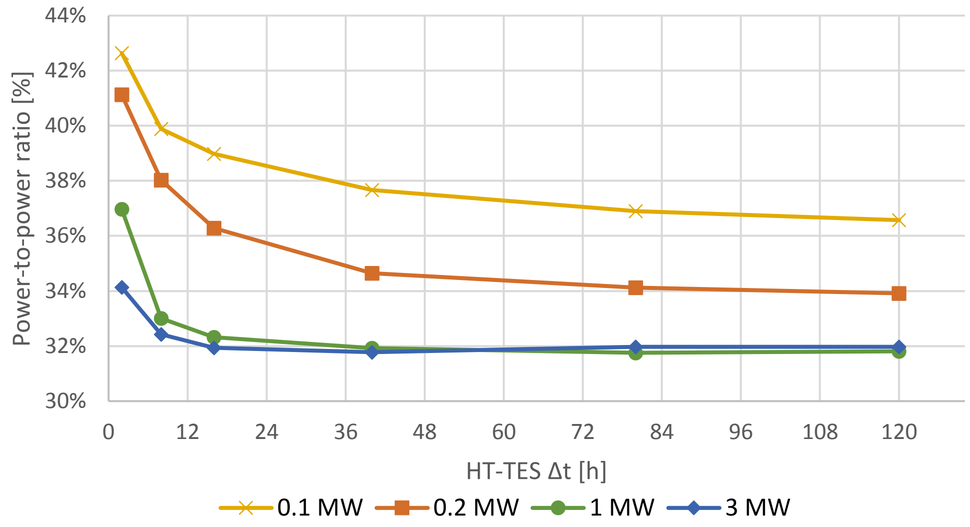

Figure 48: Power-to-power ratio of the CHEST system as function of the HT-TES capacity for different HP (and ORC) capacities.

3.2.4. Variable ratio between HP and ORC capacities

Likewise, the analysis on the ratio between HP and ORC capacities presented in Section 3.2.1, the current section describes the effect of the ORC relative capacity on the performance indicators of the CHEST system. The main difference compared to the analysis in Section 3.2.1 is that in this case the HT-TES has a limited capacity. Based on the results presented in Section 3.2.3, the investigation is limited to 4 capacities of HT-TES, sized on a value of Δt = 8 hours and 24 hours respectively, and on a HP capacity of 0.2 MW and 2 MW. The values of COP_{ref} used for the sizing of the HT-TES kept constant at the aforementioned value of 6.

The performance of the CHEST system is evaluated as function of different ratios between ORC capacity and HP capacity. The ratios chosen here are 0.25, 0.5, 1.0 and 1.2.

Figure 49 and Figure 50 show the number of full-load hours of the ORC and of the HP respectively, as a function of the ORC relative capacity in the 4 investigated scenarios.

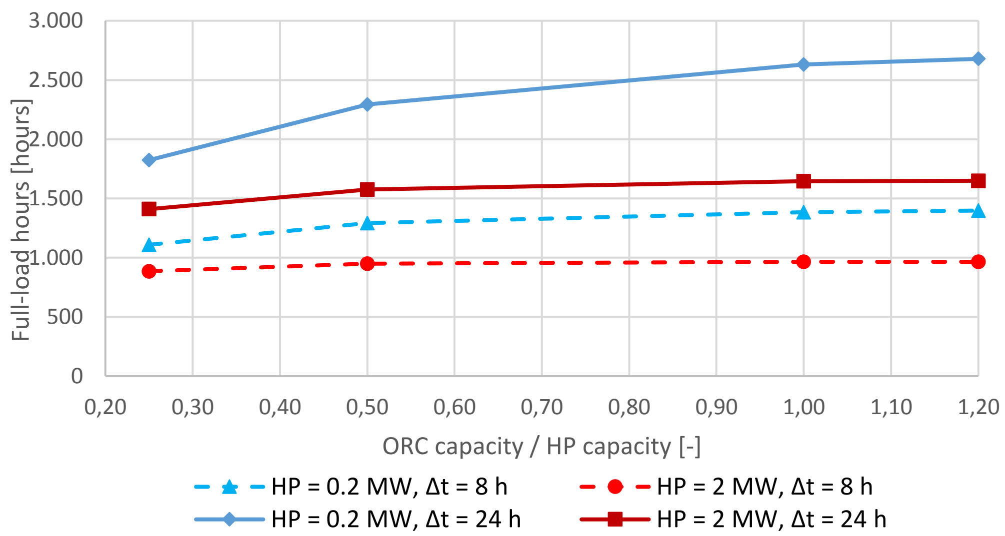

Figure 49: Full-load hours of the HP as function of the ORC relative capacity for the different HP capacities and HT-TES sizes.

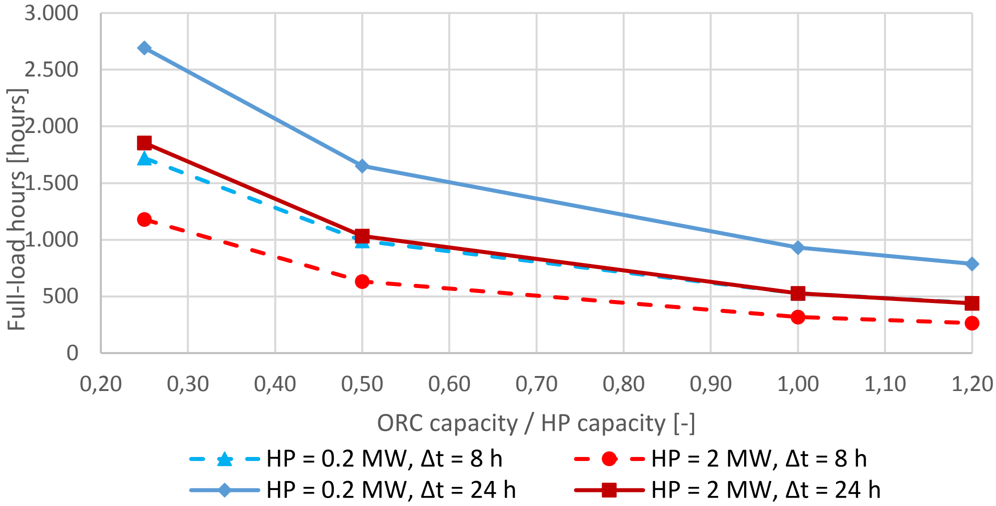

Figure 50: Full-load hours of the ORC as function of the ORC relative capacity for the different HP capacities and HT-TES sizes.

In principle, similar trends can be recognized here like in the Aalborg case with the only difference that the curves for the two HP capacities are less close to each other. An increase of the ORC capacity at a given HP capacity increases the number of HP full-load hours (slightly), but results in a decrease of the ORC full-load hours. This is due to the fact that an increase of the ORC capacity leads in an increased discharging of the HT-TES which means for the HT-HP more time to operate, but less for the ORC.

When the HT-TES is discharged faster, due to an increase of the ORC capacity, also means more heat to transfer to the HT-TES by the HP, thus greater amount of electricity is absorbed by the HP at higher ORC/HP ratios (Figure 51). However, this effect is relatively small. The result for the electricity produced by the ORC shows a similar trend (Figure 52) as well as the trend for the number of cycles (Figure 53).

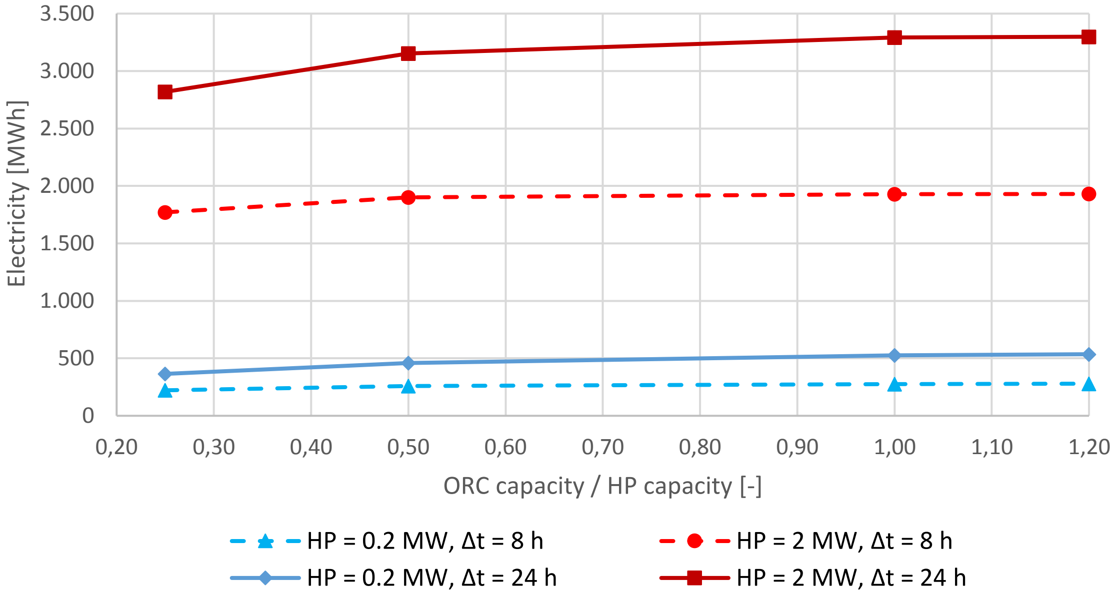

Figure 51: Electricity absorbed by the HP as function of the ORC relative capacity for the different HP capacities and HT-TES sizes.

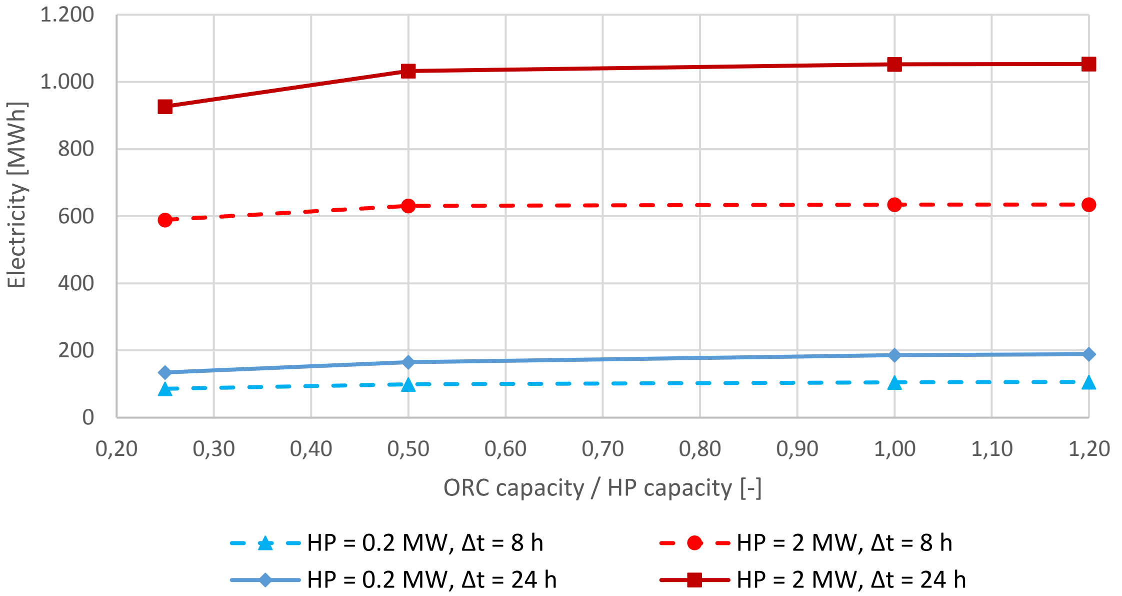

Figure 52: Electricity production from the ORC as function of the ORC relative capacity for the different HP capacities and HT-TES sizes.

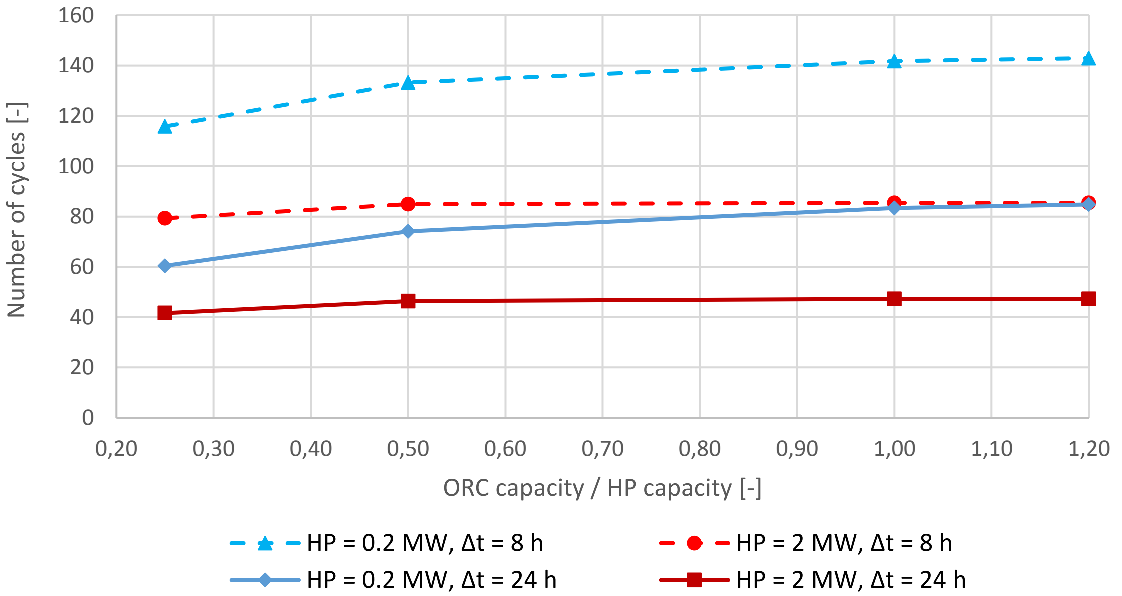

Figure 53: Number of cycles of the latent part of the HT-TES as function of the ORC relative capacity for the different HP capacities and HT-TES sizes.

Figure 54 shows that the COP shows only minor decrease of the COP with increasing ORC/HP capacity ratio which is in light with the numbers shown in Table 23. The ORC efficiency is again nearly constant, so the curves for the power-to-power ratio follow the same trend of the COP.

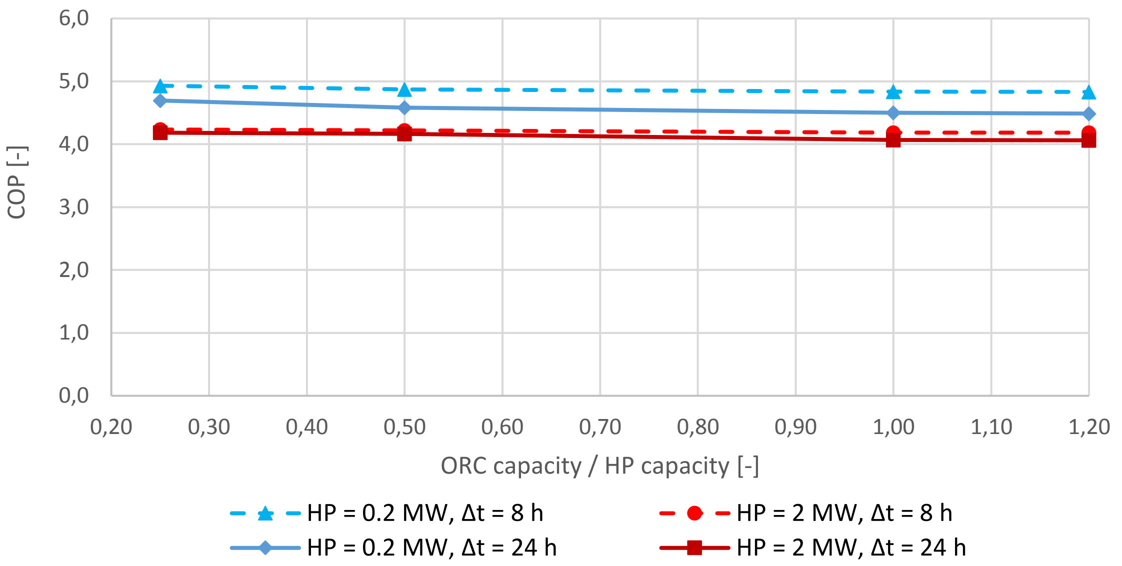

Figure 54: COP of the HP as function of the ORC relative capacity for the different HP capacities and HT-TES sizes.

3.2.5. Working fluid: R1233zd(E) against Butene

All simulations presented in the previous sections are performed assuming Butene as working fluid in both the HP loop and in the ORC loop. In this section results based on R1233zd(E) as working fluid are presented and compared to the results previously obtained for Butene. The boundary conditions chosen for the simulations are the same as those described in the previous sections. Due to the similarity between the results for a HP capacity of 1 MW and for 10 MW in Section 3.1.4, only the latter is considered here.

As regards to the ORC the findings are the same as for Aalborg case, namely the use of R1233zd(E) results in slightly higher full-load hours (Figure 55) and slightly higher electricity produced by the ORC (Figure 56).

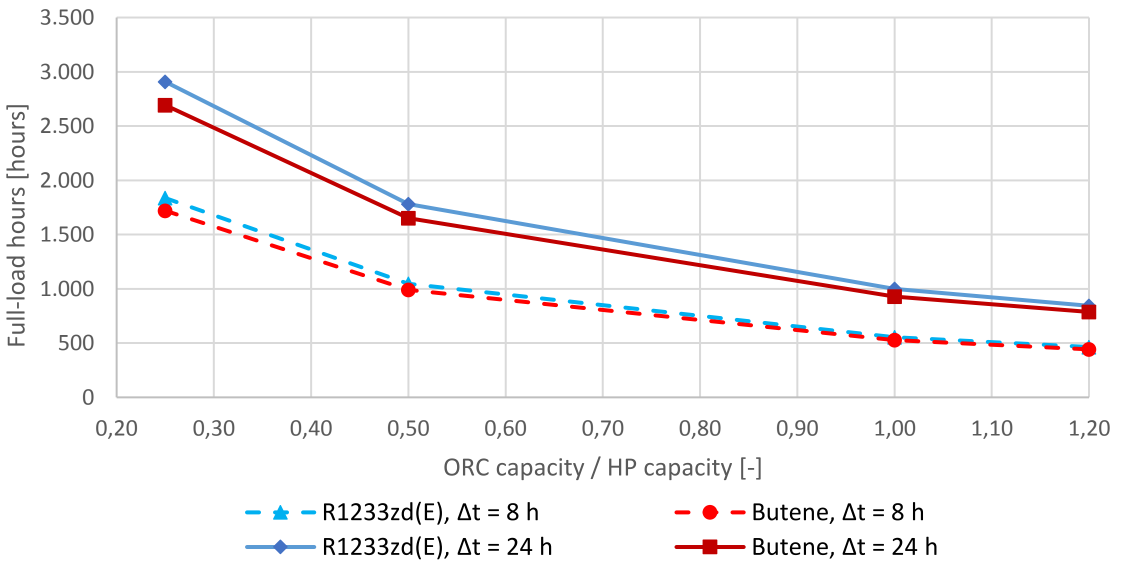

Figure 55: Full-load hours of the ORC as function of the ORC relative capacity for the different working fluids and HT-TES sizes.

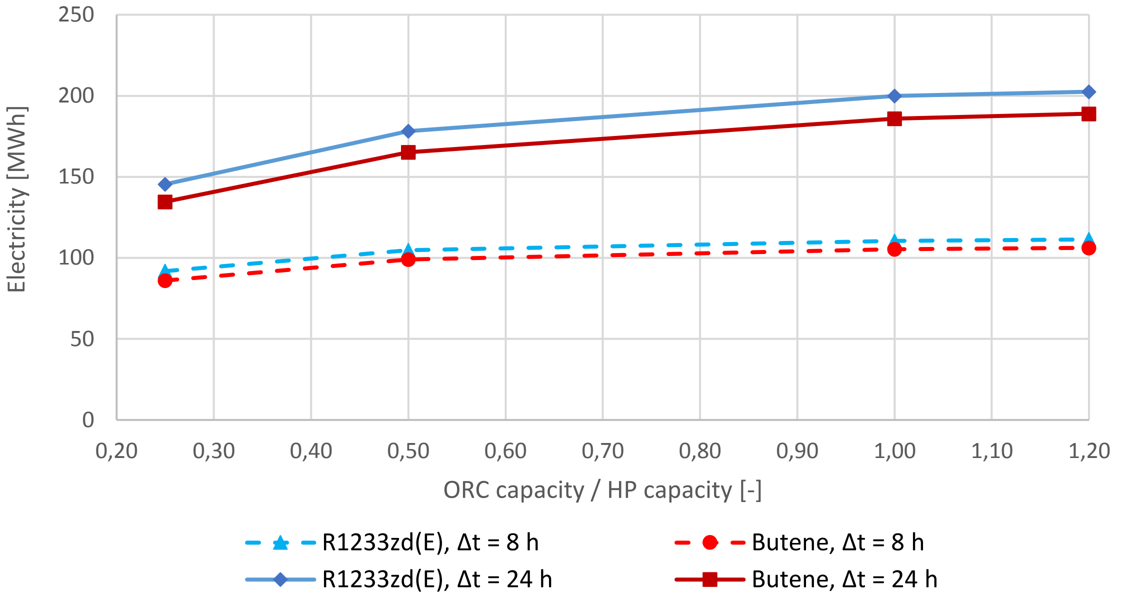

Figure 56: Electricity production from the ORC as function of the ORC relative capacity for the different working fluids and HT-TES sizes.

As for the HP, the finding in Aalborg case is that the results for the two fluids are basically the same. However, for Alpha Ventus case, butene shows slightly higher full-load hours (Figure 57) and also slightly higher electricity absorbed by the HP (Figure 58) compared to R1233zd(E).

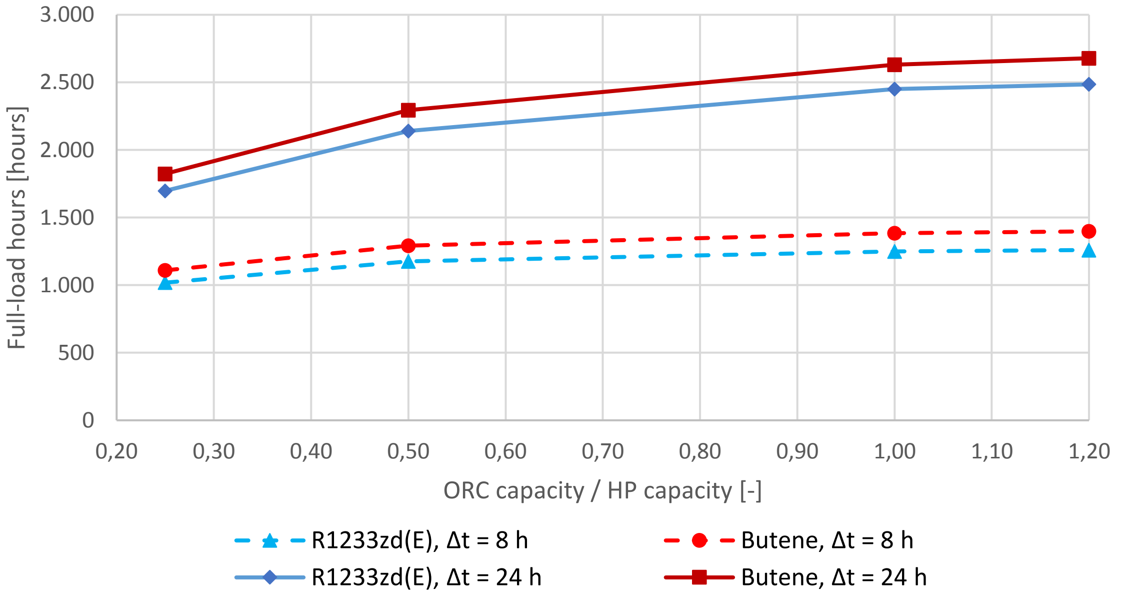

Figure 57: Full-load hours of the HP as function of the ORC relative capacity for the different working fluids and HT-TES sizes.

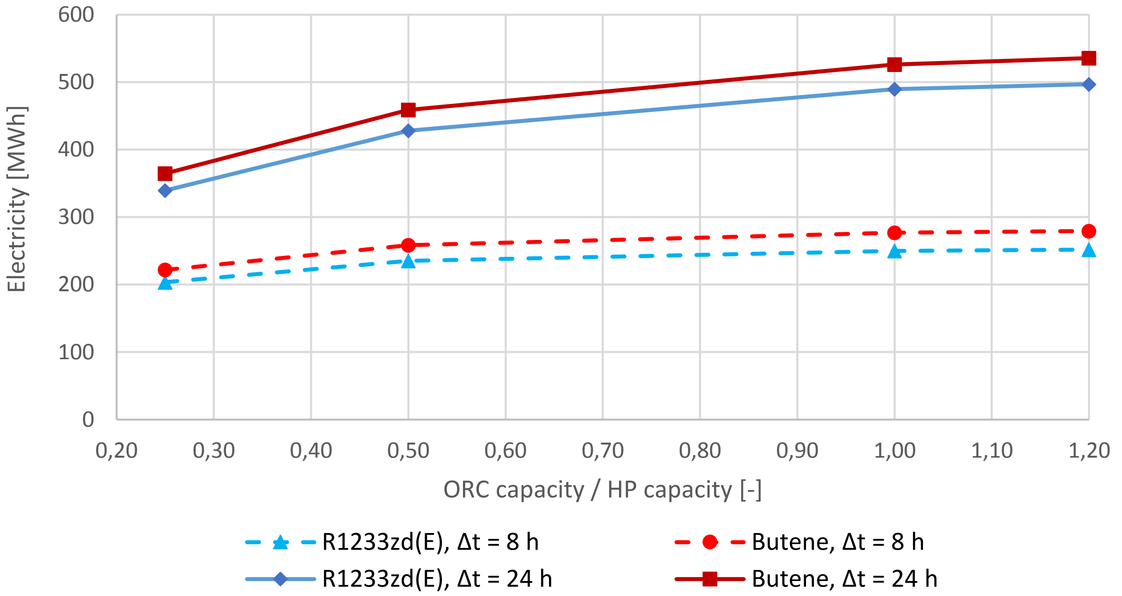

Figure 58: Electricity absorbed by the HP as function of the ORC relative capacity for the different working fluids and HT-TES sizes.

This leads to the fact that the COP of the HP is higher for butene, whereas the ORC efficiency is higher for R1233zd(E) (Figure 59 and Figure 60). The power-to-power ratio of the CHEST system, finally, is higher for R1233zd(E) (Figure 61). The number of cycles is higher for R1233zd(E) (Figure 62) while the additional heat from the boiler is almost the same with both fluids (Figure 63).

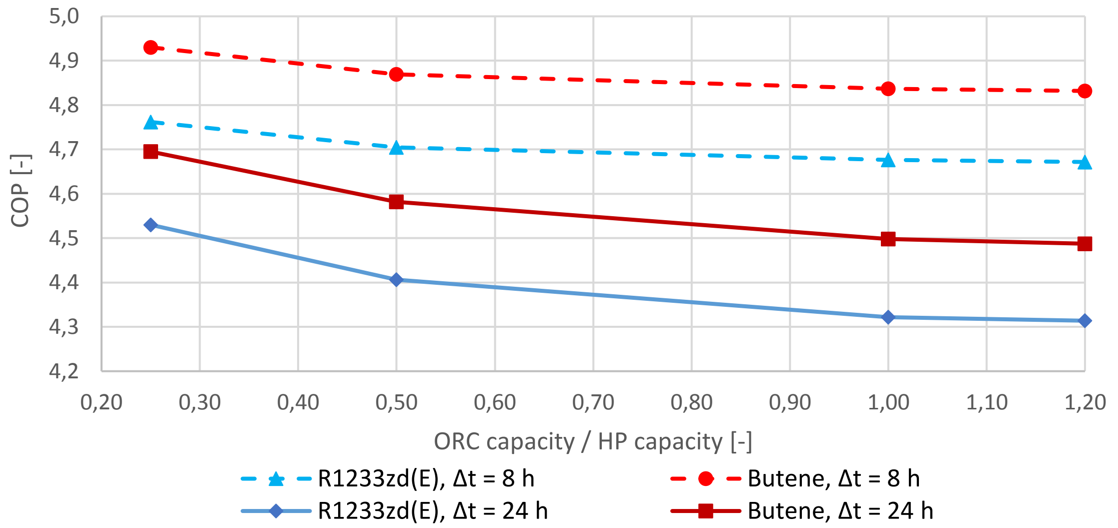

Figure 59: COP of the HP as function of the ORC relative capacity for the different fluids and HT-TES sizes.

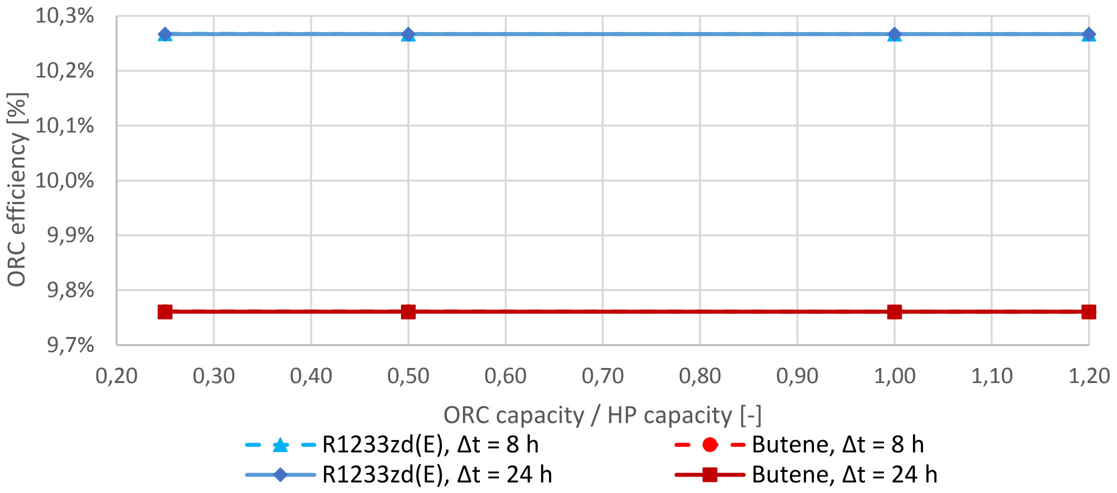

Figure 60: ORC efficiency as function of the ORC relative capacity for the different fluids and HT-TES sizes.

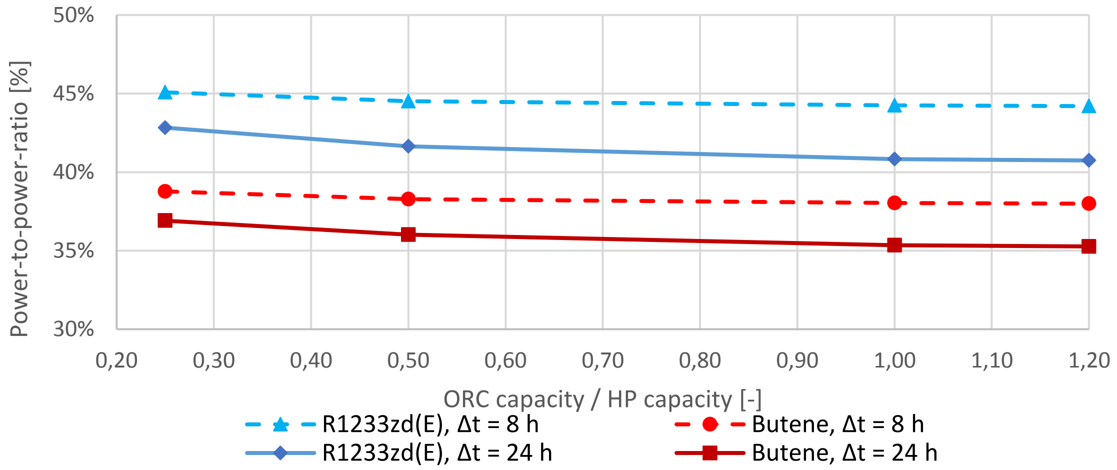

Figure 61: Power-to-power ratio of the CHEST system as function of the ORC relative capacity for the different working fluids and HT-TES sizes.

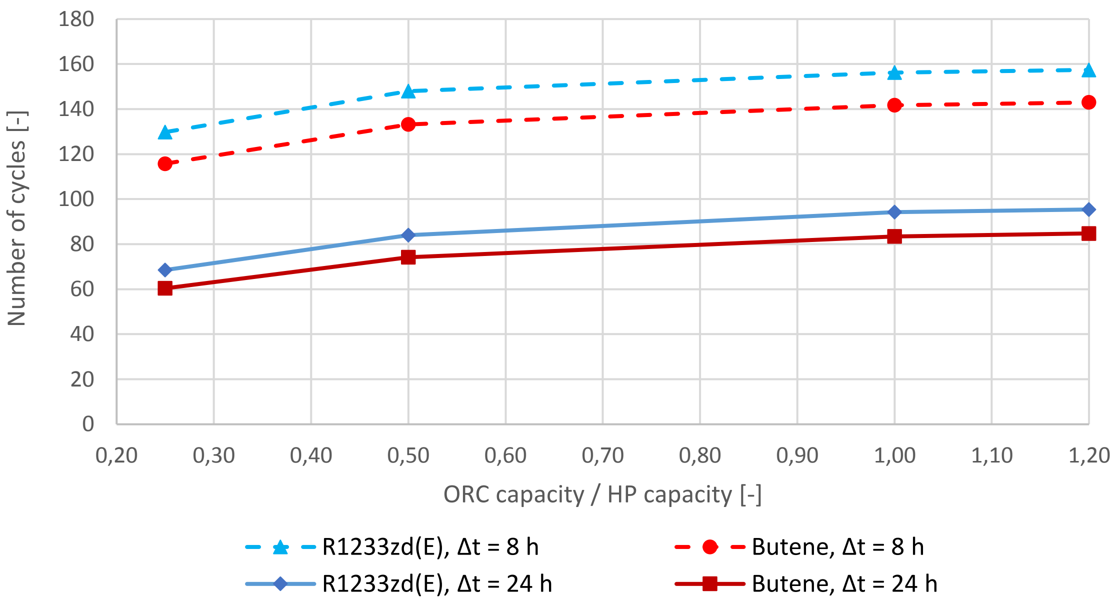

Figure 62: Number of cycles of the latent part of the HT-TES as function of the ORC relative capacity for the different working fluids and HT-TES sizes.

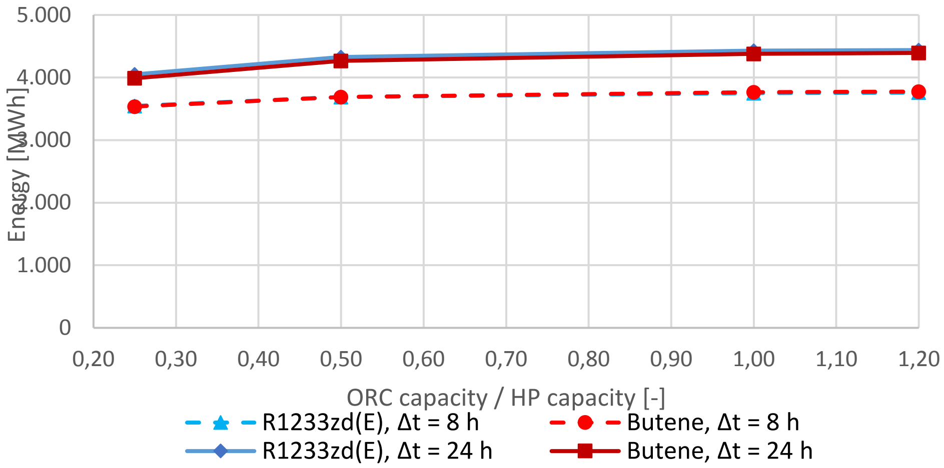

Figure 63: Heat to be dissipated from the sensible part of the HT-TES as function of the ORC relative capacity for the different working fluids and HT-TES sizes.

3.2.6. RES electricity production and electricity demand

All simulations presented in the previous sections are performed assuming a scaling of the profile of the RES electricity production such that the production is equal to the electricity demand on a yearly basis. In this section, simulations with a different ratio between RES electricity production and electricity demand are presented. The hourly profiles themselves are not changed.

In contrast to the Aalborg case, here only simulations with a ratio >1 are performed because this is, actually, the relevant boundary condition to be analysed in this special case study. As mentioned in the descriptions of this case study in deliverable D2.1 such situation is or will be common for many places in the North of Germany. For instance, the city of Emden which is located about 40 km away from the point where Alpha Ventus feeds the produced electricity into the grid, today has already a factor of RES electricity production (wind + PV) to electricity demand of 1.06 and plans to increase RES electricity production further.

However, the fact that on a yearly basis more electricity is produced by RES than electricity is demanded, does not mean that no further (conventional) electricity generators are required, because of the different profiles of production and consumption, sometimes there is electricity surplus and deficit, as shown in Figure 37.

A CHEST system reduces this deficit (as well as the surplus), since in times with less RES electricity production than energy demand, the CHEST system can deliver electricity (and vice versa, in times with more RES electricity production than energy demand, the CHEST system takes up electricity). When the ratio of RES electricity production to energy demand is high enough, then – with a suitable size of the CHEST system – it should be possible to set the deficit to 0, i.e. the remaining deficit with CHEST system (not the original one given by the RES electricity production profile and the electricity demand profile) could be 0 at any point of time. This would mean that no extra (conventional) capacities are required anymore and this results in a lower stress of the grid.

This section focuses on the analysis of how high this ratio of RES electricity production to electricity demand must be to achieve such a situation together with an appropriately sized CHEST system. This, which magnitude of further increase of wind turbine capacities is useful for a city like Emden.

For the simulations performed here, the electricity demand profile is kept constant (scaling factor of 10, Section 3.2), but the RES electricity generation profile is scaled 1/8.2 resulting in a ratio between RES electricity production and electricity demand of 2.0, and 1/3.28, resulting in a ratio of 5.0. As the maximum electricity deficit is around 2.6 MW, the ORC must have at least this capacity, otherwise the target of reducing the deficit down to 0 is not accomplishable. For simplicity, the HP and the ORC capacities are both set to 3 MW here. Simulations with a HT-TES capacity of Δt = 40, 80, 120 h are carried out and the remaining electricity deficit (with CHEST system) is calculated and compared to the original electricity deficit (without CHEST system).

For the HT-TES capacity of Δt = 120 h the reduction of the electricity deficit by the CHEST system is illustrated in Figure 64 for a ratio of 1.0 between RES electricity production and electricity demand. In Figure 65 this is shown for a ratio of 2.0 and in Figure 66 and Figure 67 for a ratio of 5.0.

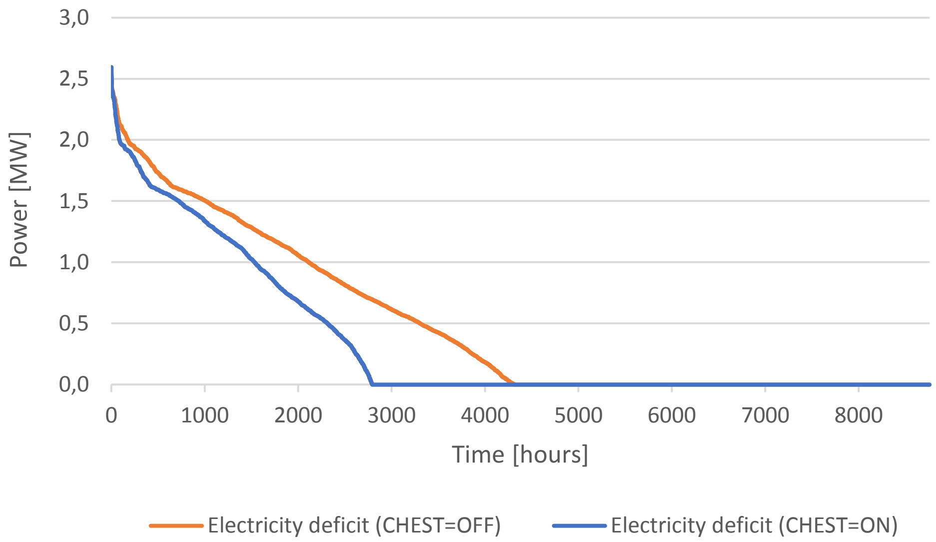

Figure 64: Comparison of the electricity deficit distribution over the year without and with CHEST system for a ratio between the RES electricity production and the electricity demand of 1.0 (HP and ORC capacity 3 MW, HT-TES Δt = 120 h).

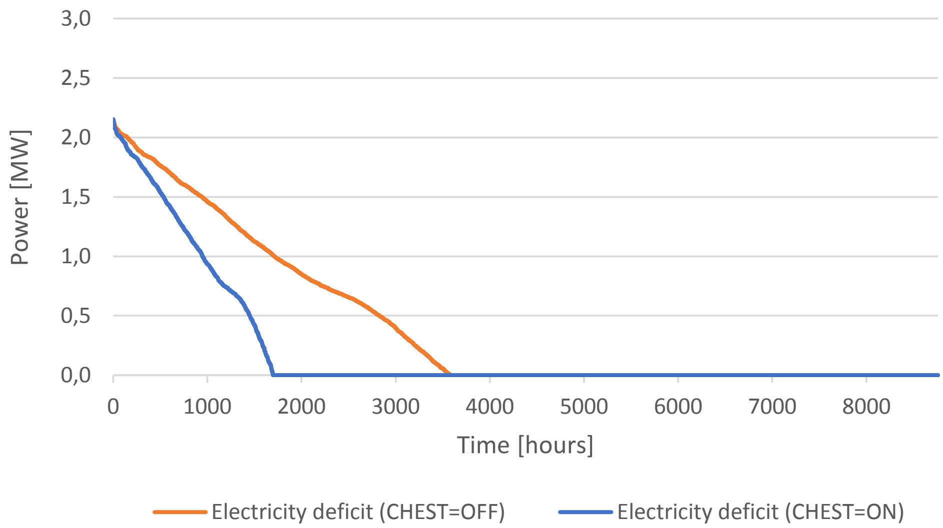

Figure 65: Comparison of the electricity deficit distribution over the year without and with CHEST system for a ratio between the RES electricity production and the electricity demand of 2.0 (HP and ORC capacity 3 MW, HT-TES Δt = 120 h).

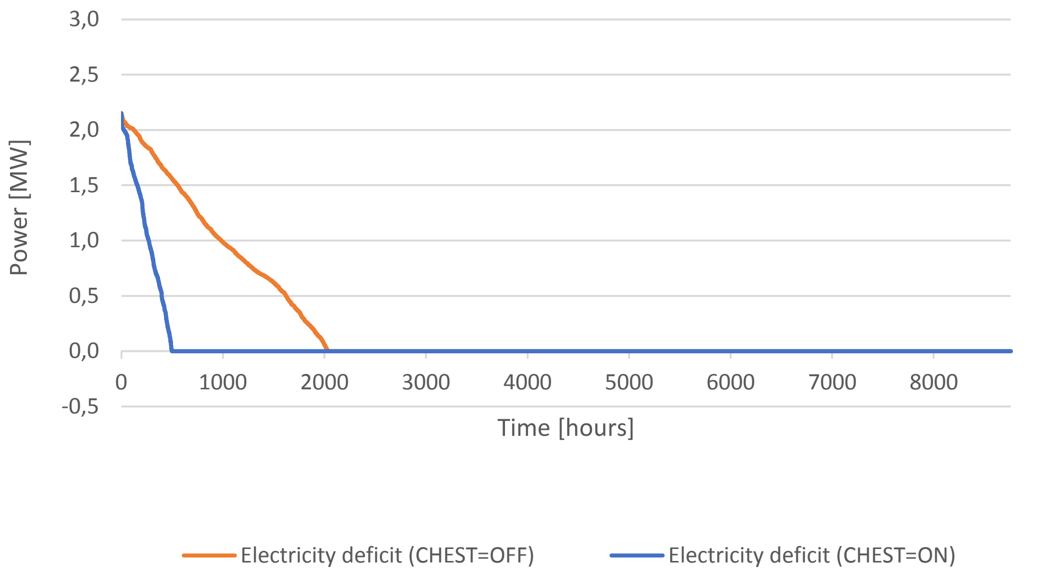

Figure 66: Comparison of the electricity deficit distribution over the year without and with CHEST system for a ratio between the RES electricity production and the electricity demand of 5.0 (HP and ORC capacity 3 MW, HT-TES size, Δt = 120 h).

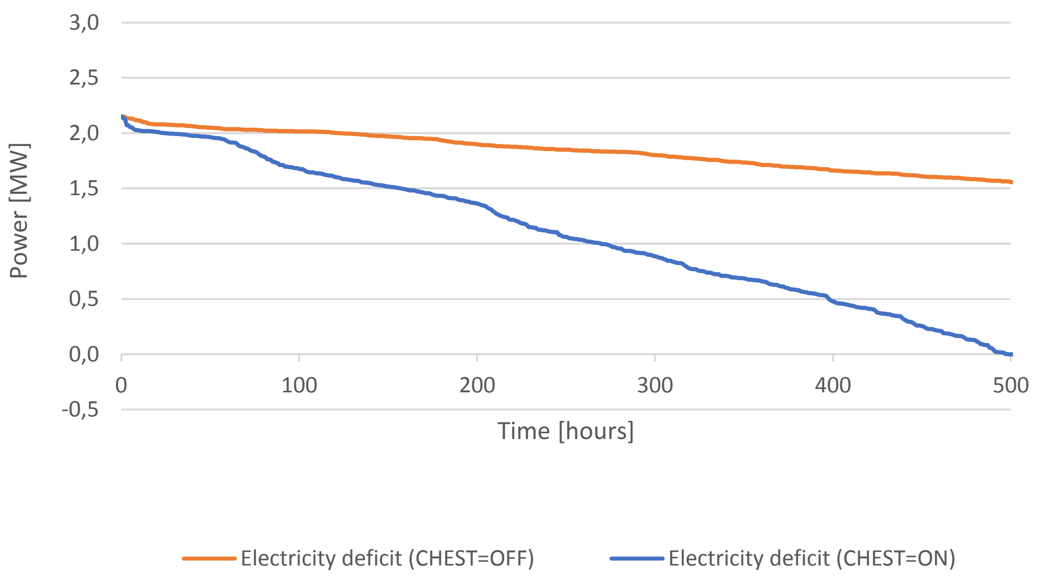

Figure 67: Detail view of Figure 66 (first 500 hours).

The figures show how the hours per year with electricity deficit are reduced by the CHEST system and how this effect becomes stronger with increasing ratio between RES electricity production and electricity demand. Of course, it must be stated that a ratio between RES electricity production and electricity demand of 5.0 is not realistic and reasonable, but it can be seen from Figure 65, the deficit becomes considerably smaller compared to the original one for a factor of 2.0 already. For a factor of 2.0 the remaining deficit with CHEST system accounts for 1,921 MWh, compared to a deficit of 4,770 MWh at a factor of 1.0 without CHEST system (Table 18). It has to be considered that the reduction of the deficit is not only due to the CHEST system, but also due to the increase of the ratio between RES electricity production to electricity demand, because of the higher electricity production the deficit as such (without CHEST system) is reduced.

In the figures above the increase of the ratio between RES electricity production and electricity demand, combined with a rather big HT-TES capacity, does not reduce the maximum value of the remaining deficit. Even for the ratio of 5.0 there is no reduction of the maximum deficit (Figure 67). As a conclusion, this capacity must still be hold available by the grid to meet the energy demand at every point of time in the year.

From this conclusion derives that only when the maximum deficit is significantly reduced, thus contributing to a lower stress of the grid, it seems justified to realize a CHEST system and increase the RES electricity production in an order of magnitude that the factor between RES electricity production and electricity production is noticeably bigger than 1.0. However, the fact that the result is not satisfying here does not mean that this is always so for every CHEST system and boundary condition. First, different sizing of the HP and ORC capacity could improve this situation. Second, the control of the CHEST system could be improved in a way that the ORC does not produce electricity in times of low electricity deficits keeping certain amount of heat in the HT-TES to be used for (predicted) times when the electricity deficit is higher. Last, but not least, also the shape of the RES electricity production and electricity demand profiles will presumably have an influence on the extent of reducing the electricity deficit.

A closer look on the simulation results presented above shows that the HT-TES is at a low state of charge most of the time in the year. For instance, for the simulation with a ratio between RES electricity production and electricity demand of 2.0 and a HT-TES storage capacity of 120 h the state of charge is never above 50 %. This means that the HT-TES storage capacity was not the limiting factor here responsible for not achieving a higher reduction of the deficit.

A simulation performed with a ratio between RES electricity production and electricity demand of 2.0 and a HT-TES storage capacity of 120 h, but now with an HP capacity of 5 MW instead of 3 MW (the ORC capacity is kept constant at 3 MW) also shows only a small effect resulting in a remaining deficit of 1,862 MWh, compared to 1,921 MWh mentioned above for the CHEST system with 3 MW HP capacity. The maximum state of charge of the HT-TES accounts for only about 30 % here.

The reason the HT-TES is at a low state of charge despite high nominal HP capacities lies on the heat side. Although there is enough electricity surplus available for the HP, its operation is limited because of missing heat. To investigate this effect another simulation is performed with again a ratio between RES electricity production and electricity demand of 2.0, a HT-TES storage capacity of 120 h, an HP capacity of 5 MW and an ORC capacity of 3 MW, but now with a RES heat production scaling factor of 2.0. This results in a remaining deficit of only 352 MWh and furthermore, the maximum remaining deficit is now also reduced at least a little bit from 2.15 MW to 2.01 MW. The reduction of the electricity deficit by the CHEST system for this simulation is shown in Figure 68.

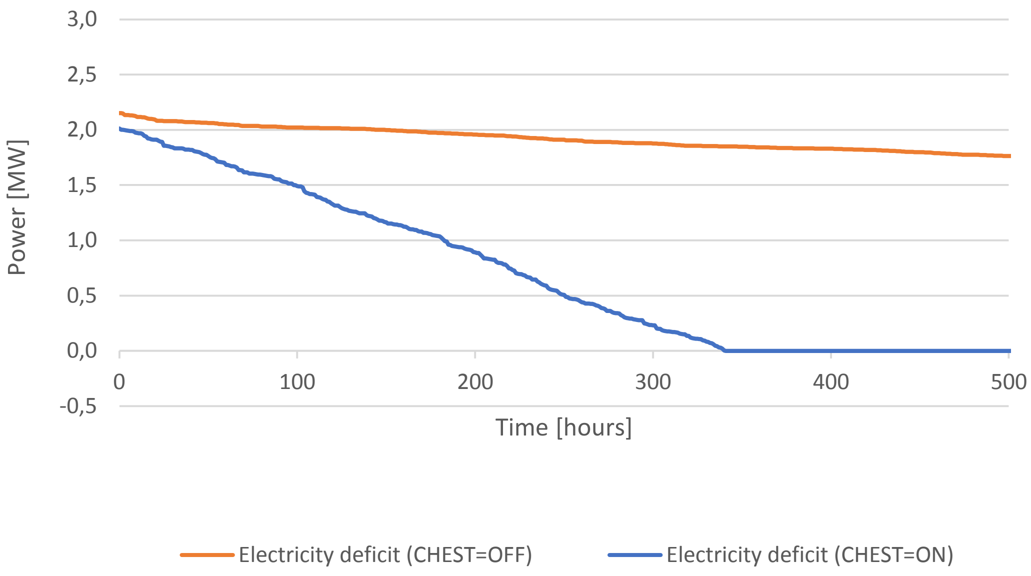

Figure 68: Comparison of the electricity deficit distribution over the year without and with CHEST system for a ratio between the RES electricity production and the electricity demand of 2.0, an HP capacity of 5 MW, an ORC capacity of 3 MW, an HT-TES size of Δt = 120 h and a RES heat production scaling factor of 2.0 (detail view for the first 500 hours)

The maximum HT-TES state of charge was about 40 % here, so the conclusion is that the HT-TES capacity can be reduced.

The simulation performed here shows that for the Alpha Ventus case, a significant reduction of the electricity deficit is not achieved by only increasing the RES electricity production, but also by increasing the RES heat production, which could also be done by carrying out power-to-heat. However, the main point here is that the CHEST system gets this additional energy input also in the form of heat and not solely in the form of electricity.

Further simulations and adaptions of the TRNSYS model (control of the ORC) will be carried out to investigate this in detail. Also, it will be analysed more deeply how this affects the performance parameters like the power-to-power ratio of the CHEST system and the boiler output.

3.2.7. Discussion

Concerning the heat side, the boundary conditions are like the Aalborg case. On a yearly basis the RES heat generation accounts for about 47 % of the DH heat demand in Alpha Ventus case compared to about 52 % in Aalborg case and the profiles of RES heat generation and DH heat demand of the two cases have in common that only in summer time there are phases when RES heat exceeds DH demand. This means the PTES can store heat in that period to be used in autumn.

Adding a CHEST system means that in case of HP operation heat is taken from the PTES and in case of ORC operation heat is injected back into the PTES. However, as it has been pointed out before for the Aalborg case, the heat going into the system is less than the one brought into which requires an additional heat input by a boiler. Hence, just from the heat side, a CHEST system does not mean a benefit, but increases (conventional) energy consumption. Besides, when implementing a CHEST system for compensation of this extra heat, RES heat generation capacities should be increased.

The benefit of the CHEST system lies in the uptake of RES electricity surplus which would otherwise be wasted. To evaluate whether the CHEST system is beneficial, the value of heat and electricity in the specific context of the case study must be known. However, this is beyond the scope of this deliverable which deals only with the energetic evaluation of the CHEST system.

For the assumed boundary conditions applied here, i.e. scaling of the electricity profiles so that the ratio between RES electricity production and electricity demand is 1.0, a CHEST system could have the following characteristics:

- nominal electric capacity of the HP around 0.3 - 0.5 MW;
- nominal capacity of the ORC which is around 50 % of that of the HP;
- nominal capacity of the HT-TES able to store 12-24 hours of electricity input to the HP;
- ratio between the storage capacity of the latent heat part of the HT-TES and the sensible heat part equal to 0.74, i.e. around the latent-to-sensible ratio of the HP.

The clean-up strategy also has to be improved in this context. Regarding the working fluid, the use of R1233zd(E) shows slightly higher power-to-power ratios. Nevertheless, as in the Aalborg case, not only the efficiency of the CHEST system should be considered, but also i.e. the performance of the individual technologies.

For a ratio between RES electricity production and electricity demand > 1.0, the nominal capacity of the ORC should be in the order of magnitude of the maximum electricity deficit, when aiming at reducing the maximum electricity deficit significantly in order to contribute to a lower stress of the electric grid. In order to significantly lower the electricity deficit, it is also necessary to look at the heat side and - if this limits the reduction – to increase the RES heat production. However, further analysis is needed here to investigate which boundary conditions, ratios between RES electricity production and electricity demand and CHEST characteristics make this aim realizable and how this affects the performance of the CHEST system. Moreover, simulations with different LT-TES capacity (in relation to the HT-TES capacity) will be carried out to investigate the heat side of the CHEST system more in detail.

4. Conclusions

The CHEST system has been described from the thermodynamic point of view. Based on this, the model developed by DLR could provide performance maps to characterize the operation of the CHEST components when the CHEST system is not integrated in the energy system. Based on the DLR's model, a TRNSYS model is developed and its operation has been accurately described, explaining the function of each component. Although some simplifications are necessary in the modelling (such as, clean-up strategy, condensation of the ORC only in the pit storage, simplified control strategy…), the TRNSYS model has proved to be suitable for a preliminary analysis of the impact of a CHEST system on a specified energy system. In this deliverable the TRNSYS model is used to simulate the integration of a CHEST system in the energy systems of Aalborg and of Alpha Ventus. The remaining case studies will be analysed in the deliverable D2.3. Then, based on the simulation results, the following conclusions can be drawn.

Larger HP and ORC capacities, as well as larger HT-TES, are characterized by larger amounts of absorbed/produced electricity, but the increment in the absorbed/produced electricity is progressively smaller at higher capacities. Consequently, in both the investigated case studies, the sizes of the CHEST components which seemed more feasible are significantly smaller than the capacities, which should be installed to minimize the electricity surplus/deficit. Indicative sizes are suggested for the different components of the CHEST system in the two investigated case studies. In the case of Aalborg, a nominal electric capacity of around 10 MW is suggested for the HP. In the case of Alpha Ventus, a smaller capacity (300-500 kW) is found more suitable. In both cases, it is found that the nominal electrical capacity of the ORC should be around 50 % that of the HP. The HT-TES should be sized to store 12-24 hours of electricity input to the HP. Regarding the repartition of the storage capacity of the HT-TES between its two parts, the ratio between the storage capacity of the latent heat part and that of the sensible heat part is recommended to be around 0.74, i.e. the latent-to-sensible ratio of the HP.

In general, the HP draws more heat (and at higher temperature) out of the low temperature storage than the heat than the ORC injected back (and at lower-temperature). Therefore, if the thermal energy balance of the overall system is considered, the CHEST operation made the system use more thermal energy compared to the case without CHEST operation as it was expected. This is due to the fact that some low-temperature heat is not be included in the model, therefore, it has to be dissipated because of the simplifications of the CHEST components and the temperature requirements of the DH network. Furthermore, the presence of the CHEST system allows displacing electricity from periods when there is an excess to periods when it lacks. To quantify this benefit, it is necessary to have information on the value of the electricity in the different periods, the value of the balancing service that a CHEST system could provide to the electrical grid, the cost of the alternatives storage and/or balancing technologies as well as the technical and economic factors which apply to the dispatch of electricity. This activity will be carried out in D2.3 and WP4.

Regarding the temperature requirements of the HT-TES, the TRNSYS model cannot be used to give recommendations. The chosen PCM (KNO_3-$LiNO_3$(eu), Section 2.1.2) set the temperature requirement for the latent part of the HT-TES to the phase change temperature of 133 °C, which determines the condensing temperature of the HP cycle and the evaporating temperature of the ORC cycle. Due to performance maps combining the performance of the HP (and of the ORC) with that of the HT-TES are used in the TRNSYS model, considering the temperature differences across the heat exchangers and other relevant requirements, relevant results about the temperature requirements of the HT-TES cannot be provided in this analysis. However, in task 2.4, it is being developed a decoupled TRNSYS model and in the deliverable D2.4 the recommendations of individual technologies will be included.

Regarding the working fluid, the use of R1233zd(E) shows a slightly better performance compared to Butene. However, other considerations should be taken into account for the choice of the working fluid. It is therefore, in WP3 and WP4 are working in the selection of the best working fluid.

5. Appendix A

This Appendix contains the performance maps of the HT-HP and of the ORC, based on the outputs of the model of the CHEST system developed by DLR in the Ebsilon Professional software.

The performance maps for both Butene and R1233zd(E) are reported.

In the tables the apostrophe following flow rates, thermal and electric power quantities denote that these quantities refer to a specific nominal power of the machine. In the performance maps of the HT-HP, the specific nominal power refers to is 1 MW of electrical power absorbed by the compressor. In the performance maps of the ORC, the specific nominal power refers to 1 MW of electrical power output from the expander.

Table 24: Performance map for the HT-HP using Butene as refrigerant (independent operation of HT-HP and ORC).

$T_{source,in}$ [°C]	$T_{source,out}$ [°C]	m'_{HW} [kg/s]	Q'_{in} [kW]	P'_{in} [kW]	Q'_{excess} [kW]	$T_{excess,in}$ [°C]	$T_{excess,out}$ [°C]	Q'_{latent} [kW]	$Q'_{sensible}$ [kW]	$m'_{sensible}$ [kg/s]
40	35	146.0	3050.8	1039.3	889.0	70	26.7	1338.9	1798.7	19.2
50	45	162.5	3395.9	1044.0	780.9	70	37.3	1525.3	2070.0	15.1
60	55	181.7	3798.3	1049.4	621.0	70	47.9	1761.5	2401.2	12.3
70	65	204.5	4279.4	1055.9	387.9	70	58.4	2066.2	2816.9	10.3
80	75	232.4	4871.8	1064.0	46.5	70	68.9	2468.5	3356.0	8.80
90	85	292.5	6146.2	1081.1	0.0	70	70.0	3042.9	4118.7	7.59
100	95	383.2	8071.4	1106.9	0.0	70	70.0	3880.9	5230.3	6.59

Table 25: Performance map for the ORC using Butene as refrigerant (independent operation of HT-HP and ORC).

$T_{sink,in}$ [°C]	$T_{sink,out}$ [°C]	Q'_{latent} [kW]	$Q'_{sensible}$ [kW]	$m'_{sensible}$ [kg/s]	P'_{out} [kW]	m'_{CW} [kg/s]	Q'_{out} [kW]
15	25	2568.0	3490.5	12.8	912.7	122.4	5116.8
20	30	2761.5	3577.5	13.1	907.1	129.3	5402.1
30	40	3225.5	3763.8	13.8	894.6	145.3	6063.3
40	50	3829.5	3967.9	14.5	879.9	164.9	6884.1
50	60	4643.3	4192.1	15.4	862.4	190.0	7936.9

Table 26: Performance map for the HT-HP using R1233zd(E) as refrigerant (independent operation of HT-HP and ORC).

$T_{source,in}$ [°C]	$T_{source,out}$ [°C]	m'_{HW} [kg/s]	Q'_{in} [kW]	P'_{in} [kW]	Q'_{excess} [kW]	$T_{excess,in}$ [°C]	$T_{excess,out}$ [°C]	Q'_{latent} [kW]	$Q'_{sensible}$ [kW]	$m'_{sensible}$ [kg/s]
40	35	143.9	3006.9	1038.7	992.4	75	25	1591.0	1398.7	14.7
50	45	161.0	3363.2	1043.4	894.8	75	36	1833.8	1614.2	11.6
60	55	180.6	3776.4	1049.0	753.8	75	47	2134.8	1872.8	9.57
70	65	204.1	4271.8	1055.7	552.8	75	57	2517.0	2193.3	8.06
80	75	233.1	4886.9	1064.0	264.7	75	68	3016.3	2605.1	6.88
90	85	278.9	5858.9	1077.1	0.0	75	75	3704.1	3166.4	5.93
100	95	364.5	7677.7	1101.5	0.0	75	75	4721.0	3991.3	5.14

Table 27: Performance map for the ORC using R1233zd(E) as refrigerant (independent operation of HT-HP and ORC).

$T_{sink,in}$ [°C]	$T_{sink,out}$ [°C]	Q'_{latent} [kW]	$Q'_{sensible}$ [kW]	$m'_{sensible}$ [kg/s]	P'_{out} [kW]	m'_{CW} [kg/s]	Q'_{out} [kW]
15	25	2897.5	3246.3	11.9	947.0	123.7	5169.6
20	30	3112.4	3306.5	12.1	943.5	130.4	5447.6
30	40	3625.8	3437.7	12.6	935.8	146.1	6098.4
40	50	4289.6	3582.7	13.2	926.6	165.6	6914.6
50	60	5177.8	3741.3	13.7	915.7	190.8	7970.2

References

[Bauer. 2012]. Bauer. T., Steinmann. W.-D., Laing. D., Tamme. R. Chapter 5: Thermal energy storage materials and systems. 2012. Annual Review of Heat Transfer, Vol. 15, pp.131-177, Begell House Inc.

[Jockenhöfer. 2018]. Jockenhöfer. H., Steinmann. W. D., Bauer, D. Detailed numerical investigation of a pumped thermal energy storage with low temperature heat integration. 2018. Energy, 145, pp. 665–676, https://doi.org/10.1016/j.energy.2017.12.087.

[Mazzarella. 1992]. Mazzarella. L. *Multi-flow stratified thermal storage model with full-mixed layers*. 1992. Retrieved 31/08/2018 from http://trnsys.de/download/en/ts_type_342_en.pdf.

[NIST. 2018]. National Institute of Standards and Technology (NIST). 2018. *REFPROP Database* Version 10. Available at www.nist.gov/srd/refprop.

[STEAG. 2018]. STEAG. EBSILON®Professional. 2018. Available at www.steag-systemtechnologies.com/en/products/ebsilon-professional/.